DISSERTATION

METAL ORGANIC FRAMEWORKS AS HETEROGENEOUS NITRIC OXIDE CATALYSTS FOR USE IN THE DEVELOPMENT OF THERAPEUTIC POLYMER MATERIALS

Submitted by

Jacqueline L. Harding

Department of Chemistry

In partial fulfillment of the requirements

For the Degree of Doctor of Philosophy

Colorado State University

Fort Collins, Colorado

Fall 2014

Doctoral Committee:

Advisor: Melissa Reynolds

Amy Prieto
Debbie Crans
Travis Bailey
Deanna Worley

ABSTRACT

METAL ORGANIC FRAMEWORKS AS HETEROGENEOUS NITRIC OXIDE CATALYSTS FOR USE IN THE DEVELOPMENT OF THERAPEUTIC POLYMER MATERIALS

Implantable polymeric medical devices are subject to surface biofouling due to the deposition of microbial agents and the accumulation of proteins at the material interface. Consequently, medical devices which are intended for beneficial functions can become a potentially fatal threat. As a result biofouling resistant materials are vigorously sought through the manipulation of material surface properties and by eluting therapeutics on the material surface. Nitric oxide (NO) is a bioactive agent generated by most nucleated cells in the human body and is known to mediate antimicrobial and antithrombus effects while maintain the capacity to promote the proliferation of healthy tissues. As such, the development of NO releasing biomaterials is known to reduce incidences of surface biofouling. However, current NO releasing materials are limited to short lifetimes of used based on limited capacity of exogenous NO which can be incorporated into the material. In order to circumvent this problem the goal of this research is to develop a biomaterial which generates NO from an endogenously supplied source.

Metal organic frameworks (MOFs) were selected for investigation as heterogeneous catalysts for the generation of NO from bioavailable NO donors, S-nitrosothiols (RSNOS). MOFs were evaluated as NO catalysts based on their capacity to react with various RSNO substrates and their maintained structural integrity under reaction conditions. Presented herein is the successful demonstration of a Cu-MOF for the catalytic generation of NO from bioavailable RSNOs donors. However, the limited stability of this proof of principle MOF in aqueous solution prompted the development of a MOF-NO catalyst that is suitable for physiological applications through tuning the organic ligands used in the construction of the framework. Finally a two-fold demonstration of the feasibility towards designing composite MOF based

biomaterials is presented as blended materials prepared via commercial manufacturing processes and via surface growth of MOFs on flexible polymeric substrates.

ACKNOWLEDGEMENTS

The journey is long filled with twists and turns that make it impossible to see what lies ahead. However, here at this weigh station it is easy to look back and recount all of the influences and opportunities, which have led me to my current position. With that I would like to begin by thanking my parents who have provided me with a lifetime of opportunity too not only accomplish my dreams but also all of my whims and fantasies. My sister of course who found herself more often than not roped into something that she knew from the get go was crazy but never ceases to sign up for the next round. Thank you for never making me feel that I am limited and that anything is possible.

Along the way I have encountered countless teachers, some in the classroom and some on the playground, all of which have provided me with the bricks to build a firm foundation. Most notably I would like to thank my graduate advisor Melissa Reynolds, whose timing could not have been better. When we met I was lost and ready to lead myself down an alternate path. Thank you for helping me stay the course because I know now beyond a shadow of a doubt that this is my true path.

Finally, I would like to thank those who have been running right there with me for the obstacle course that is grad school: Michelle, Zander, Riley, and Imogene (aka Stinky). Thank you Riley for always being at my side ready to go anytime and for the great big hugs you give when I need it most. Imogene for teaching me that sometimes it’s best to just speak up and tell the world what you need because it will answer and you will find yourself loved because of your quirks not

despite them. Zander for being the rock and reminding me everyday of the importance of getting out there and climbing the hill no matter how much it hurts. Michelle for never letting me feel like I am all alone no matter how much I want to believe it and most importantly for reminding me that where we are going cruise control is not an option and that its best to just roll with it.

I can’t wait to check in at the next station.

Dr. Jacqueline Harding

TABLE OF CONTENTS

Chapter 1

An Introduction to the Development of Therapeutic Biomaterials

Synopsis

Research Problem: Implantable polymeric medical devices are subject to surface biofouling due to the deposition of microbial agents and the accumulation of proteins at the material interface. Consequently, medical devices which are intended for beneficial functions can become a potentially fatal threat. As a result biofouling resistant materials are vigorously sought through the manipulation of material surface properties and by eluting therapeutics on the material surface. These approaches are currently met with only limited success due each approaches inherent limitation of counting either infectious microbes or the adhesion of thrombus forming biomolecules to the material surface.

Research Goal: The development of a biomaterial which generates the bioactive agent nitric oxide from an endogenous source to counter the negative effects of surface biofouling via integration of the device into the host environment.

Research Hypothesis: Nitric oxide is a bioactive agent generated by most nucleated cells in the human body known to mediate antimicrobial effects and promote the proliferation of healthy tissues. Therefore the development of an NO releasing material which can sustain the generation of physiologically relevant levels of NO by relying on endogenous supplies of NO over the device lifetime will result in the development of an antifouling material surface with potentially regenerative effects.

Research Approach:

1) In chapter 2 a method for the accurate quantification and reporting of bioavailable NO generated from NO donors in cell media solutions used for *in vitro* studies is presented. This work aims to

identify possible sources of discrepancies in the literature used to report therapeutic levels of NO by identifying riboflavin as an effective NO scavenging agent found as an additive in cell media solutions. Once established the method developed here was applied to a collaborative effort with the Vigh group in the neuroscience department at Colorado State University to measure the therapeutic dosage of NO needed to stimulate diseased retinal cells. These findings are not reported in the text, but the full manuscript is available in the appendix.

- Harding, J. L.; Reynolds, M. M. *Analytical Chemistry* **2014**, *86*, 2025.

2) Chapter 3 discusses the use of a metal organic framework (MOF) for the catalytic generation of NO from bioavailable small molecule NO donors, S-nitrosothiols (RSNO). In this work the well studied Cu-MOF, CuBTC, was shown to catalytically generate NO. The reactivity of the catalyst was determined based upon the rate of NO generation with each of the investigated RSNO substrates and was found to be influenced based on substrate size and polarity of terminal functional groups. The MOF catalyst remained intact following reaction with the RSNOs, but only when a non aqueous solvent, ethanol, was used. Further exploration into the importance of the metal ion active site was shown using iron and aluminum based MOFs.

   - Harding, J. L.; Reynolds, M. M. *Journal of the American Chemical Society* **2012**, *134*, 3330.

3) Presented in chapter 4 is the development of a MOF NO catalyst with structural stability in biological fluids. In this work triazolae based ligand is coordinated to Cu2+ metal centers resulting in the formation of a robust framework towards aqueous environments. This material is shown to resist degradation even when exposed to biological fluids and maintains its activity as an NO catalyst.

   - Harding, J.L.; Metz, J.M.; and Reynolds, M.M. *Advanced Functional Materials* **2014**, DOI:10.1002/adfm.201402529

4) Chapter 5 outlines the feasibility of incorporating MOF NO catalysts into the polymeric matrix of existing medical devices utilizing commercial extrusion processes. In order to successfully

implement MOFs for use in therapeutic materials it is essential that existing manufacturing processes not require substantial modification. Furthermore, MOFs must retain their structural and chemical properties once incorporated into a device. As a result MOF-poly materials prepared according to commercial manufacturing methods were evaluated based on the structural integrity and reactivity of the material towards NO generation. Mechanical properties of the prepared material were not assessed.

- Harding, J. L.; Reynolds, M. M. *Journal of Materials Chemistry B* **2014**, *2*, 2530.

5) In chapter 6 a method for the deposition of MOF crystals on the surface of flexible polymeric substrates is presented. The uniform deposition of MOF thin films on surfaces to form composite materials for use as membranes or supported heterogeneous catalysts is highly desirable, however many current approaches rely on the use of rigid inorganic substrates that are impractical for many real world applications. Instead this work presents a facile room temperature synthesis of covalently attached MOF crystals on the surface of a flexible organic substrates. This method results in the growth of crystals with uniform size and excellent surface coverage on the substrate that is indifferent to substrate size, topology, and topography making it an excellent method for incorporating MOF particles onto the surface of prefabricated materials.

- Manuscript in preparation

Research Conclusions: This research represents a complete body of work from the development of an analytical method for evaluating the behavior of MOF NO catalysts to their ultimate incorporation into functional devices intended for biological applications.

Project Background

Medical Device Biofouling. Medical devices are a major component in the healthcare industry ranging from simple yet useful devices (Class I) such as tongue depressors and bandages to life-saving treatment options (Class III) including pacemakers and vascular stents.[1] While Class I materials are generally

representative of a benign classification that pose little risk to patients, the Class III materials are considered high risk and are susceptible to resulting in adverse effects including patient injury or infection.[2] Implantable devices are subject to the deposition of microbial agents on the material surface and the foreign body response which results in the accumulation of proteins and microbes on the surface of the device shown in Figure 1, posing a high risk for device impairment.[3-5] Furthermore, the increasing use of invasive medical procedures for the implantation of devices leads to an increased risk for the development of device associated infections. Current estimates place the occurrence of nosocomial bacterial related infections at 65% and are associated with the growth of bacterial biofilms on device surfaces. [6] Severe biofouling of medical devices, ultimately resulting in device failure can only be corrected by the removal and replacement of the device through costly invasive procedures. Given the broad scope of medical devices in use and the complexity of physiological environments to which they are exposed makes the design of antifouling materials a challenge requiring multiple avenues of approach.[4]

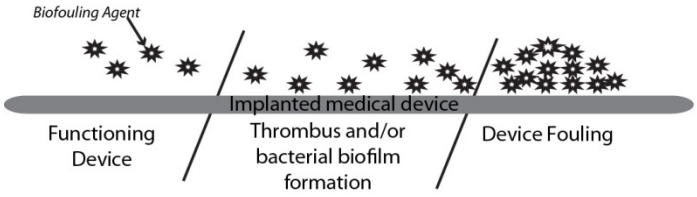

Figure 1. Deposition of microbial or protein based biofouling agents on the surface of a medical device ultimately resulting in device surface biofouling.

While, the exact mechanisms of attachment of bioagents to the surface of medical devices is not well understood, physical and chemical surface properties are known to influence the type and extent of surface fouling [7]. Upon insertion into a liquid environment a conditioning layer immediately forms composed of lipids and glycoproteins onto the device surface.[2,7-9] The composition of the conditioning layer is dictated by the device surface properties, including charge and hydrophillicity, and environmental factors such as pH and temperature. The composition of the conditioning layer subsequently influences

what types of bacteria strains can colonize on the surface and the likelihood of thrombus formation which is the aggregation of proteins and platelets on a surface that results in the formation of a blood clot [7,10]. Once a suitable environment for attachment is established bacterial species are capable of adhering to the surface and proliferating into microcolonies eventually forming biofilms. Biofilms found on blood contacting devices often include a large portion of host clotting proteins and immune cells intended to isolate the infection and prevent the formation of sepsis [10,11].

Biocompatibility of materials is a defining condition for the use of any synthetic material for a biological application. However, the term biocompatibility is a bit ambiguous and is most commonly used in reference to the toxicity associated with the material and the likelihood of an adverse effect resulting from use of the material. In consideration of the current limitations of existing implantable devices with regards to their susceptibility towards biofouling, current medical device technology does not represent a truly biocompatible system. Instead the design materials therefore must go beyond function by also considering the feasibility of the device intergrating with the host environment by countering the negative effects associated with surface biofouling [12] and ultimately facilitate the restoration of physiological function.

Maintaining medical devices in a homeostatic environment with the biological interface is key for their sustained usage. The design of next generation biomedical devices is aimed at preventing surface fouling through passive and active approaches by the manipulation of physical and chemical surface properties to create anti-adhesive materials based on their ability to prevent the adhesion of noxious biomolecules (Figure2a-c) or antimicrobial by denaturing infectious microbes and subsequently restricting the proliferation of biofilms (Figure 2d-e). [13-21] While each approach is effective for the intended application the combined activity of anti-adhesive and antimicrobial functionalities into a single material would ultimately enhance the antifouling properties of medical devices [22,23] and with careful tuning may even facilitate the materials integration with the host environment.

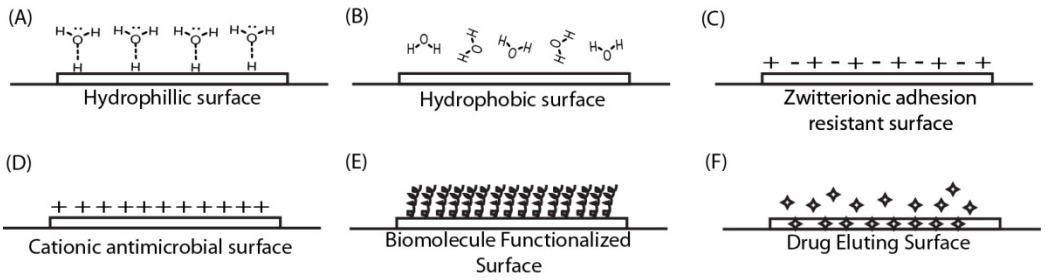

Figure 2. Strategies in device design for antifouling polymeric surfaces a) anti-adhesive hydrophilic materials b)anti-adhesive hydrophobic materials c) anti-adhesive zwitterionic surface functionalization d) antimicrobial cationic surfaces e) antimicrobial or anti-adhesive biomolecule coated surfaces f) therapeutic drug eluting surfaces

Development of Bioinspired Materials. The foreign body response is associated with the most adverse fouling effects, as result the functionalization of material surfaces with biomolecules is an advantageous approach for cloaking implanted medical devices. The controlled deposition of biomolecules on the surface of the device can create a physical and chemical barrier between fouling agents and the device surface without impairing the functionality of the device.[24] Deposition of surfaces with biomolecules such as peptides offers the advantage of being inherently biocompatible and the associated cationic charge imparts antimicrobial activity. [25-28] The use of antimicrobial peptides peptides is effective against a broad range of microbes including pathogenic bacterial strains of *Pseudomonas aeruginosa, Staphylococcus aureus, Streptococcus gordonii, Fusobacterium nucleatum* and *Porphyromonas gingivalis.* [25] However, the antimicrobial activity of biomolecule peptides is closely associated with the identity of the peptide in use and furthermore peptide functionalization of surfaces do no prevent the deposition of fouling agents. Instead a biomolecule with multiple modes of action that can be continuously expressed on the material surface is quintessential.

The most ubiquitous of all biomolecules, nitric oxide (NO) is generated as a part of the healthy function of most nucleated cells in the human body and is responsible for cellular signaling process in the cardiovascular, immune, and nervous systems. [29-34] Biosynthesis of NO is a result of the reaction of L-

arginine with nitric oxide synthase (NOS), of which there are three: endothelial (eNOS), nervous (nNOS), and immune (iNOS). [35-37] As shown in Figure 3, the effect of NO is concentration dependent ranging from proliferative and protective effects at low concentration (1-30nM) to cytotoxic at higher concentrations (≥100nM).[38] Both eNOS and nNOS maintain a low output of NO on cellular surfaces as normal physiological function in healthy hosts and a deficiency in NO is closely associated with the formation of arterial thrombus [39-41]. However, iNOS is associated with immune responses and is the only NOS enzyme in which NO generation can be induced as result of inflammation or infection [42,43]. As such, the levels of NO generated by iNOS are high and aimed at creating cytotoxic and biocidal effects. Macrophages are the primary sources of NO generated during immune responses and the subsequent antimicrobial action of NO is thought to occur via the mutation of microbial DNA, inhibition of DNA repair and synthesis in the microbe, and neutralization by peroxynitrite [43]. As a result the development of NO releasing biomaterials offers the combined advantages of drug eluting materials with biomolecule functionalization to create a biomimetic surface.

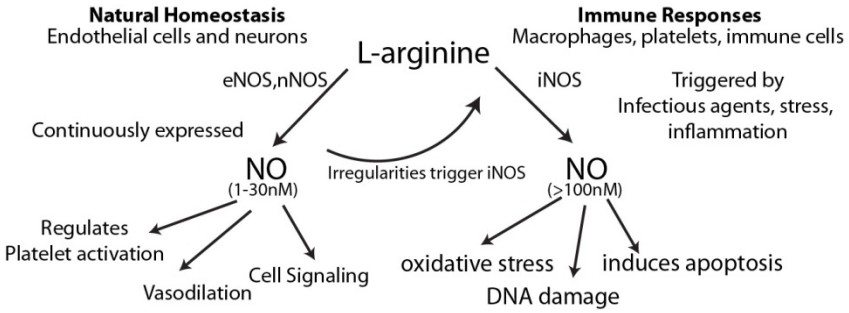

Figure 3. Role of NO in regulating a homeostatic environment and generating an immune response

Classical Design of NO Biomaterials. As a biomolecule capable of antimicrobial, thrombolytic, and proliferative effects NO releasing materials are the subject of extensive investigations for combating medical device fouling and promoting device integration with the biological environment. Rather than

relying on enzymatic pathways for NO generation, small molecule NO donors, such as diazeniumdiolates[44-47] or S-nitrosothiols[48,49] (Figure 4), can be incorporated directly into polymeric matrices of existing devices as blended materials or covalently adhered to the surface.[50] The release of NO from donor molecules is triggered in physiological conditions by pH and a temperature driven pathways for diazeniumdiolates (Figure 4a) and heat, light, and in the presence of catalytic Cu^{2+} ions for RSNOs (Figure 4b). The release of NO from the donors incorporated into biomaterials results in site localized effect where the amount of NO generated is easily tuned based on the composition of the donor molecule. The use of NO donors are advantageous for tuning the dosage of NO delivered from a material due to the variable half-lives exhibited between 1 second and 24 hours.[45,51] The incorporation of NO releasing groups into medical devices is established as effective for the prevention of thrombus and biofilm formation on [19,52-55]. However, the shortcoming of current design properties however is the limited supply of NO that can be incorporated into the polymeric matrices, which ultimately limits the materials therapeutic lifetime of use.

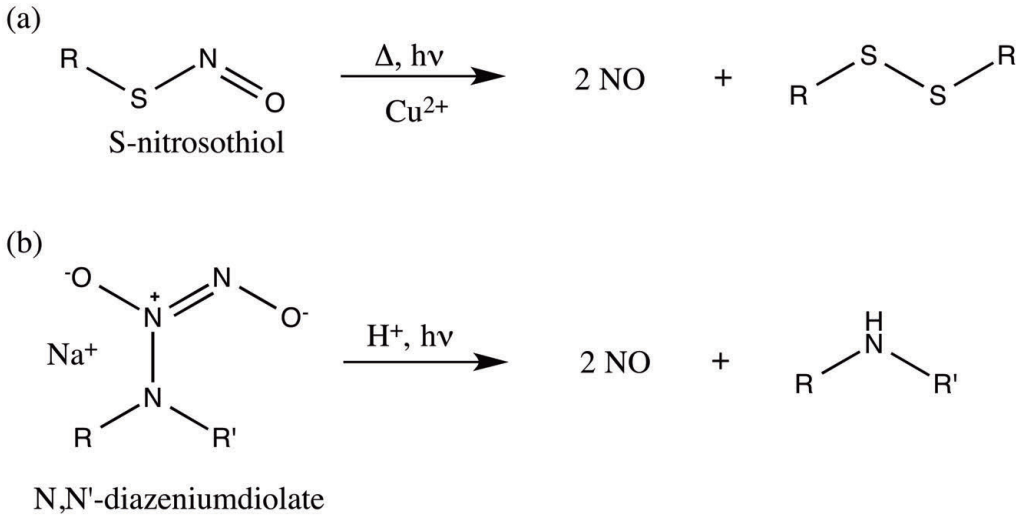

Figure 4. Small molecule NO donors and corresponding NO release pathways (a) S-nitrosothiols (RSNO) and (b) Diazeniumdiolates

Designing a Catalytic NO Material. An ideal NO material will maintain a continuous supply for the duration of the device lifetime or until the successful integration of the device within the physiological environment is achieved. Towards this end it is necessary to reimagine our approach to the development of NO materials, where rather than relying on incorporated reservoirs of NO we instead access the supplies of NO that are naturally being generated. Due to the rapid reactivity of NO ($t_{1/2}$ = <1ms) the body has devised transport mechanisms of NO through the blood stream in the form of S-nitrosothiols present as both small molecule and protein pound derivatives of the amino acid L-cysteine.[49,56] Therefore, as shown in Figure 5 the development of NO materials with long term NO release properties will capitalize on the potential for the catalytic generation of NO from endogenous RSNOs through the incorporation of Cu^{2+} catalysts within the polymeric matrix of devices.

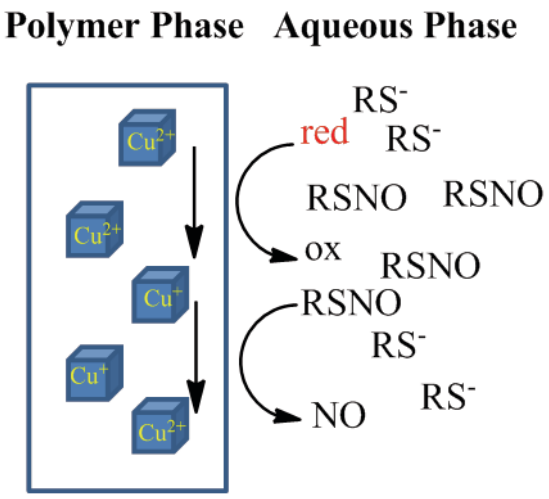

Figure 5. Incorporation of a Cu-catalyst into the matrix of a polymeric material for the sustained generation of NO from bioavailable RSNO substrates

Copper is an essential trace element found exclusively in protein bound configurations as enzymatic active sites.[57] Notably protein bound Cu^{2+} ions are capable of reacting with bioavailable RSNOs resulting in the generation of NO. Subsequently, exploration of macromolecular Cu^{2+} complexes embedded into the matrix of polymeric materials via covalent attachment to the polymeric backbone or as blended materials.[58-61] In each case the generation of NO from bioavailable RSNOs was demonstrated, however

rapid leaching of the Cu-active site was observed resulting in deactivation of the material. As such, based on the current state of research in the field of catalytic NO materials it is essential to progress towards the development of robust Cu catalyst that can withstand the physiological environment while maintaining its capacity to catalytically generate NO from endogenous RSNOs.

Porous Solid State NO Catalysts. Porous solid state materials including zeolites and metal organic frameworks (MOFs)[62-66] have drawn interest for use as NO materials due to their robust architectures and wide applicability. In particular MOFs have garnered increased interest in recent years with an excess of a 4000 publications in 2013 alone. The abundance of structurally distinct frameworks is a result of the versatile combinations of organic ligands and the metals selected for the synthesis. As such, MOFs have found applicability in a wide range of applications from gas storage to catalysis as a result of the robust 3D crystalline networks that exhibit permanent porosity with tunable pore size and the reversible adsorption of substrates.

The variable chemical and physical properties of MOFs make them promising platforms for biomedical applications due to their potential design for biodegradability, and tunability for a wide range of applications.[64,67-70] Towards this end the large pore volumes of MOFs have made them attractive candidates for use as drug delivery vehicles.[68,71] In particular the precedent for gas storage applications of MOFs has led to explorations of MOFs as NO delivery vehicles.[64,72-74] As NO materials, MOFs can be loaded with NO as a physisorbed guest or through post synthetic modification of the framework for functionalization with covalently attached diazeniumdiolate NO donors. The use of MOFs as NO materials presents the highest loading capacity of any NO material to date, however a lack of capacity for tuning NO release kinetics and the finite supply of NO within the material ultimately limits the applicability.

The exploration of MOFs as NO catalysts which rely on an endogenous sources of NO has the potential to impart long lasting delivery of NO and tunable NO generation kinetics. There are three approaches for

using MOFs as catalysts: First, active sites are located as a function of the metal ligand coordination cluster which forms the secondary building unit. Secondly, macrocyclic ligands such as porphyrin incorporated as a component of the MOF ligand subsequently bind a metal ion such as Zn, Fe, Mn, and Cu to create a bioinspired catalytic framework. Third, post synthetic modification of the MOF to incorporate catalytic species into the network either by covalently modifying the organic ligand or encapsulation of the active species within the MOF pore space. In this work I will focus on the use of the a Cu-based coordination cluster as the active site for reaction with RSNOs, described in Figure 6.

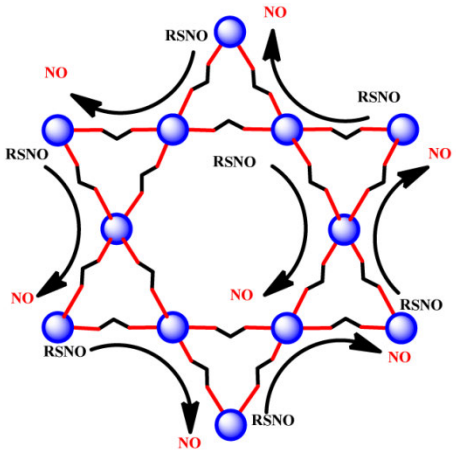

Figure 6. RSNO NO donor substrates reacting with coordinatively unsaturated Cu active sites incorporated as the framework secondary building unit.

Frameworks designed to utilize the metal coordination cluster as the active metal site must allow for the coordination of the substrate without incurring structural damage. Towards this end coordinatively unsaturated MOFs have successfully catalyzed numerous organic transformation reactions and are even successful for generating enantioselctive products.[75,76] The development of MOF-NO catalysts therefore necessitates the use of a framework with coordinatively unsaturated Cu^{2+} metal centers in order to facilitate the adsorption of RSNO species. In addition, the porosity of the framework is essential for permitting the substrates access towards the catalytic centers and has the secondary advantage of

imparting substrate selectivity into the material. Most importantly however for the sustained use of the material as a BioMOF catalyst the framework must remain robust within the physiological environment.

While extremely promising materials for an extensive range of applications, the use of MOFs as functional materials requires that the fine particles be incorporated into a secondary support. [77] Towards this end MOF composite materials have been explored in membrane science for chemical separations or sensing and even as heterogeneous catalysts. The key requirement for the preparation of MOF composite materials is after fabrication of the material it is essential that the MOF remains structurally and chemically unaffected without compromising functionality. The formation of a composite material can proceed via two routes 1) incorporating MOF particles directly into the matrix of a secondary support as a blend, or 2) chemical attachment of MOFs to the surface of substrates via *in situ* growth.[78] MOF particles dispersed throughout a polymeric matrix impart a high degree of versatility towards the types of applications that the materials can be used for due to the flexibility of the support substrate. However, the limitation with this approach is the lack of uniformity in the layer of MOF crystals. Advantageously, the direct growth of MOFs onto surfaces results in the controlled deposition of uniform MOF thin film coatings with control over the thickness of the deposited layer, orientation of the crystal face, and even patterned surface deposition.[79,80] However, the formation of MOF thin films onto substrate surfaces is primarily reported for rigid inorganic surfaces rather than flexible organic materials. This work will explore the development of MOF composite materials using both approaches.

Research Summary. The primary goal of this research is to develop catalytic NO materials which utilize bioavailable RSNO substrates to generate nonfouling implantable medical devices. A crucial step for the development of NO materials is the ability to accurately quantify NO. In this work the author explores the use of chemiluminescence based NO analysis for the accurate quantification of NO generated in cell media solutions to mimic in vitro studies and present a case study for the applicability of designing NO materials (Chapter 2). Presented next is the successful demonstration of a Cu-MOFs for the catalytic generation of NO from bioavailable RSNOs donors (Chapter 3). However the limited stability of this

proof of principle MOF in aqueous solution prompted the development of a MOF-NO catalyst that is suitable for physiological applications through tuning the organic ligands used in the construction of the framework (Chapter 4). Finally a two-fold demonstration of the feasibility towards designing composite MOF based biomaterials is presented as blended materials prepared via commercial manufacturing processes (Chapter 5) and via surface growth of MOFs on flexible polymeric substrates. This research represents a complete body of work from the development of an analytical method for evaluating the behavior of MOF NO catalysts to their ultimate incorporation into functional devices.

References

1. 10993, I. O. f. S.
2. Gilbert, P.; McBain, A. J.; Rickard, A. H.; Schooling, S. R. In *Medical Biofilms*; John Wiley & Sons, Ltd: 2003, p 73.
3. Banerjee, I.; Pangule, R. C.; Kane, R. S. *Advanced Materials* **2011**, *23*, 690.
4. Harding, J. L.; Reynolds, M. M. *Trends in Biotechnology* **2014**, *32*, 140.
5. Jiang, S. Y.; Cao, Z. Q. *Advanced Materials* **2010**, *22*, 920.
6. Donlan, R. M. In *Medical Biofilms*; John Wiley & Sons, Ltd: 2003, p 29.
7. Jass, J.; Surman, S.; Walker, J. T. In *Medical Biofilms*; John Wiley & Sons, Ltd: 2003, p 1.
8. Costerton, J. W.; Stewart, P. S.; Greenberg, E. P. *Science* **1999**, *284*, 1318.
9. Wai, S. N.; Mizunoe, Y.; Jass, J. In *Medical Biofilms*; John Wiley & Sons, Ltd: 2003, p 97.
10. Keefer, L. K. *Nature Materials* **2003**, *2*, 357.
11. Pitt, W. G.; Park, K.; Cooper, S. L. *Journal of Colloid and Interface Science* **1986**, *111*, 343.
12. Walker, J. T.; Surman, S.; Jass, J. In *Medical Biofilms*; John Wiley & Sons, Ltd: 2003, p 255.
13. Chen, S. F.; Li, L. Y.; Zhao, C.; Zheng, J. *Polymer* **2010**, *51*, 5283.
14. Cheng, G.; Zhang, Z.; Chen, S.; Bryers, J. D.; Jiang, S. *Biomaterials* **2007**, *28*, 4192.
15. Li, X.; Yu, Q.; Zhang, Y. X.; Wu, Z. Q.; Chen, H. *Acta Polymerica Sinica* **2011**, 812.
16. Epstein, A. K.; Wong, T. S.; Belisle, R. A.; Boggs, E. M.; Aizenberg, J. *Proceedings of the National Academy of Sciences of the United States of America* **2012**, *109*, 13182.
17. Siedenbiedel, F.; Tiller, J. C. *Polymers* **2012**, *4*, 46.
18. Timofeeva, L.; Kleshcheva, N. *Applied Microbiology and Biotechnology* **2011**, *89*, 475.
19. Charville, G. W.; Hetrick, E. M.; Geer, C. B.; Schoenfisch, M. H. *Biomaterials* **2008**, *29*, 4039.
20. Grainger, D. W. *Expert Opinion on Biological Therapy* **2004**, *4*, 1029.
21. Takahashi, H.; Letourneur, D.; Grainger, D. W. *Biomacromolecules* **2007**, *8*, 3281.
22. Zou, P.; Hartleb, W.; Lienkamp, K. *Journal of Materials Chemistry* **2012**, *22*, 19579.

23. Wang, B. L.; Ren, K. F.; Wang, H.; Ji, J. *Acs Applied Materials & Interfaces* **2013**, *5*, 4136.
24. Green, J. B. D.; Fulghum, T.; Nordhaus, M. A. *Biointerphases* **2011**, *6*, MR13.
25. Costa, F.; Carvalho, I. F.; Montelaro, R. C.; Gomes, P.; Martins, M. C. L. *Acta Biomaterialia* **2011**, *7*, 1431.
26. Forbes, S.; McBain, A. J.; Felton-Smith, S.; Jowitt, T. A.; Birchenough, H. L.; Dobson, C. B. *Biomaterials* **2013**, *34*, 5453.
27. Bilek, M. M. M.; Bax, D. V.; Kondyurin, A.; Yin, Y. B.; Nosworthy, N. J.; Fisher, K.; Waterhouse, A.; Weiss, A. S.; dos Remedios, C. G.; McKenzie, D. R. *Proceedings of the National Academy of Sciences of the United States of America* **2011**, *108*, 14405.
28. Hequet, A.; Humblot, V.; Berjeaud, J. M.; Pradier, C. M. *Colloids and Surfaces B-Biointerfaces* **2011**, *84*, 301.
29. Palmer, R. M. J.; Ferrige, A. G.; Moncada, S. *Nature* **1987**, *327*, 524.
30. Ignarro, L. J. *Circulation Research* **1989**, *65*, 1.
31. Grisham, M. B.; Jourd'Heuil, D.; Wink, D. A. *The American Physiological Society* **1999**, G315.
32. Wink, D. A.; Mitchell, J. B. *Free Radical Biology and Medicine* **1998**, *25*, 434.
33. Thomas, D. D.; Flores-Santana, W.; Switzer, C. H.; Wink, D. A.; Ridnour, L. A. In *Nitric Oxide (Second Edition)*; Ignarro, L. J., Ed.; Academic Press: San Diego, 2010, p 3.
34. Bogdan, C. *Nature Immunology* **2001**, *2*, 907.
35. Palmer, R. M. J.; Ashton, D. S.; Moncada, S. *Nature* **1988**, *333*, 664.
36. Gross, S. S.; Wolin, M. S. *Annu. Rev. Physiol.* **1995**, *57*, 737.
37. Marletta, M. A. *Trends in Biochemical Sciences* **1989**, *14*, 488.
38. Carpenter, A. W.; Schoenfisch, M. H. *Chemical Society Reviews* **2012**, *41*, 3742.
39. Moncada, S.; Higgs, E. A. *British Journal of Pharmacology* **2006**, *147*, S193.
40. Loscalzo, J. *Circulation Research* **2001**, *88*, 756.
41. Ignarro, L. J.; Napoli, C.; Loscalzo, J. *Circulation Research* **2002**, *90*, 21.
42. MacMicking, J.; Xie, Q.-w.; Nathan, C. *Annual Review of Immunology* **1997**, *15*, 323.

43. Nathan, C.; Shiloh, M. U. *Proceedings of the National Academy of Sciences* **2000**, *97*, 8841.

44. Chakrapani, H.; Showalter, B. M.; Citro, M. L.; Keefer, L. K.; Saavedra, J. E. *Organic Letters* **2007**, *9*, 4551.

45. Davies, K. M.; Wink, D. A.; Saavedra, J. E.; Keefer, L. K. *Journal of the American Chemical Society* **2001**, *123*, 5473.

46. Keefer, L. K.; Flippen-Anderson, J. L.; George, C.; Shanklin, A. P.; Dunams, T. M.; Christodoulou, D.; Saavedra, J. E.; Sagan, E. S.; Bohle, D. S. *Nitric Oxide: Biology and Chemistry* **2001**, *5*, 377.

47. Smith, D. J.; Chakravarthy, D.; Pulfer, S.; Simmons, M. L.; Harabie, J. A.; Citro, M. L.; Saavedra, J. E.; Davies, K. M.; Hutsell, T., C.; Mooradian, D. L.; Hanson, S. R.; Keefer, L. K. *Journal of Medicinal Chemistry* **1999**, *39*, 1148.

48. Al-sa'doni, H. H. *Current Medicinal Chemistry* **2004**, *11*, 2679.

49. Butler, A. R.; Rhodes, P. *Analytical Biochemistry* **1997**, *249*, 1.

50. Frost, M. C.; Reynolds, M. M.; Meyerhoff, M. E. *Biomaterials* **2005**, *26*, 1685.

51. Askew, S. C.; Barnett, D. J.; McAninly, J.; Williams, D. L. H. *Journal of the Chemical Society Perkin Transaction 2* **1995**, *8*, 741.

52. Lu, Y.; Slomberg, D. L.; Sun, B.; Schoenfisch, M. H. *Small* **2013**, *9*, 2189.

53. Annich, G. M.; Meinhardt, J. P.; Mowery, K. A.; Ashton, B. A.; Merz, S. I.; Hirschl, R. B.; Meyerhoff, M. E.; Bartlett, R. H. *Critical Care Medicine* **2000**, *28*, 915.

54. Sulemankhil, I.; Ganopolsky, J. G.; Dieni, C. A.; Dan, A. F.; Jones, M. L.; Prakash, S. *Antimicrobial Agents and Chemotherapy* **2012**, *56*, 6095.

55. Mowery, K. A.; Schoenfisch, M. H.; Saavedra, J. E.; Keefer, L. K.; Meyerhoff, M. E. *Biomaterials* **2000**, *21*, 9.

56. Giustarini, D.; Milzani, A.; Colombo, R.; Dalle-Donne, I.; Rossi, R. *Clinica Chimica Acta* **2003**, *330*, 85.

57. Tapiero, H.; Townsend, D. M.; Tew, K. D. *Biomedicine & Pharmacotherapy* **2003**, *57*, 386.

58. Hwang, S.; Cha, W.; Meyerhoff, M. E. *Angew. Chem.* **2006**, *118*, 2811.

59. Hwang, S.; Meyerhoff, M. E. *Biomaterials* **2008**, *29*, 2443.

60. Oh, B. K.; Meyerhoff, M. E. *Journal of the American Chemical Society* **2003**, *125*, 9552.

61. Puiu, S. C.; Zhou, Z.; White, C. C.; Neubauer, L. J.; Zhang, Z.; Lange, L. E.; Mansfield, J. A.; Meyerhoff, M. E.; Reynolds, M. M. *Journal of Biomedical Materials Research Part B: Applied Biomaterials* **2009**, 203.

62. *Metal-organic frameworks design and application*; Wiley: Hoboken, N.J., 2010.

63. Corma, A.; García, H.; Llabrés i Xamena, F. X. *Chemical Reviews* **2010**, *110*, 4606.

64. Hinks, N. J.; Mckinlay, A. C.; Xiao, B.; Wheatley, P. S.; Morris, R. E. *Microporous and Mesoporous Materials* **2010**, *129*, 330.

65. Horcajada, P.; Gref, R.; Baati, T.; Allan, P. K.; Maurin, G.; Couvreur, P.; Ferey, G.; Morris, R. E.; Serre, C. *Chemical Reviews* **2012**, *112*, 1232.

66. Janiak, C. *Dalton Transactions* **2003**, 2781.

67. Barron, P. M.; Wray, C. A.; Hu, C. H.; Guo, Z. Y.; Choe, W. *Inorganic Chemistry* **2010**, *49*, 10217.

68. Della Rocca, J.; Liu, D. M.; Lin, W. B. *Accounts of Chemical Research* **2011**, *44*, 957.

69. Horcajada, P.; Gref, R.; Baati, T.; Allan, P. K.; Maurin, G.; Couvreur, P.; Férey, G.; Morris, R. E.; Serre, C. *Chemical Reviews* **2011**, *112*, 1232.

70. McKinlay, A. C.; Morris, R. E.; Horcajada, P.; Ferey, G.; Gref, R.; Couvreur, P.; Serre, C. *Angewandte Chemie-International Edition* **2010**, *49*, 6260.

71. Horcajada, P.; Serre, C.; Maurin, G.; Ramsahye, N. A.; Balas, F.; Vallet-Regi, M.; Sebban, M.; Taulelle, F.; Ferey, G. *Journal of the American Chemical Society* **2008**, *130*, 6774.

72. McKinlay, A. C.; Xiao, B.; Wragg, D. S.; Wheatley, P. S.; Megson, I. L.; Morris, R. E. *Journal of the American Chemical Society* **2008**, *130*, 10440.

73. Miller, S. R.; Alvarez, E.; Fradcourt, L.; Devic, T.; Wuttke, S.; Wheatley, P. S.; Steunou, N.; Bonhomme, C.; Gervais, C.; Laurencin, D.; Morris, R. E.; Vimont, A.; Daturi, M.; Horcajada, P.; Serre, C. *Chemical Communications* **2013**, *49*, 7773.
74. Xiao, B.; Wheatley, P. S.; Zhao, X.; Fletcher, A. J.; Fox, s.; Rossi, A. G.; Megson, I. L.; Bordiga, S.; Regli, L.; Thomas, K. M.; Morris, R. *Journal of the American Chemical Society* **2007**, *129*, 1203.
75. Alaerts, L.; Seguin, E.; Poelman, H.; Thibault-Starzyk, F.; Jacobs, P. A.; De Vos, D. E. *Chemistry European Journal* **2006**, *12*, 7353.
76. Wu, C.-D.; Hu, A.; Zhang, L.; Lin, W. *Journal of the American Chemical Society* **2005**, *127*, 8940.
77. Adams, R.; Carson, C.; Ward, J.; Tannenbaum, R.; Koros, W. *Microporous and Mesoporous Materials* **2010**, *131*, 13.
78. Betard, A.; Fischer, R. A. *Chemical Reviews* **2012**, *112*, 1055.
79. Centrone, A.; Yang, Y.; Speakman, S.; Bromberg, L.; Rutledge, G. C.; Hatton, T. A. *Journal of the American Chemical Society* **2010**, *132*, 15687.
80. Shekhah, O.; Wang, H.; Kowarik, S.; Schreiber, F.; Paulus, M.; Tolan, M.; Sternemann, C.; Evers, F.; Zacher, D.; Fischer, R. A.; Woll, C. *Journal of the American Chemical Society* **2007**, *129*, 15118.

Chapter 2

Accurate Measurement of NO Bioavailability Released from Donors Under *in vitro* Conditions[1]

Synopsis

Nitric oxide (NO) is an essential messenger in human physiology, mediating cellular processes ranging from proliferation to apoptosis.[1-5] The effects of NO are concentration dependent and control over the instantaneous amount of NO available to cells is essential for determining the therapeutic NO dosages for various applications. As such, the development of NO therapeutic materials relies on accurate quantitative NO measurements that provide both total NO release from the NO donor as well as instantaneous NO concentrations.[6] Based on the complexity of the cell media environment, inaccurate NO reporting often occurs for *in vitro* studies.[7] These inaccuracies result from using inert media such as phosphate buffer saline (PBS), failing to account for the reactivity of media components. In this work, we describe a method for directly quantifying the instantaneous and total amounts of NO from commonly used NO donors in commercially available cell media routinely used for endothelial and neural cell lines. A riboflavin-tryptophan complex found in the media was identified as the major scavenger of NO in the cell media and likely reacts with NO via a radical-radical reaction. This finding significantly impacts the amount of available NO. The scavenging effects are concentration dependent on the riboflavin-tryptophan complex and the NO release rate from the NO donor. The results of this study provide insights

[1] *The work presented herein is published in the journal Analytical Chemistry with Melissa M. Reynolds as a joint author and is used with permission. The body of work presented here was assembled by this author.* *Anal. Chem. 2014, 86, 2025.*

on the exogenous amounts of NO that are present in cell media and may provide an explanation for differences in NO dosages between buffer experiments and *in vitro* and *in vivo* studies.

Introduction

The history of nitric oxide as a therapeutic can be traced back over one hundred years in the form of physicians prescribing nitroglycerin for treating angina.[8,9] Yet it wasn't until the discovery of NO as the endothelial relaxation factor responsible for vasodilation of blood vessels that the therapeutic potential of NO was realized.[10,11] Since a scientific explosion towards understanding the physiological role of NO has taken place and revealed that the effects are ubiquitous, although highly concentration dependent (see chapter 1). Towards this end the utility of NO therapeutic materials has been investigated for applications spanning the spectrum between regeneration of healthy tissues and as chemotherapeutics.[1,12-16] However, the practical application of therapeutic NO materials requires careful dosage tuning in order to illicit a desired response.

While the importance of NO is recognized there is much debate regarding the feasibility and utility of use. One such example is the effects of NO towards stimulating the angiogenic growth of blood vessels. As previously mentioned NO plays a critical role as the endothelial relaxation factor and it is hypothesized that it is also responsible for stimulating angiogenic growth, however there is much debate in the literature regarding its ultimate effectiveness.[17-20] From these reports it is clear that while in some instances the effects of NO are advantageous in other cases there is no clear effect. Prior to concluding whether or not angiogenic growth can be facilitated by NO it is crucial to evaluate the variability of NO materials that are used including the type of NO material, the concentration of the donor, and also the type of media used for these experiments must be taken into consideration. As a result of isolating the different types factors used we can thereby determine the therapeutic range of NO required for angiogenic growth that is dependent only on the proper dosage of NO needed to illicit the response.

The determination of accurate NO dosage to achieve a desired cellular response is imperative towards the effective use of NO materials. While the variable NO release rates from donors is an obvious factor when it comes to selecting an appropriate material, the influence of the reaction medium is often overlooked.[6,7] Often times experiments aimed at determining the instantaneous amount of NO released from the materials and evaluation of subsequent cellular responses are performed as an independent experiment where NO release measurements are carried out in inert buffer solutions compared to the complex biological mediums that are used for in vitro studies.

In order to accurately measure the amount of NO that is available to elicit a cellular response, an effective method for evaluating the total NO released from NO donors under *in vitro* conditions is highly desirable. Cell and tissue culture media are composed of 3 primary additive groups: amino acids, inorganic salts, and vitamins. Formulations vary based upon manufacturer, media type, and the addition of supplemental serum. The complexity of cell media solutions combined with the reactive nature of NO provides ample opportunity for the presence of scavengers to reduce the amount of available NO. As such, the identification of potential scavenging agents present in the cell media solution that can potentially interfere with the availability of NO from donors is essential towards understanding concentration mediated effects of NO in cells through *in vitro* studies.

Common spectroscopic and electrochemical methods for the direct and indirect measurement of NO include the Griess assay,[21,22] electrochemical sensors,[23] and chemiluminescence detectors.[24] Recently, the Schoenfisch group surveyed the use of these commonly used methods for their ability to quantitatively measure NO in a range of media types.[7] This work demonstrated significant differences in the amount of NO measured using each technique, where chemiluminescence was the only method that provided accurate quantification of total NO based upon the theoretical payload of the sample. The ability to measure the NO payload from NO-releasing materials is highly valuable for determining the total amount of NO that is available to target sites. Traditionally, the release of NO from materials is evaluated in phosphate buffered saline (PBS) held at physiological pH (7.4) and temperature (37 °C). Substitution of

the sampling medium from PBS to a biologically-relevant media, such as saliva, urine, and cell growth media, results in significant variations in the amount of detected NO.[7]

In this work a chemiluminescence based sampling method for quantifying the NO release from two classes of common NO donors, *N*-diazeniumdiolates and *S*-nitrosothiols, in carbonate buffered media routinely used for endothelial and neural cell lines is presented. While cell culture experiments require aerobic conditions, chemiluminescence measurements of NO are conducted in an anaerobic environment in order to determine the NO scavenging effects of cellular media solutions without interference associated with the rapid reactivity of NO with O_2. The NO scavenging effects of each media type are determined by a direct comparison of the measured amount of NO in inert buffer solution. The extent of scavenging was found to be variable based on the cell media used and the half-life of NO generation from each donor. Upon closer inspection of the subtle differences in media composition it was determined that the vitamin additive riboflavin is the principal scavenging agent in a concentration dependent manner. These findings are significant for the accurate quantification and reporting of bioavailable NO generated from NO materials used under *in vitro* conditions.

Experimental Methods

Materials. All reagents were obtained from commercial vendors and used without further purification: *N,N'*-dimethyl-1,6-diaminohexane (TCI America), L-cysteine, (98%, Alfa Aesar), spermine, (97%, Alfa Aesar), *t*-butyl nitrite, (90%, Aldrich), riboflavin, (98%, Alfa Aesar), L-tryptophan, (99%, Alfa Aesar), L-tyrosine (97%, Aldrich), sodium hydroxide (Fisher Scientific), cupric chloride dihydrate (99%, Fisher Scientific), phosphate buffered saline tablets (EMD), and acetonitrile (EMD). Cell media solutions of MCDB 131, without glutamine (EC media) and neurobasal A (NB media) were obtained from Invitrogen and used without further modification. Compressed gasses were obtained from commercial vendors of nitrogen, 99.999%, oxygen, argon, 5% carbon dioxide balanced with nitrogen were supplied by Airgas and nitric oxide from Matheson.

*Preparation of NO donors***.** 1) Diazeniumdiolates were prepared in accordance with previously published procedures.[26] In brief, to a specialized pressure vessel, 500 mg of the parent amine, *N*,*N'*-dimethyl-1,6-diaminohexane for MAHMA/NO or spermine for SPER/NO, was added to 40 mL of acetonitrile equipped with a stir bar. The vessel was sealed and attached to a specialized NO reactor. The vessel was purged with argon gas to remove any oxygen, followed by the introduction of 80 psi of NO. The amine was reacted with NO under pressurized conditions for 24 h, after which time the diazeniumdiolate formed as a white precipitate. The product was filtered, washed with acetonitrile (3 x 30 mL), and dried under vacuum to remove residual solvents. The diazeniumdiolates were evaluated for purity by UV-vis spectroscopy based on the characteristic absorbance feature at 252 nm. More specifically, each donor was prepared at 0.1 mM in sodium hydroxide (0.1 mM) and quantified according to the absorbance value at 252 nm (ε=7300 M^{-1} cm^{-1} for MAHMA/NO and ε=8500 M^{-1} cm^{-1} for SPER/NO.) The prepared NO donors were stored in the freezer. *2) S-nitrosothiols: S*-nitrosocysteine (CysNO) was prepared by adding 6 x 10^{-5} mol *t*-butyl nitrite to an ice cold solution of 0.05 M L-cysteine in 1 mL of DI water. The reaction was stirred in an ice bath for twenty minutes until the solution was a transparent, dark red. The resulting concentration of CysNO was determined by UV-vis spectroscopy via an absorption feature at 545 nm (ε=15 M^{-1} cm^{-1}).

Quantification of NO. Nitric oxide was quantified using a GE chemiluminscence-based nitric oxide analyzer (NOA). In brief, 15 mL of sampling solution (PBS or cell media) was added to a customized NOA sampling vessel fitted with a pH probe. The headspace of the reaction vessel was sampled continuously at a rate of 200 mL min^{-1}. A nitrogen flow gas was introduced into the system headspace at a rate of 184 mL min^{-1} and simultaneously bubbled into the solution at 16 mL min^{-1}. In experiments using cell growth media, the bubbling gas was substituted for a 5% CO_2, 95% N_2 in order to maintain a pH of 7.4. The injection port was capped and a micro-sized pH probe connected to a pH meter (Fisher 50x series) was inserted into the side-port. The NOA was calibrated with 0 and 45 ppm NO standards. The pH meter was calibrated at pH 4, 7 and 10. In all experiments, the solution temperature was maintained at

37 °C using a circulating water bath. Aliquots of the NO donor solutions were introduced into the sample injection port using a glass Hamilton syringe to give an initial solution concentration of 1 x 10^{-6} M. The resulting NO release was recorded in 1 s intervals. NO release for CysNO is initiated by a copper catalyst. As such catalytic amounts of Cu^{2+} ions (5 mol% Cu^{2+} compared to CysNO) was added to the reaction solution from a 1 x 10^{-6} M stock solution of $CuCl_2$. The theoretical amount of total NO was determined based on the initial concentration of NO donor added to the system. The concentration of the stock NO donor solution was determined by UV-vis, as described above.

NO Scavenging Experiments based on cell media. Riboflavin and tryptophan were examined as components of the cell media with the potential to act as NO scavengers. Stock solutions of 1 mM tryptophan and 0.1 mM riboflavin were prepared in Millipore purified water (18 MΩ resistance). In order to mimic the EC and NB media conditions, riboflavin and tryptophan were added to PBS (15 mL) at concentrations corresponding to those found in the commercially available cell media solutions. The concentration of riboflavin differed by two orders of magnitude between EC and NB media and was 0.01 μM and 1.06 μM, respectively. The media concentration of tryptophan in EC and NB media was 20.1μM and 78.4 μ M, respectively. A complete list of additives for each media type is provided in the supporting information (see Table S1). MAHMA/NO was added at an initial concentration of 1μM to the riboflavin/tryptophan PBS solutions. The scavenging efficiency of the additives was determined based on the quantified NO with each additive evaluated individually as well as in combination. Each experiment was performed at n > 3 with the averages and standard deviations reported.

Scavenging agent ratio effects. In the first set of experiments the ratio of riboflavin was varied with respect to reducing agents, tryptophan or tyrosine. Stock solutions of 0.1 mM MAHMA/NO, 0.1 mM riboflavin, 10 mM tryptophan, and 0.1mM tyrosine were prepared in DI water. Experiments were performed in PBS at pH=7.4. In each experiment the concentrations of MAHMA/NO and riboflavin were maintained at a 1:1 ration at 0.001 mM. Tryptophan or tyrosine were added to the reaction between 1 and 1000 equilavents compared to riboflavin. Due to solubility limitations for tyrosine when the ratio was

1:1000 with riboflavin the concentration of riboflavin anf MAHMA_NO were reduced to 0.1 μM and tyrosine was kept at the stock concentration of 0.1mM prepared directly in PBS. In experiments where the effects of riboflavin versus the concentration of NO were evaluated by maintaining a fixed concentration of riboflavin (1 μM) and tryptophan (100 μM). The concentration of the MAHAM/NO as the NO donor was then varied between 0.1 μM and 10 μM. The resulting NO was quantified by chemiluminescence. The amount scavenged NO was calculated by subtracting the theoretical yield of NO from the actual yield. Each experiment was performed in triplicate.

Statistical Analysis. Statistical t-tests were performed on each data set to determine statistical differences at the 95% confidence interval.

Results and Discussion

Sample Chamber Design. Nitric oxide release from NO donors was evaluated in PBS or cell media solutions using chemiluminescence based detection. Traditionally, nitrogen is used as an inert carrier gas for chemiluminescence measurements where it is introduced into the headspace of the vessel and bubbled directly into the solution (see Figure 1). In the case of cell media solutions, a 5% CO_2 / 95% nitrogen carrier gas is employed in order to maintain the solution pH in the range of typical cell culture protocols, and to mimic the percentage of CO_2 in the blood stream. In order to ascertain that the solution pH is maintained in the appropriate range, the sampling setup was fitted with a pH probe for continuous monitoring. The initial pH of the media was 7.65; after 10 min of CO_2/N_2 bubbling into the solution, the pH reached 7.4 and was maintained for the duration of the experiment.

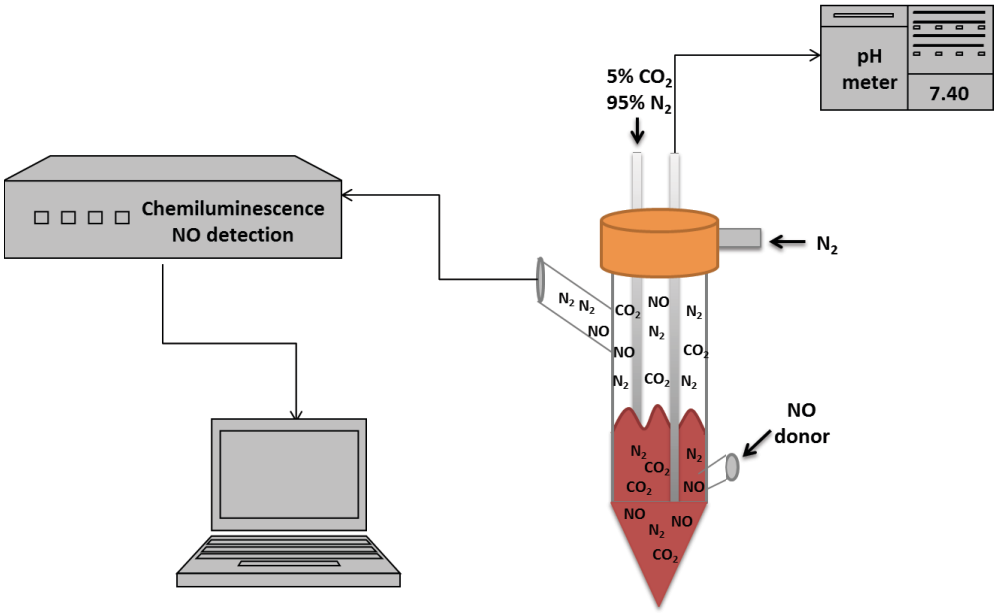

Figure 1. Measurement setup for the real-time quantification of NO released in media solutions with simultaneous monitoring of pH.

Prior to this work, real-time accurate quantification of NO generated in biological media using chemiluminescence has been difficult due to the ability to maintain the pH of the carbonate buffer in the physiological range. Maintaining a constant pH of 7.4 is important for two reasons: first, cell studies are performed at a constant pH of 7.4 which imitate body conditions, and with deviations of $\pm$ 0.15 units causes cell death,[25] and second, both *N*-diazeniumdiolates and *S*-nitrosothiol NO donors are well known to have pH dependent decomposition mechanisms.[26] By measuring the pH over the course of the reaction, we ensure that any observed differences in NO release across various media is a direct result of the medium and not changes in the reaction environment. Since CO_2 does not react with NO under these conditions, substitution of CO_2 for part of the nitrogen carrier gas allows the buffer capacity to be maintained without disrupting the gas flow that is required to maintain accurate kinetics measurements. In the absence of CO_2 gas, the pH of the media increased to 9.7, which is unsuitable for biological applications; whereas, when CO_2 is added at a rate of 16mL min^{-1}, the pH of the solution is maintained at pH 7.4.

NO Quantification from NO Donors in Biological Media. The generation of NO from *N*-diazeniumdiolates and *S*-nitrosothiol donors in various *in vitro* conditions was investigated by considering PBS, endothelial cell medium (EC medium) and neurobasal cell medium (NB medium). The NO donors selected for this study are the *N*-diazeniumdiolates MAHMA/NO and SPER/NO and the S-nitrosothiol CysNO, shown in Figure 2. As a basis for comparison, we first determined the total payload of each donor using standard measurement method in PBS. The amount of NO recovered from each donor in the various cell media solutions was then compared to the total recovered in PBS (Figure 3). In EC medium, the total amount of NO measured from the decomposition of either MAHMA/NO or CysNO was not statistically different at the 95% confidence interval compared to measurements in PBS. However, substitution of the NO donor for SPER/NO in EC medium resulted in a statistically significant difference compared to PBS, with a 30% decrease in the amount of measured NO. Experiments performed with NB medium resulted in a 60% decrease in NO recovery compared to PBS for MAHMA/NO and CysNO, while SPER/NO in NB medium resulted in complete suppression of the measureable NO.

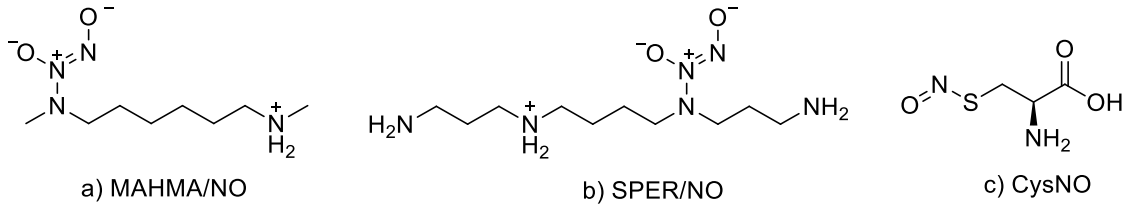

Figure 2. The NO donor investigated included the *N*-diazeniumdiolate donors a) MAHMA/NO b) SPER/NO and the *S*-nitrosothiol donor c) CysNO.

The generation of NO from the investigated donors is contingent on environmental conditions, including temperature and pH. The decrease in the total NO release over the course of the experiment observed in the cell media could be attributed to either incomplete decomposition of the NO moiety or rapid scavenging by media components. The pH of the medium environment significantly influences the stability of the NO donor, ultimately leading to variability in the rate of NO release that can contribute to

discrepancies in the amount of recorded NO. In order to ascertain if the observed discrepancies in NO recoveries across the different media types is due to fluctuations in pH, we continuously monitored the solution pH for the entire duration of the measurement for each media type and donor (Table 1). In each case, the reaction pH was consistent and maintained in the physiological range, indicating that there are not differences in the NO recoveries due to pH changes over the course of the NO releasing period. Additional evidence to support that the medium environment does not impact the release of NO from each donor is provided by the NO release half-lives shown in Table 1. Half-lives are based on the total amount of NO recovered from each experiment and reported as the time when half of the NO was measured. For each NO donor, the half-life of NO generation, regardless of the total amount recovered from the cell media solutions, remained consistent with the half-life observed for PBS, which indicates that, of the total amount of NO that is released, the kinetics of the NO release does not change, only the amount of NO changes in a given period of time. On the basis of these results, we can conclude that the decrease in measured NO is a direct result of NO scavenging by media components rather than stabilization of the NO donor moiety. In order to properly report the necessary dosage of NO for stimulating a cellular response, it is essential to determine which components of the cell media are responsible for the scavenging of NO in each individual media.

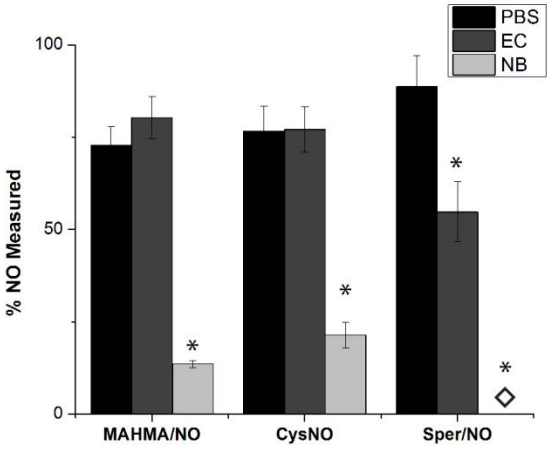

Figure 3. Comparison of the cell media solutions to PBS based upon the total amount of NO recovered from each NO donor. The * denotes a significant difference at the 95% confidence interval compared to PBS within each NO donor data set.

Table 1. Summary of solution pH and reaction half-life for each donor and medium combination. Half-life standard deviations (n=3) are reported at the 95% confidence interval.

NO donor	Media	$t_{1/2}$ (min)	pH
MAHMA/NO	PBS	1.3 ± 0.5	7.37 ± 0.02
MAHMA/NO	EC	1.2 ± 0.4	7.39 ± 0.01
MAHMA/NO	NB	1.9 ± 0.7	7.38 ± 0.02
CysNO	PBS	6.5 ± 0.8	7.37 ± 0.01
CysNO	EC	6.7 ± 0.6	7.38 ± 0.02
CysNO	NB	7.6 ± 0.8	7.39 ± 0.03
SPER/NO	PBS	32.8 ± 4	7.38 ± 0.02
SPER/NO	EC	30.8 ± 2	7.39 ± 0.03
SPER/NO	NB	n/a	7.38 ± 0.02

Effect of Media Additives. The significant difference in NO recovery amounts between EC medium and NB medium for each of the NO donors examined suggests that media additives play a crucial role in the availability of NO. It is important to note that the scavenging experiments were performed without the addition of supplemental serum that is regularly used in cell culture experiments. Constituents of serum often include growth factors, proteins, hormones, and vitamins that could potentially increase NO scavenging. In this work the primary concern is the identification of NO scavenging agents found as additives in cell media solutions. In Appendix A a complete list of the media components for EC and NB media as provided by the manufacturer. Comparison of the additive lists indicated that the concentration of riboflavin (vitamin B2) in NB media (1.06×10^{-3} M) exceeded that of the EC media (1.01×10^{-5} M) by two orders of magnitude and exceeded the initial concentration of NO donor (1×10^{-6} M) for both media

types. As an essential nutrient in promoting cellular growth, riboflavin is a common additive in cellular media; however, the concentration is varied based on cellular needs. Riboflavin and has been cited previously as an NO scavenging agent in the presence of oxygen by facilitating the generation of superoxide, resulting in the generation of peroxynitrite upon reaction with NO.[45] By studying the effect of riboflavin as an NO scavenger under conditions found for cell media used for *in vitro* studies, we were able to highlight an alternative pathway for NO scavenging by riboflavin.

As a member of the flavin family of compounds, riboflavin is able to undergo 1 and 2 electron reductions to form the radical semiquinone or hydroquinone species in the presence of a proper oxidant, see Figure 4.[27] Tryptophan, an essential amino acid added to cell media solutions, has been noted as early as the 1950s as an oxidant for the reduction of riboflavin to the reactive radical semiquinone.[28] As a radical species, NO is especially susceptible to the reaction with the radical semiquinone species in the form of a radical-radical reaction. In order to evaluate the hypothesis that the riboflavin-tryptophan complex is an active NO scavenging agent in cell media solutions, we simulated the concentrations of both riboflavin and tryptophan from each of the cell media types using PBS as our reaction medium.

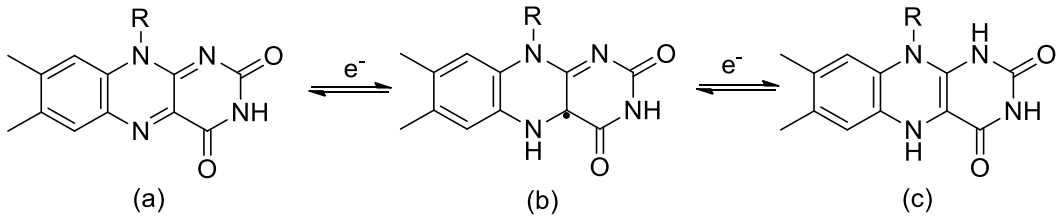

Figure 4. The various oxidation states of the flavin family: flavin undergoes a two electron reduction from a) quinone to b) radical semiquinone, and c) hydroquinone.

In Figure 5, the NO scavenging efficiency of riboflavin and tryptophan, used independently and in combination, is compared to results in PBS and the respective medium types using MAHMA/NO and SPER/NO as the source of NO. For experiments designed to mimic the concentrations of riboflavin and tryptophan in EC media, using MAHMA/NO as the donor, the amount of NO recovered was not statistically different at the 95% confidence interval compared to either PBS or EC media (Figure 5a). However, at the elevated concentrations for each component found in NB media, the measured NO for the combined use of riboflavin and tryptophan was statistically equivalent to results observed for NB media (Figure 5b). At NB concentrations with MAHMA/NO, the scavenging efficiency of riboflavin alone was only half as efficient at scavenging NO compared with the riboflavin-tryptophan combination. Compared to PBS, the riboflavin-tryptophan complex scavenged 60% of the available NO. The sole use of tryptophan, however, did not statically alter the amount of measured NO when compared to PBS buffer.

The relatively short half-life of MAHMA/NO ($t_{½}$ = 1.3±0.5 min at 37 °C, pH 7.4,) results in the release of a bolus of NO, elevating the concentration of NO in solution at a rate that exceeds the scavenging potential of the riboflavin-tryptophan complex. To explore this effect, we have paralleled our scavenging experiments with the use of SPER/NO ($t_{½}$ = 33±4min at 37 °C, pH 7.4). When added to a solution containing both riboflavin and tryptophan under EC conditions, the total amount of measured NO is statistically equivalent to the results obtained for EC media (Figure 5c). Similarly, NO release was not observed for the riboflavin and tryptophan experiments in NB conditions (Figure 5d). Based on our results with MAHMA/NO, we expect that the use of riboflavin alone will have a pronounced effect on the amount of NO recovered at both the EC and NB media concentrations using SPER/NO as the donor. Under NB type conditions, NO release was not measureable whereas under EC conditions, the amount of NO recovered was not statistically different from results obtained for the PBS control. In concurrence with results from MAHMA/NO, the sole use of tryptophan did not result in a statistical difference in measured NO compared to PBS for either EC or NB conditions using SPER/NO as the NO donor.

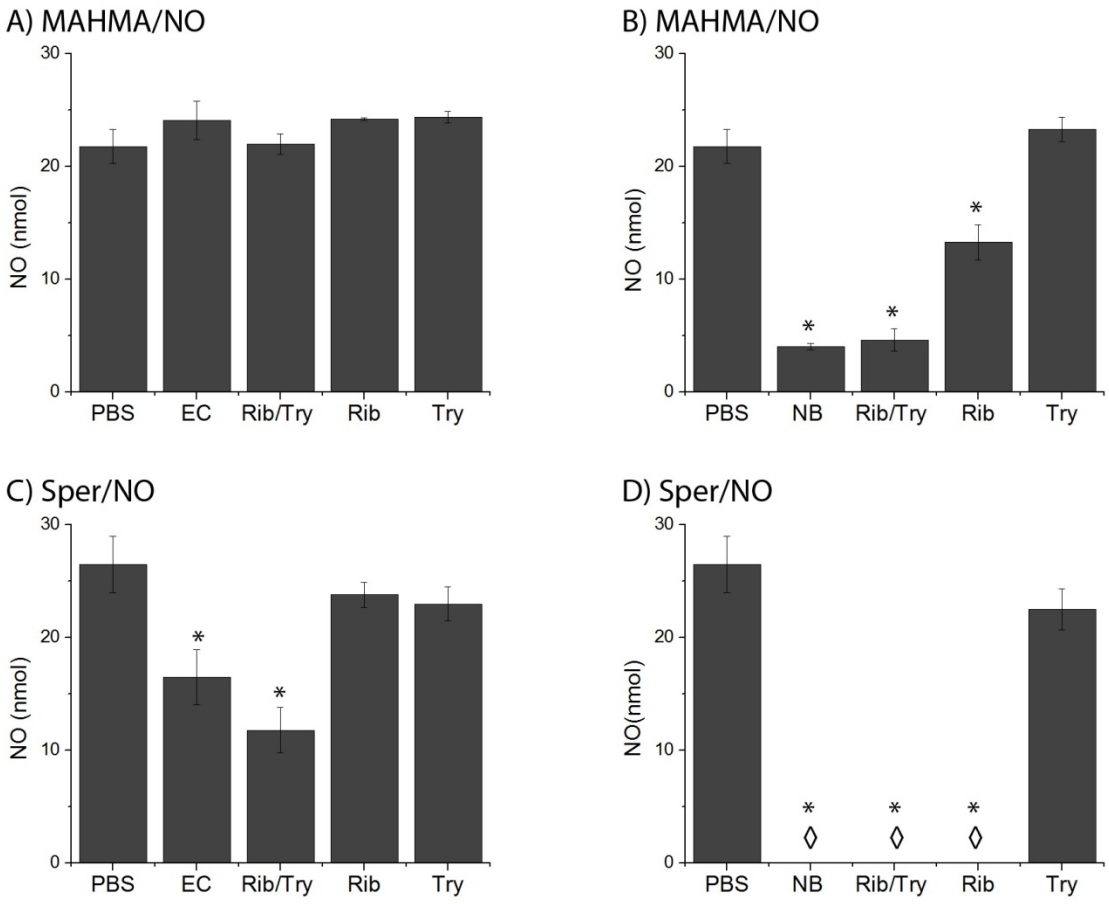

Figure 5. Comparison of NO release in PBS solutions with riboflavin and tryptophan added at concentrations that correspond to the varying media types a) MAHMA/NO under EC media conditions, b) MAHMA/NO under NB media conditions, c) SPER/NO under EC media conditions, d) SPER/NO under NB media conditions. Values are reported as an average ± standard deviation for n=3. Asterisks denote statistical differences compared to PBS at the 95% confidence interval.

Effect of scavenging agent ratios. The cell media solutions used in this work differ in riboflavin concentration by two orders of magnitude and drastic difference in NO scavenging were observed. Furthermore, the ratio of riboflavin to tryptophan varied significantly at 1:100 and 1:1000 for NB and EC media, respectively. As a result, in order to evaluate the role of riboflavin and tryptophan concentrations with respect to NO scavenging, the relationship between riboflavin and tryptophan must be considered

along with the ratio of NO to available riboflavin. This will in turn be useful for predicting the extent of scavenging in media types not addressed in this work by providing a general understanding of the role of riboflavin and tryptophan as NO scavengers.

Riboflavin is identified as the reagent primarily responsible for NO scavenging, whereas tryptophan alone has no effect as shown in Figure 5b; however, the addition of tryptophan to a solution containing riboflavin notably enhances the incidence of scavenging. The scavenging efficiency of riboflavin is attributed to the abundance of reduced riboflavin in the solution. Therefore, by increasing the ratio of tryptophan in solution there is an increase in the amount of the semiquinone scavenging species in solution. To examine the optimal ratio of tryptophan:riboflavin needed to maximize scavenging, we varied the ratio between zero and one thousand equivalents of tryptophan to riboflavin, shown in Figure 6. In each of these experiments, the ratio of riboflavin to NO remained constant. In the absence of tryptophan, riboflavin scavenges approximately 40% of the available NO in the system. The addition of a single equivalent of tryptophan to the solution does not enhance the scavenging efficiency compared to riboflavin alone. As the ratio of tryptophan is further increased to 10, 100, and 1000 equivalents there is a notable increase in the NO scavenging. The most efficient riboflavin : tryptophan ratio was noted to be 1:100, scavenging 70% of the NO generated. Further increasing the amount of tryptophan to a 1000 fold excess did not enhance the efficiency of scavenging; instead a slightly diminished efficiency of NO scavenging was noted.

With the numerous additives in cell growth media, the likelihood of additional reducing agents for riboflavin is high. Of these components tyrosine, a non-essential amino acid, is known to facilitate charge transfer reactions with flavin compounds. In the cell media solutions investigated, the concentration of tyrosine is 100 μM and 4 μM in EC and NB media, respectively. Similar to experiments with tryptophan, we varied the ratio of tyrosine to riboflavin and quantified the amount of resulting NO, Figure 6. Analogous to tryptophan, there is no increase in the scavenging efficiency when tyrosine is used at a 1:1 ratio with tryptophan. The maximum scavenging efficiency of 50% with tyrosine as the reducing agent is

observed at a 10 fold excess. Further additions of tyrosine to 100 and 1000 fold excesses do not contribute to an increase in scavenging beyond the 50% observed at a 10 fold excess. In comparison to tryptophan, tyrosine is a less effective reducing agent with riboflavin when considering NO scavenging.

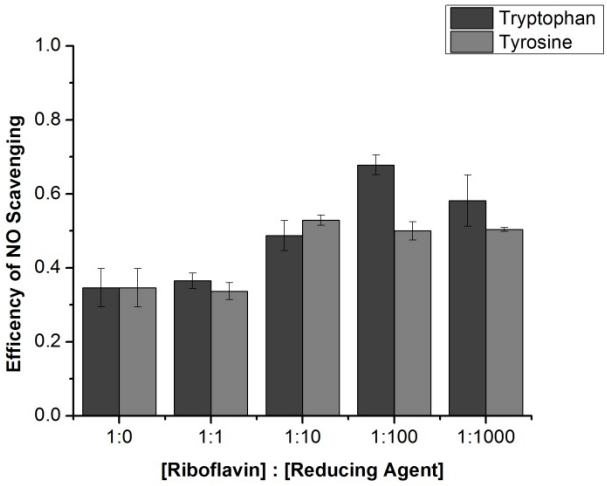

Figure 6. NO scavenging efficiency of riboflavin at variable ratios of reducing agents tryptophan or tyrosine. Values are reported based on the percentage of NO that is scavenged. Values are reported for triplicate measurements at the 95% confidence interval.

As such, the combined use of tryptophan and tyrosine increases the ratio of the reducing agent to riboflavin to over a 1000-fold excess for both media types. However, we have established that, despite the increasing presence of reducing agents, it is the riboflavin concentration that ultimately dictates scavenging. To investigate the combined effects of tyrosine and tryptophan on NO scavenging with riboflavin, we performed experiments that mimicked the conditions found for EC and NB media types. Using MAHMA/NO as the NO donor, we found that tyrosine/tryptophan experiments did not impact the observed scavenging when compared to results with cell media. As a result, it is clear that the ratio of riboflavin to reducing agents is important. Once the concentration of reducing agents exceeds the threshold of efficacy, further increasing the concentration of reducing agents does not influence the scavenging efficiency of riboflavin towards NO.

Now that we have established the role of reducing agents towards NO scavenging, we must consider the effect of the absolute concentrations of NO and riboflavin towards scavenging. In experiments using the two cell media formulations, the amount of riboflavin present in solution differed by two orders of magnitude, resulting in very little NO scavenged in EC media compared to large scavenging effects in NB media. This indicates that, in addition to the riboflavin : tryptophan ratio, the amount of riboflavin compared to NO also plays a role. To determine the effect of riboflavin concentration on the amount of NO scavenging, we varied the ratio of NO donor to riboflavin from 10:1 to 1:10 in 5 equivalent increments, shown in Figure 7. It is important to note that since we are using a diazeniumdiolate as the NO donor, each equivalent actually produces 2 equivalents of NO. In these experiments, a fixed concentration of riboflavin and tryptophan were used at the optimal ratio of 1:100.

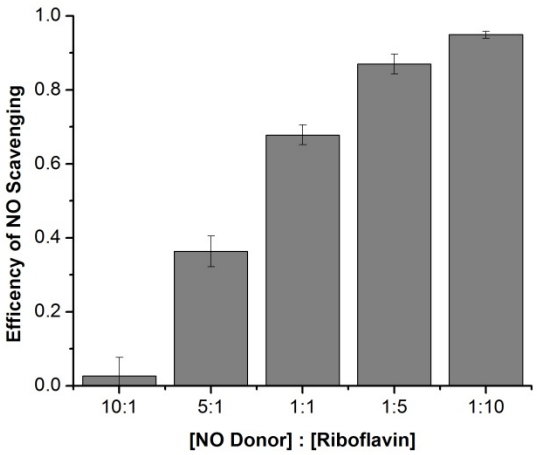

Figure 7. NO scavenging efficiency of riboflavin at variable ratios of NO donor. Values are reported based on the percentage of NO that is scavenged. Values are reported for triplicate measurements at the 95% confidence interval.

In experiments where the concentration of NO donor exceeded the amount of riboflavin 10:1, scavenging was not observed, Figure 7. As the ratio of riboflavin increased at increments of 5 equivalents, the efficiency of scavenging was enhanced with 95% of the NO scavenged when riboflavin was in 10 molar excess to the NO donor. With each successive 5 equivalent increase in the riboflavin concentration with respect to NO donor, the scavenging efficiency was increased, see Figure 7. These results indicate that for the most effective scavenging of NO is observed when the concentration of riboflavin is in excess of the NO in the system. This was especially evident when we compared the NO scavenging results between MAHMA/NO and Sper/NO in the cell media.

Conclusion

The determination of NO dosages required to elucidate a cellular response necessitates that the effects of the cell media solutions on NO availability be accounted for. In this work, a method is established for measuring the amount of available NO released from NO donors when added to cell media solutions whose pH is maintained using a carbonate buffer system. The complexity of the media solutions offers a rich environment for the reaction of NO with various components. Variations in the riboflavin content of the cell media was found to result in scavenging of NO. The efficiency of NO scavenging by riboflavin was deduced to be dependent on the absolute concentration of riboflavin with respect to the concentration of NO. In addition, riboflavin scavenging efficiency was found to be dependent on the presence of reducing agents, including tryptophan and tyrosine, in an excess of at least 100 fold to achieve maximum scavenging efficiency.

References

1. Bogdan, C. *Nature Immunology* **2001**, *2*, 907.
2. Carpenter, A. W.; Schoenfisch, M. H. *Chemical Society Reviews* **2012**, *41*, 3742.
3. Giustarini, D.; Milzani, A.; Colombo, R.; Dalle-Donne, I.; Rossi, R. *Clinica Chimica Acta* **2003**, *330*, 85.
4. Gross, S. S.; Wolin, M. S. *Annu. Rev. Physiol.* **1995**, *57*, 737.
5. Lowenstein, C. J.; Dinerman, J. L.; Snyder, S. H. *Ann. Intern. Med.* **1994**, *120*, 227.
6. Coneski, P. N.; Schoenfisch, M. H. *Chemical Society Reviews* **2012**, *41*, 3753.
7. Hunter, R. A.; Storm, W. L.; Coneski, P. N.; Schoenfisch, M. H. *Analytical Chemistry* **2013**, *85*, 1957.
8. Ignarro, L. J.; Lippton, H.; Edwards, J. C.; Baricos, W. H.; Hyman, A. L.; Kadowitz, P. J.; Gruetter, C. A. *Journal of Pharmacology and Experimental Therapeutics* **1981**, *218*, 739.
9. Ignarro, L. J.; Napoli, C.; Loscalzo, J. *Circulation Research* **2002**, *90*, 21.
10. Moncada, S.; Higgs, E. A. *British Journal of Pharmacology* **2006**, *147*, S193.
11. Palmer, R. M. J.; Ferrige, A. G.; Moncada, S. *Nature* **1987**, *327*, 524.
12. de Mel, A.; Murad, F.; Seifalian, A. M. *Chemical Reviews* **2011**, *111*, 5742.
13. MacMicking, J.; Xie, Q.-w.; Nathan, C. *Annual Review of Immunology* **1997**, *15*, 323.
14. Naghavi, N.; de Mel, A.; Alavijeh, O. S.; Cousins, B. G.; Seifalian, A. M. *Small* **2013**, *9*, 22.
15. Privett, B. J.; Broadnax, A. D.; Bauman, S. J.; Riccio, D. A.; Schoenfisch, M. H. *Nitric Oxide-Biology and Chemistry* **2012**, *26*, 169.
16. Seabra, A. B.; Duran, N. *Journal of Materials Chemistry* **2010**, *20*, 1624.
17. Cooke, J. P. *Artherosclerosis Supplements* **2003**, *4*, 53.
18. Del Gaudio, C.; Baiguera, S.; Boieri, M.; Mazzanti, B.; Ribatti, D.; Bianco, A.; Macchiarini, P. *Biomaterials* **2013**, *34*, 7754.

19. Jones, M. K.; Tsugawa, K.; Tarnawski, A.; Baatar, D. *Biochemical and Biophysical Research Communication* **2004**, *318*, 520.
20. Kang, C. K.; Lim, W. H.; Kyeong, S.; Choe, W. S.; Kim, H. S.; Jun, B. H.; Lee, Y. S. *Colloids and Surfaces B-Biointerfaces* **2013**, *102*, 744.
21. Sun, J.; Zhang, X. J.; Broderick, M.; Fein, H. *Sensors* **2003**, *3*, 276.
22. Fox, J. B. *Analytical Chemistry* **1979**, *51*, 1493.
23. Privett, B. J.; Shin, J. H.; Schoenfisch, M. H. *Chemical Society Reviews* **2010**, *39*, 1925.
24. Bates, J. N. *Neuroprotocols: A Companion to Methods in Neurosciences* **1992**, *1*, 141.
25. Haber, R. J. *Western Journal of Medicine* **1991**, *155*, 146.
26. Davies, K. M.; Wink, D. A.; Saavedra, J. E.; Keefer, L. K. *Journal of the American Chemical Society* **2001**, *123*, 5473.
27. Zheng, Y. J.; Ornstein, R. L. *Journal of the American Chemical Society* **1996**, *118*, 9402.
28. Isenberg, I.; Szentgyorgyi, A. *Proceedings of the National Academy of Sciences of the United States of America* **1958**, *44*, 857.

Chapter 3

Metal Organic Frameworks as Nitric Oxide Materials[2]

Synopsis

The traditional approach to NO materials is based on the incorporation of an exogenous supply of NO. While this approach is effective for inhibiting surface biofouling the effects are often short lived due to the finite reservoir of incorporated NO. Instead the development of NO materials with sustained NO release must rely on renewable sources of NO supplied in the blood stream as S-nitrosothiols. As such the incorporation of Cu catalysts into the matrix of polymeric materials facilitates the surface localized generation of NO from bioavailable substrates. Metal organic frameworks (MOFs) are robust and versatile materials with emerging interest in biomedical applications and are explored in this work for their potential as NO catalysts.

The reactivity of the archetypal Cu-MOF, CuBTC, as a catalyst for NO generation from RSNO substrates was determined based on the real time measurement of NO. Catalytic turnover was observed for CuBTC where repeat usage did not impact the reactivity of the catalyst. The selectivity of CuBTC towards RSNOs was determined based on variations in substrate size and polarity of incorporated functional groups. Structural integrity of CuBTC following reaction with the RSNOs was evaluated by assessing the resulting crystallininty of the reacted particles via powder X-ray diffraction (pXRD). Finally, the influence of the metal ion used in the construction of the framework towards reactivity with RSNOs was

[2] *The work presented herein is published in the journal Analytical Chemistry with Melissa M. Reynolds as a joint author and is used with permission. The body of work presented here was assembled by this author. © 2014 American Chemical Society, Anal. Chem. 2014, 86, 2025.*

determined using iron and aluminum based MOFs. This work represents a proof of principle for the use of MOFs as NO catalysts, however substantial improvements in the aqueous stability of the framework are needed for biological applicability.

Introduction

Metal organic frameworks (MOFs) are a unique class of solid state materials whose periodic assembly of coordination clusters of metal ions and organic linking ligands, referred to herein as secondary building units (SBUs), results in the formation of a porous crystalline network in 1, 2, or 3 dimensions.[1-3] As a result an infinite combination metal ions and ligands of MOFs can be tuned for a wide range of applications including gas storage,[4-6] chromatography,[7-9]and catalysis[10-12] to name a few. MOFs initially drew strong correlations to zeolites and were touted as being up and coming versatile materials for numerous industrial applications. However unlike zeolites which have a strictly inorganic composition and can withstand temperatures in excess of 1000 °C, the organic component of MOFs restricts the thermal stability of MOFs up to 500 °C.[3] Furthermore, the SBUs dictate the structural and chemical features of MOFs and are governed by the constraints of metal ligand coordination chemistry and are therefore subject to stability considerations in air and in solution. As a result through the rational design of frameworks based on the judicious selection of metal ions and ligands MOFs can be tailored for specific applications.

An emerging field of interest for the application of MOFs is in biomedicine as imaging contrast agents,[13] drug delivery vehicles,[14-16] and as bioinspired catalysts.[17,18] First and foremost the preparation of MOFs for biomedical applications necessitates a biofriendly composition that will not result in adverse effects or toxicity related complications once in use. To date studies regarding biocompatibility of MOFs are scarce, however rational design of bioMOFs dictates that only metal ions that are innate to the biological environment including Fe, Ca, Mg, Zn, or Cu should be used. As for the ligands polycarboxylic or imidazole linkers are shown to have minimal toxicity owning to their high polarity that permits easy

clearance from the body.[14,19] Considering the porous nature of MOFs the most facile route to use in biomedicine is the encapsulation of therapeutic agents and the subsequent deliver through host/guest, diffusion, or degradation processes. In particular, nitric oxide (NO) can be incorporated into the framework in accordance with traditional MOF gas storage approaches as a physisorbed guest or it can be grafted onto functionalities contained within the framework in an approach known as post synthetic modification.[15,20-24] As far as NO materials are concerned MOFs functionalized with exogenous NO report the highest loading capacities of any material to date, however uncontrollable release kinetics and ultimate depletion of the NO reservoir remain a limiting factor for their use.[25] While the release of large boluses of NO is known to have immediate positive effects as an antimicrobial agent, long term effects aimed at preventing surface deposition of fouling agents on device surfaces and regenerative effects require the sustained and controlled delivery of NO for periods in excess of a year.

The design of long term NO materials requires the use of endogenous NO donors rather than the direct incorporation of exogenous NO donors into the material matrix. Readily available NO donors found circulating in the blood stream in concentrations up to 10 uM as NO storage and transport vehicles are RSNOs.[26,27] The liberation of NO from RSNOs is known to proceed via a Cu^{2+} catalyzed reaction shown in equation 1.[28,29] As such the design of MOF NO catalysts should be equipped with Cu^{2+} metal ions as the active site. The use of MOFs as biocatalysts is an emerging field that is dominated by the inclusion of protein mimetic active sites, such as porphyrin macrocycles,[17,30] as a component of the ligand in the construction of the framework. The use of these bioinsipred MOF catalysts have shown to be successful for mediating many charge transfer based reactions, however the increased size and flexibility of the framework imparted by the active site containing ligands results in collapsible frameworks generally requiring use only in the gas phase.[18,30] As an alternative MOFs with coordinatively unsaturated metal centers in the SBU are effective for catalyzing many organic reactions and exhibit structural robustness over both gas and solution phase reactions.

$$2\ RSNO \xrightarrow{Cu^{2+}} 2\ NO + RSSR \quad \text{(equation 1)}$$

For purposes of this proof of principle work the commercially available Cu-MOF, CuBTC[31] was selected as the investigated MOF NO catalyst. CuBTC is amongst the most researched frameworks to date owing to its archetypal assembly into a robust porous (9Å x 9Å) 3-dimensional framework with coordinatively unsaturated Cu^{2+} metal centers and limited hydrolytic stability.[32-34] The SBU of CuBTC is consists of two octahedrally coordinated Cu^{2+} ions coordinated to the carboxyl functionalities of 1,3,5-benzenetricarboxylic acid (BTC) bridging ligands forming a carboxylate paddle wheel complex, shown in Figure 1a.[31] The axial positions of each Cu^{2+} ion are occupied by labile water molecules, which upon dehydration results in a Cu-MOF with coordinatively unsaturated metal ions available for driving catalytic reactions. The accessibility of Cu active sites, hydrolytic stability, and large pores of CuBTC make it a promising choice for investigating the potential reaction with RSNO substrates resulting in the catalytic generation of NO, Figure 1b.

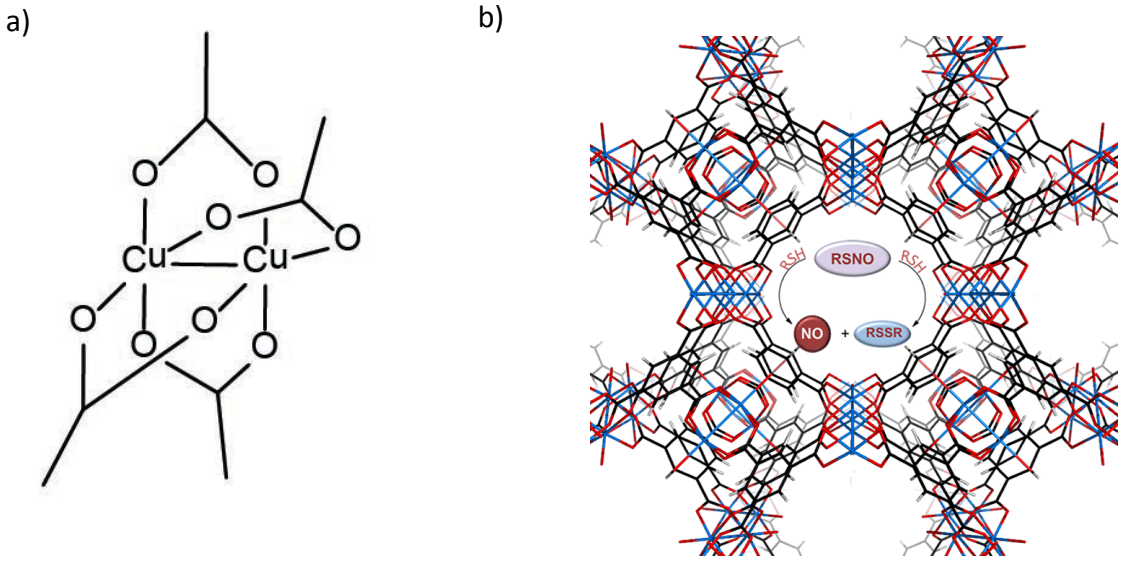

Figure 1. a) Dinuclear Cu^{2+} Carboxylate paddlewheel active site of CuBTC. B) Illustration of RSNO decomposition to produce NO via a MOF catalyst with coordinatively unsaturated Cu^{2+} metal centers

The suitability of a MOF as an NO catalysts is contingent upon the structural stability of the material under the reaction conditions and the capacity of the material to catalytically generate NO from bioavailable RSNO substrates. The reactivity of the CuBTC with bioavailable RSNO S-nitrosocysteine (CysNO), according to equation 2, was evaluated by directly monitoring the formation of the product NO. The structural integrity of CuBTC was determined based upon the characteristic diffraction patterns of the material obtained by pXRD and analysis of the reaction solution for Cu resulting from degradation of the framework. Subsequently, the relationship between substrate structure and reactivity with CuBTC was examined using seven RSNO substrates that differed based on size and polarity of incorporated functional groups. Finally, the role of the metal ion contained within the framework was evaluated in order to confirm the necessity of having a Cu metal center as the active site.

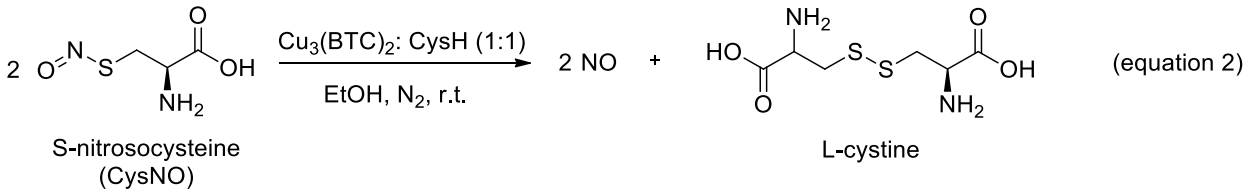

(equation 2)

Experimental Methods

Materials. All reagents were purchased from commercial vendors and used without further purification. $Cu_3(BTC)_2$ was purchased as Basolite C300 from Aldrich (St. Louis, Missouri). Mercaptans used in this work include L-cysteine (Alfa Aesar), cysteamine (Fluka), thioglycolic acid (Sigma-Aldrich), thiolactic acid (Sigma-Aldrich), 2-mercaptoethanol (Amresco), D,L-homocysteine (Sigma-Aldrich), and 3-mercaptopropionic acid (Sigma Aldrich). Reagent grade ethanol (96%) was purchased from Mallinckrodt Chemical (Phillipsburg, New Jersey), and *t*-butyl nitrite (90%) was purchased from Acros Organics (New Jersey, USA). Ultra high purity N_2 and O_2 gases for the NOA measurements were supplied by Airgas (Denver, Colorado). Water was purified using a Millipore purification system set at 18 MΩ for all experiments.

MOF Activation. $Cu_3(BTC)_2$ was activated by heating the material to 100 C under vacuum for 8 hours. Following activation the materials were stored under desiccant until use. After activation the material underwent a color change from unactivated cyan blue to a very dark blue. A comparative evaluation of the effect of activated and unactivated $Cu_3(BTC)_2$ for CysNO decomposition was done according to the previously specified procedure. It is of note that upon addition to the ethanol solution the activated particle immediately assumed the light cyan blue color of unactivated materials due to interaction with the solvent. A comparison of the NO release profiles is shown in SI figure 1. The resulting NO release profiles indicate that there is initially an increase in the rate of the reaction, however the same trend is observed in both cases. Therefore, in order to maintain consistency in the initial extent of hydration all experiments reported here in utilized the activated materials.

Preparation of S-nitrosothiols. RSNOs were prepared *in situ* by adding $5x10^{-5}$ mol of the appropriate thiol to 1mL of Millipore water followed by addition of excess ($1x10^{-4}$ mol) nitrosating agent, *t*-butyl nitrite. For each of the thiols investigated, the reaction solution was covered and protected from light with an aluminum foil wrapper and placed in an ice bath at 0 °C. After 15 min, the reaction solution was purged with N_2 under vacuum for 5 min to remove unreacted *t*-butyl nitrite. Complete removal of *t*-butyl nitrite was verified by UV-Vis spectroscopy following the disappearance of the characteristic 6 point absorbance features between 330-410 nm. The concentrations of the RSNO solutions were monitored by UV-Vis spectroscopy following the absorbance band at 545 nm.

Determination of molar extinction coefficients of RSNOs. *S*-nitrosothiols were prepared from a stock solution of 0.05 M thiol with 2x excess of *t*-butyl nitrite added as the nitrosating agent. After reacting in an ice bath for 15 min the solution was purged with N_2 to remove the excess *t*-butyl nitrite and the system was evacuated under vacuum to assure complete removal of residual *t*-butyl nitrite. Using a UV-vis spectrometer the maximum absorbance feature at 545 nm for each RSNO was recorded. Under the conditions of excess nitrosating agent, 100% conversion of the thiol moieties to RSNOs was assumed. Using Beer's law, we determined the molar extinction coefficient of each RSNO based on the starting

thiol concentration assuming complete nitrosation based on the resulting absorbance value. Each experiment was done in triplicate and the resulting molar extinction coefficients for each RSNO are as follows: Thiol: λ(nm), (ε(M^{-1} cm^{-1})); *S*-nitrosocysteine (CysNO): 545, (14.5); *S*-nitrosocysteamine (CysamNO): 545, (14.5)); *S*-nitrosohomocysteine (HcysNO): 545, (16.5); *S*-nitroso-3-mercaptopropionic acid (MPANO): 550, (15.8); *S*-nitrosothioglycolic acid (TGANO): 545, (16.5); *S*-nitrosothiolactic acid (TLANO): 545, (16.5); *S*-nitrosomercaptoethanol (MeNO): 545, (13.8).

Quantification of NO. Direct NO measurements were made using chemiluminescent detection with a GE 280i Nitric Oxide Analyzer (NOA). In reactions requiring a catalyst, the catalyst was added prior to the addition of RSNO. The MOF catalyst, $Cu_3(BTC)_2$ was added directly to the NOA reaction vessel prior to the addition of the solvent. Using an analytical balance accurate to the one ten thousandth of a gram a total of 0.1 mg $Cu_3(BTC)_2$ totaling a copper content of 0.5 μmol Cu^{2+}. A 0.5 μmol aliquot of $CuCl_2 \cdot 2H_2O$ was injected from a 0.05 M stock $CuCl_2 \cdot 2H_2O$ directly into the solvent solution. The solvent ethanol was added in 2 mL quantities to a specialized reaction vessel and was deoxygenated with a flow of N_2 gas set to 200 mL/min with a simultaneous sampling rate of 200 mL/min under vacuum into the NOA reaction chamber. The reaction vessel was protected from light with aluminum foil wrapping and exposed to ambient temperature at 22 °C. An aliquot containing 1 μmol RSNO ($2x10^{-5}$ L stock solution) was introduced to the reaction flask via a side injection port. The resulting NO product was collected at one second intervals and processed using Microsoft Excel 2010. All experiments were performed in triplicate and the average and standard deviation reported for the total NO recovered (mol) and the half-lives (s).

pXRD measurements. Powder x-ray diffraction (pXRD) measurements were collected using a ScintagX2 pXRD equipped with a Cu Kα (λ=1.5406 Å)radiation source. Scans were taken at a speed of 3°/min and a step size of 0.02°.

ATR-IR measurements. Infrared spectra was collected on a Nicolet 6700 FTIR spectrometer equipped with a diamond attenuated total reflectance accessory (ATR), Figure S3. All data was processed using Omnic 8 FTIR software. All experiments were conducted in triplicate.

Measurement of nonframeworkCu^{II}. After the 2:1:1 CysNO:CysH: MOF-Cu^{II} reaction (experiment #5 in Table S1) was complete, the $Cu_3(BTC)_2$was removed from the reaction mixture. The filtered ethanol reaction solution was evaporated, and the residual material was reconstituted with 2mL H_2O. The resulting solution was evaluated for copper content according to EPA method 200.8 using a Perkin Elmer ICP-OES.[2] The copper content was found to be $2.5 \pm 0.6 \times 10^{-7}$ M or 0.1% of the total MOF Cu^{2+} content. All experiments were conducted in triplicate and the average and standard deviation reported.

Results and Discussion

Solvent Stability Measurements of CuBTC. The stability of MOFs in aqueous environments is one of the critical challenges towards designing BioMOFs. CuBTC is a promising material because it has exhibited moisture stability, by coordinating H_2O molecules and suggested for use as a desiccant. As such to begin the exploration of CuBTC as a MOF NO catalyst it is essential to investigate the robustness towards immersion in an aqueous environment. To this effect the structural integrity of CuBTC was evaluated following immersion in deionized water and also in phosphate buffered saline at pH7.4 in order to simulate mediums that are used for in vitro studies of biomaterials. The integrity of the material following aqueous immersion was evaluated by comparing the crystalline fingerprint of the starting material with the particles collected post immersion using pXRD, shown in Figure 2. CuBTC particles immersed in DI water for a 24h period resulted in irreversible alterations in the crystallinity of the material. This indicates that the material cannot withstand exposure to an aqueous environment.

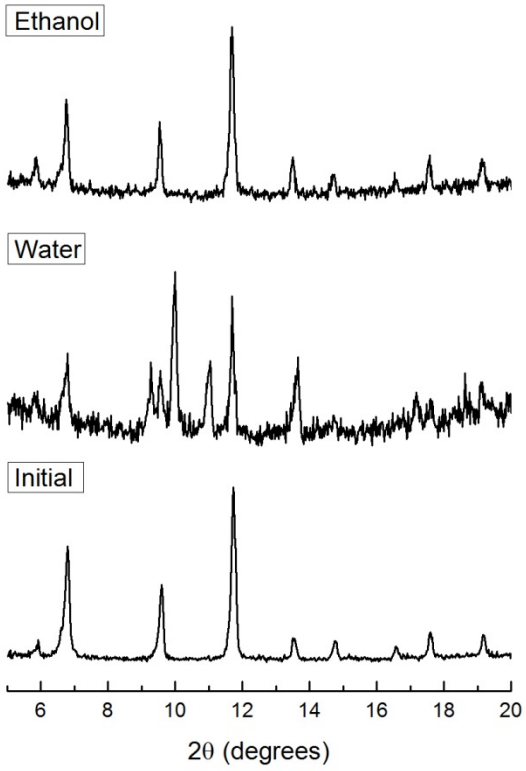

Figure 2. Solvent stability studies of CuBTC after a 24h soak in water and ethanol at room temperature.

Despite the lack of aqueous stability of CuBTC, the ultimate goal of this research is to demonstrate that feasibility of developing a MOF-NO catalyst. Therefore an alternative solvent medium must be explored which does not impact the stability of the framework, while allowing for the miscibility of the substrate. To this effect ethanol was investigated on the basis that it is used as the cosolvent in the synthesis of CuBTC and is also known to solvate low molecular weight RSNO species.[31] As shown in Figure 2 immersion of CuBTC in ethanol did not alter the crystallinity of the particles. As a result ethanol is the solvent medium selected for evaluating CuBTC as a MOF NO catalyst.

Investigation of CuBTC as an NO Catalyst. The reactivity of CuBTC towards the generation of NO from CysNO in an ethanolic solution shown in Scheme 1 was assessed by measuring the resulting NO in real time using chemiluminescence based detection. The resulting NO release profile when 2 equivalents

CysNO per Cu^{2+} active site are injected into the reaction medium is shown in Figure 3. NO release was sustained over a 10 hour period after which time the CysNO was fund to be depleted based on the total amount of NO recovered from the system indicating a catalytic turnover number of 2, shown in Table 1. In comparison to control experiments which did not contain a Cu catalyst and rather assessed the autocatalytic decomposition of CysNO after 10 hours only 17% of the available NO added to the system was recovered. These results are shown in conjunction with the CuBTC catalyzed NO release profile shown in Figure 3. As such these results demonstrate that CuBTC can successfully catalyze the generation of NO from a bioavailable RSNO.

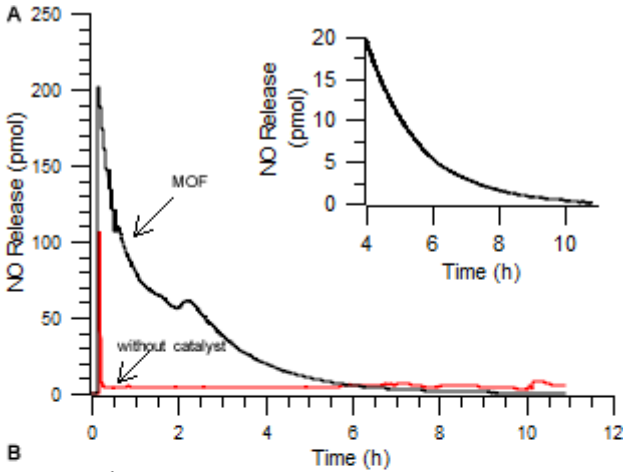

Figure 3. NO release curves from the (red) uncatalyzed decomposition of CysNO and (black) CuBTC catalyzed decomposition of CysNO

The utility of CuBTC as a catalyst however requires that the material be effective as a catalyst with increased turnover efficiency. As shown in Table 1 when 10 and 15 fold excess of CysNO is added to the reaction system the turnover number was shown to increase accordingly. These results indicate that the catalyst is capable of propagating the reaction as long as there is available substrate for the reaction. In a separate study the feasibility of catalyst recycling was assessed. In this experiment CuBTC was reacted until completion with 2 equivalents of CysaNO, after which time CuBTC was removed from the reaction solution, rinsed, and added to a fresh solution containing an additional 2 equivalents of CysNO. This

process was repeated in triplicate and the resulting NO release profiles for the 4 trials is shown in Figure 4. Notably the reactivity of the fresh CuBTC catalyst is faster than the subsequent trials being complete in 10h compared to the 14h to reach completion with the recycled particles. However, the consistency of the reactivity of the recycled particles suggests that no loss in reactivity is observed. However, the evidence at hand indicates that the catalytic activity of CuBTC towards NO generation is dependent upon the availability of substrates. As such in a biological system where the supply of RSNOs is continuously maintained the lifetime of NO release from the material is only subject to the structural integrity of the catalyst.

Table 1. CuBTC turnover with various equilavents of CysNO substrate

Conditions	**Catalyst Turnover**[a]
CysNO:MOF-Cu^{II}(2:1)	1.9±0.1
CysNO:MOF-Cu^{II} (10:1)	9.8±0.3
CysNO:MOF-Cu^{II} (15:1)	15.0±0.1
CysNO:MOF-Cu^{II}Recycling	8.0±0.3

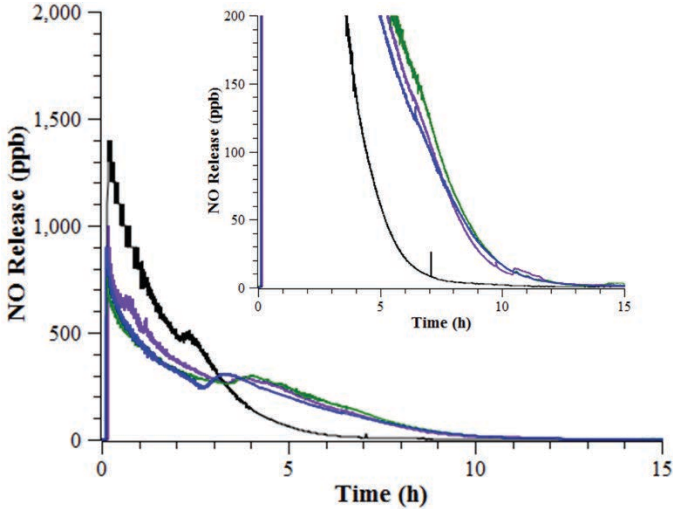

Figure 4. Recycling experiments overlayed in real time over 4 consecutive uses.

Catalyst Structural Stability Assessment. In order to verify that the observed reactivity towards NO generation is truly an artifact of CuBTC and not solvated Cu^{2+} ions resulting from the degradation of the framework analogous NO generation experiments were performed using the copper salt, $CuCl_2$ as the catalyst. In each experiment the amount of Cu^{2+} added to the reaction is equivalent to the total amount of Cu incorporated as CuBTC. Using this approach if all the framework was to fully degrade releasing solvated Cu^{2+} ions we should see similar reactivity. Towards this end the reactivity of CysNO in the presence of solvated Cu^{2+} ions listed in Table 2 is increased by an order of magnitude from 9.64 ± 0.26nM s^{-1} with CuBTC to 161 ± 18 nM s^{-1} when $CuCl_2$ is used as the catalyst. The slow reactivity of CuBTC catalyst compared to solvated Cu^{2+} ions is attributed to the accessibility of the active sites and the heterogeneity of the MOF catalyst. The active sites in CuBTC are embedded within the framework matrix requiring diffusion of the substrates through the pore space for accessibility. Furthermore, as a heterogeneous catalysts an addition energetic requirement is posed by requiring the adsorption of substrates from the solution faces onto the heterogonous catalyst.[35] Taken together these results strongly suggest that MOF bound Cu^{2+} ions are responsible for the observed reactivity.

In order to verify the structural integrity of CuBTC particles following reaction with CysNO the particles were filtered post reaction from the solution for analysis via pXRD and ATR-IR and the filtrate was assessed by elemental analysis for copper content. After removal from the reaction solution the MOF particles were rinsed and subsequently activated. Upon activation the MOF particles underwent the characteristic color change for CuBTC from tourquoise (unactivated) to dark blue (activated), which is indicative of a structurally intact framework.[31] The resultant crystallinity of the particles was evaluated by pXRD and compared to the unreacted particles shown in Figure 5. Identical diffraction patterns indicate that the structural integrity of the framework remains unaffected after reaction with CysNO.

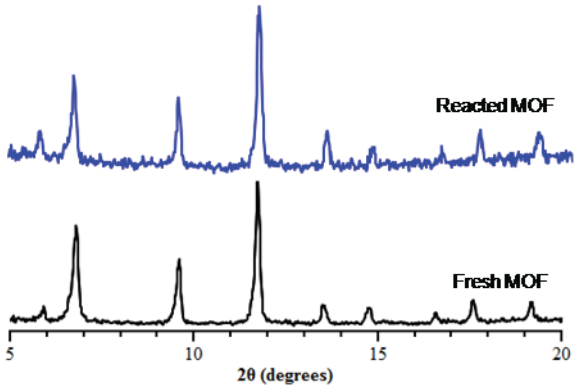

Figure 5. Powder XRD pattern of CuBTC as fresh particles (bottom) and after reaction with CysNO (top)

In a separate study to verify that small amounts of Cu^{2+} ions were not leached into solution and may contribute to the observed NO generation the reaction filtrate was evaluated for copper content using ICP-OES via EPA method 200.8. The residual copper in the solution was found to be 0.1 ± 0.08% of the total MOF copper content. A separate NO release study aimed at assessing the contribution of the Cu^{2+} ions that are present in solution towards the observed NO generation was established. As shown in Figure 6, an aliquot of $CuCl_2$ equivalent to the concentration of leached ions determined by elemental analysis was added to the reaction solution containing CysNO. The addition of this low concentration of Cu^{2+} ions was found to not increase the rate of NO generation when compared to blank control measurements. As a result it is clear that intact CuBTC particles are responsible for the observed catalytic activity towards NO generation.

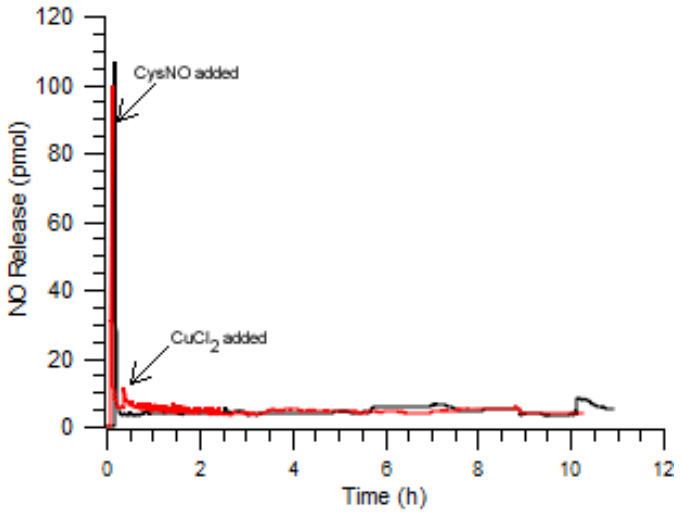

Figure 6. Investigation of contribution of solution based Cu^{2+} ions towards the generation of NO from CysNO.

Investigation of Substrate Structure on the Reactivity of the Material. The successful demonstration of CuBTC as a NO catalyst prompts further investigation into the selectivity of the material with alternative RSNOs. Investigations of MOFs as materials for separations applications have made note of the importance of the pore size for effectively separating substrates of various molecular sizes and the electrostatic environment within the pore channels facilitates interaction with substrates via van der waals interactions and is effective for use as a chromatographic column even effective for enantiomeric species.[7,9,36] The effect of substrate structure on reactivity with CuBTC was evaluated by selecting seven RSNO substrates, shown in Figure 7, based on subtle variations in molecular size and polarity. In order to compare only the effects of substrate size RSNO pairs were selected that differed only by the addition of a carbon atom in the molecular backbone and are (TgaNO)/(MPANO) and (HcysNO)/CysNO. Investigation of the effects of polarity is based on a 2 carbon backbone with substituted amino (CysamNO), hydroxyl (MeNO), and carboxyl (TGANO) terminal functional groups including; secondly the effects of adding an additional functionality, either an amino group (MPANO/CysNO) or a methyl group (TGANO/TLANO), to the carbon back bone were assessed. A summary of the rates of NO generation from each substrate comparing the uncatalyzed reaction with that of CuBTC and solvated Cu^{2+} ions is presented in Table 2.

Table 2. Rate of NO Generation from various RSNOs

RSNO	Blank (nM s^{-1})	CuBTC (nM s^{-1})	$CuCl_2$ (nM s^{-1})
CysNO	2.55 ± 0.21	10.4 ± 0.2	161 ± 18
CysamNO	2.23 ± 0.30	21.3 ± 0.9	231 ± 12
HcysNO	3.22 ± 0.19	3.10 ± 0.94	157 ± 12
MPANO	2.80 ± 0.11	4.56 ± 0.68	214 ± 19
MeNO	1.60 ± 0.27	11.1 ± 1.6	264 ± 23
TGANO	2.30 ± 0.60	20.1 ± 1.1	515 ± 73
TLANO	1.23 ± 0.10	26.1 ± 1.7	441 ± 45

All rates are reported at 25 °C. Data points were run in triplicate and reported to the 95% confidence interval.

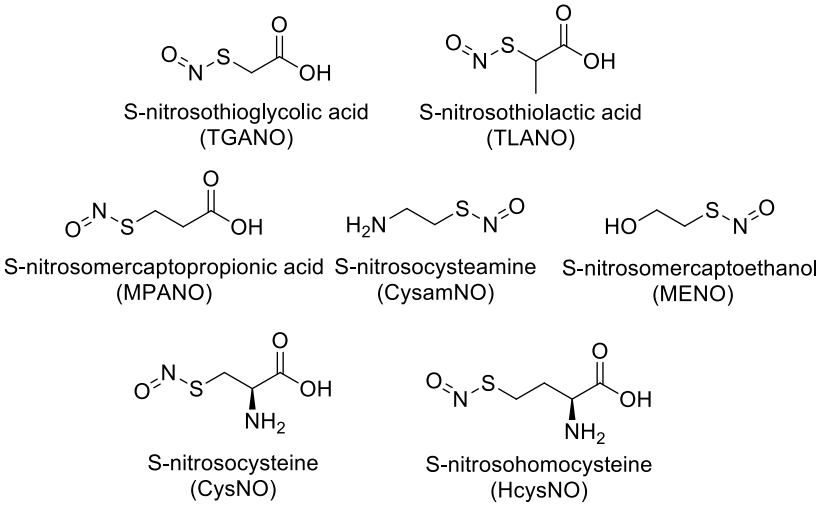

Figure 7. Molecular structures of S-nitrosothiol substrates probed for structure/reactivity studies

The reactivity of CuBTC with each substrate was evaluated based on the rate of NO generation. The reactivity of CuBTC based on the substrate size was evaluated with structurally analogous substrate pairs, TGANO/MPANO and CysNO/HcysNO, which differed only by the addition of a single carbon atom in the molecular backbone. From each pair the smaller substrate, TGANO and CysNO were found to be more reactive than their larger analouges. The use of CuBTC resulted in a 5 fold increase in the rate of NO generation for CysNO compared to the uncatalyzed reaction, however the rate for HcysNO remained unchanged comparatively. Interestingly, the reactivity of CysNO and HcysNO with solvated Cu^{2+} ions are equivalent at 161 ± 18 nM s^{-1} and 157 ± 12 nM s^{-1}, respectively. Where CysNO/HcysNO is concerned considering the similar rates of reactivity for solvated Cu^{2+} catalysts and autocatalytic decomposition , but

a lack of activity with CuBTC it is reasonable to conclude that the increased size of HcysNO precludes interaction with the active sites of the MOF catalyst and accounts for the lack of reactivity. Based on these findings it is reasonable to expect that the larger MPANO substrate would exhibit slower rate of reactivity compared to TGANO, however if the substrate size is the sole determining factor in reactivity of CuBTC then it would also be reasonable to expect that the reactivity of the 3-carbon chain MPANO would be on par with the 3 carbon CysNO substrate. However based on the reactivity data the rate of NO generation with MPANO is merely doubled compared to the 5-fold increase in rate observed for CysNO indicating that the addition of amino functional group plays a contributing role in substrate reactivity with CuBTC.

The interior pore environment of CuBTC is hydrophilic, demonstrated by the facile adsorption of water molecules into the pore space. Increasing the polarity of CysNO with the inclusion of the amino groups therefore increases the affinity of the framework for adsorption into MOF pores and accessibility to the Cu active sites, compared to the similarly sized MPANO. To further support the influence of substrate polarity on the reactivity with CuBTC as a catalyst we can consider the 2 carbon chain pair TGANO and TLANO which differ by the inclusion of a methyl group on the carbon backbone of TLANO. According to our previous findings it is reasonable to expect that the reactivity of TLANO would be diminished compared to TGANO due to the inclusion the nonpolar functional group. However, following reaction with CuBTC the rate of NO generation from TLANO at 26.1 ± 1.7 nM s^{-1} is greater than that of TGANO at 20.1 ± 1.1 nM s^{-1}. These seemingly contradictory results can be explained by the small molecular size of TLANO which can be easily accommodated in the pore space of the MOF and the inclusion of the hydrophobic methyl group diminishes the affinity of the framework for the substrate allowing for more facile diffusion of the substrate to the active sites.

To examine the extent of electronic influences on the reactivity of the RSNOs with the MOF catalyst, RSNOs were selected with diverse terminal electron withdrawing R groups on the β carbon: (i) amino (CysamNO), hydroxyl (MeNO), and (iii) carboxyl (TGANO) moieties. In the presence of the MOF, the

rate of NO generation from MeNO 11.1 ± 1.6 nM s^{-1} is the slowest whereas the rate for CysamNO and TGANO were doubled at 21.3 ± 0.9 nM s^{-1} and 20.1 ± 1.1 nM s^{-1}, respectively. These differences in substrate reactivity when a MOF catalyst is utilized can be explained by the affinity of the ancillary functional groups with the framework walls, where increasing affinity results in decreased rates of NO generation.

Alternative Metal Ions as RSNO Catalysts. To verify that the Cu metal ions are in fact the active sites and the resulting NO is not an artifact of host/guest chemistry an iron based MOF with similar pore dimensions was selected. The use of an Fe based MOF is ideal for evaluating the contribution of the metal center as the active site since Fe^{3+} is known to have limited success towards the decomposition of RSNOs resulting in the liberation of NO.[29] Under analogous conditions to NO release measurements with CuBTC, the Fe-MOF Fe(BDC)[17] was added to the reaction solution containing CysNO as the substrate. After a 15h period the generated NO in the presence of Fe(BDC) was equivalent to the results observed for the autocatalytic decomposition of CysNO, shown in Figure 8. Surprisingly however literature reports indicate that Fe(BDC) is capable of driving thiol oxidation reactions suggesting that accessibility of the metal centers is not the reason for the lack of observed activity. Taken together these results confirm the importance of the Cu active site for catalyzing the release of NO.

The established redox mechanism for the decomposition of RSNOs using homogenous Cu^{2+} ions suggest that the Cu^{1+} species interacts with the thiol component and the ancillary functional groups forming a cyclic intermediate resulting in homolytic cleavage of the S-N bond to generate the thiyl radical, NO, and Cu^{2+}.[29] In contrast, the active site of $Cu_3(BTC)_2$ precludes bidentate coordination of the ligand based on the availability of only one open coordination site around the copper ion. Furthermore, it is unclear at this time whether or not MOF catalysts with the metal centers as active sites are capable of undergoing redox behavior without incurring structural damage. Instead it has been established that the active Cu^{2+} metal center of CuBTC behaves as a Lewis acid catalyst and there is little evidence in support of redox capacity

of the material.[37] With these two conflicting mechanisms supplied for the catalyst and thiol it begs the question of which pathway the reaction between CuBTC and RSNOs proceeds.

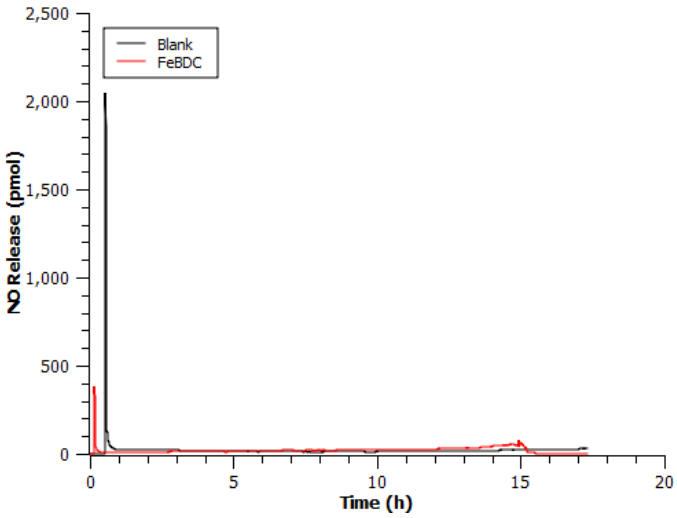

Figure 8. Reactivity of FeBDC towards catalyzing NO generation from CysNO

Recent work outlining the interactions of RSNO substrates with Lewis acids indicates that the RSNO resonance forms dictate the types of interactions that they may have with catalysts as well as the resulting products from S-N cleavage. The S, N, and O atoms of the *S*-nitroso group are each able to serve as a Lewis base and coordinate to the acid Cu^{2+} site. The interaction of a Lewis acid with the RSNO results in the generation of NO radical through coordination of the nitrogen atom.[37] Coordination of the nitrogen atom to the acidic Cu^{2+} active site of CuBTC would then result in the cleavage of the S-N bond while forming a nitrosyl as an intermediate. Cleavage of the S-N bond will likely be facilitated by substituents which can effectively stabilize the thiyl radical species and are most likely to be electron donating substituents. The increase in the reactivity of RSNOs with CuBTC as a catalyst directly corresponded to the presence of electron donating groups in proximity to exert inductive effects on the S-nitroso group.

To probe the reactivity of RSNOs with a Lewis acid catalyst aluminum was selected as the metal ion catalyst due to its redox inaccessible nature and well known activity as a Lewis acid activity. To probe the

effects of a known Lewis acid the aluminum salt $AlCl_3$ was used to investigate the reactivity of Al^{3+} ions with RSNOs. As shown in Figure 9a solvated Al^{3+} ions catalyze the decomposition of over a 5 hour period before depleting the available substrate in comparison to the uncatalyzed reactivity of the material. These results are the first report of the feasibility of using Al^{3+} as a catalyst for the generation of NO from RSNOs. In comparison to solvated Cu^{2+} ions which catalyze RSNO decomposition via a redox pathway, Al^{3+} reactivity with RSNOs proceeding via a Lewis acid pathway results in a significant decrease in the reaction rate.

To further probe the feasibility of using Al^{3+} ions as metal ions for the liberation of NO from RSNOs the MOF the aluminum MOF Al(BDC) was investiged as an NO catalyst. The reaction of Al(BDC) with CysNO shown in Figure 9b, results in an NO release profile that is reminiscent of CuBTC, however the reaction rate is reduced by half taking 20 hours to reach completion. The slowed reactivity of Al(BDC) compared to CuBTC is consistent with the more facile reaction of Cu^{2+} ions with RSNOs compared to Al^{3+}. However this demonstration of the feasibility of using Al^{3+} ions as RSNO catalysts as well as the importance of the choice of metal ion for driving this reaction.

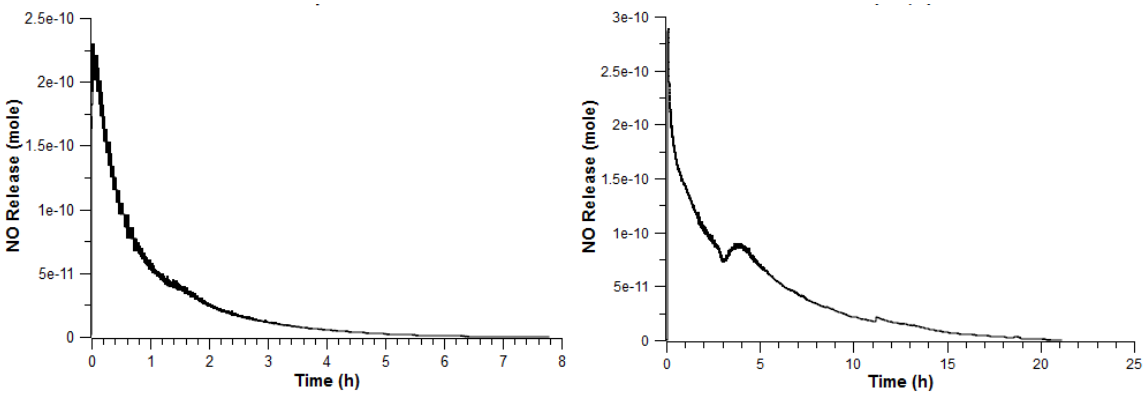

Figure 9. NO release profile of CysNO decomposition catalyzed by (left) AlCl3 and (right) AlBDC

Conclusion

In this work the first demonstration of a robust solid state Cu catalyst for the generation of NO is presented. Increased interest in the use of MOFs in in biomedicine has spurred the development of MOF drug delivery vehicles and biocatalysts. In this work a MOF is demonstrated for the first time to catalyze the generation of a bioactive molecule, NO, with the ultimate intention of use in a therapeutic setting. However, the Cu-MOF catalyst used in this work is subject to degradation in an aqueous environment ultimately precluding the use of this framework in a biomedical application for extended use. Notably, from this proof of principle work information regarding the selectivity of MOFs with substrates was determined based on size and electrostatic constraints. Furthermore, the importance of Cu atoms as the catalytic center was established by probing the reactivity of alternative MOFs with Al^{3+} and Fe^{3+} metal centers.

References

1. Stock, N.; Biswas, S. *Chemical Reviews* 2012, *112*, 933.
2. Eddaoudi, M.; Moler, D. B.; Li, H.; Chen, B.; Reineke, T. M.; O'Keeffe, M.; Yaghi, O. M. *Acc. Chem. Res.* 2001, *34*, 319.
3. Li, H.; Eddaoudi, M.; O'keeffe, M.; Yaghi, O. M. *Nature* 1999, *402*, 276.
4. Collins, D. J.; Zhou, H. C. *Journal of Materials Chemistry* 2007, *17*, 3154.
5. Furukawa, H.; Yaghi, O. M. *Journal of the American Chemical Society* 2009, *131*, 8875.
6. Morris, R. E.; Wheatley, P. S. *Angew. Chem. Int. Ed.* 2008, *47*, 4966.
7. Chen, B.; Liang, C.; Yang, J.; Contreras, D. S.; Clancy, Y. L.; Lobkovsky, E. B.; Yaghi, O. M.; Dai, S. *Angewandte Chemie International Edition* 2006, *45*, 1390.
8. Gu, Z. Y.; Yang, C. X.; Chang, N.; Yan, X. P. *Accounts of Chemical Research* 2012, *45*, 734.
9. Han, S.; Wei, Y.; Valente, C.; Lagzi, I.; Gassensmith, J. J.; Coskun, A.; Stoddart, J. F.; Grzybowski, B. A. *Journal of the American Chemical Society* 2010, *132*, 16358.
10. Corma, A.; García, H.; Llabrés i Xamena, F. X. *Chemical Reviews* 2010, *110*, 4606.
11. Isaeva, V. I.; Kustov, L. M. *Petroleum Chemistry* 2010, *50*, 179.
12. Yoon, M.; Srirambalaji, R.; Kim, K. *Chemical Reviews* 2011, *112*, 1196.
13. Della Rocca, J.; Liu, D. M.; Lin, W. B. *Accounts of Chemical Research* 2011, *44*, 957.
14. Horcajada, P.; Gref, R.; Baati, T.; Allan, P. K.; Maurin, G.; Couvreur, P.; Férey, G.; Morris, R. E.; Serre, C. *Chemical Reviews* 2011, *112*, 1232.
15. Keskin, S.; Kizilel, S. *Industrial & Engineering Chemistry Research* 2011, *50*, 1799.
16. Sun, C. Y.; Qin, C.; Wang, X. L.; Su, Z. M. *Expert Opinion on Drug Delivery* 2013, *10*, 89.
17. Barron, P. M.; Wray, C. A.; Hu, C. H.; Guo, Z. Y.; Choe, W. *Inorganic Chemistry* 2010, *49*, 10217.
18. Shultz, A. M.; Farha, O. K.; Hupp, J. T.; Nguyen, S. T. *Journal of the American Chemical Society* 2009, *131*, 4204.

19. Zhang, J.-P.; Zhang, Y.-B.; Lin, J.-B.; Chen, X.-M. *Chemical Reviews* 2012, *112*, 1001.
20. Ingleson, M. J.; Heck, R.; Gould, J. A.; Rosseinsky, M. J. *Inorganic Chemistry* 2009, *48*, 9986.
21. McKinlay, A. C.; Xiao, B.; Wragg, D. S.; Wheatley, P. S.; Megson, I. L.; Morris, R. E. *Journal of the American Chemical Society* 2008, *130*, 10440.
22. McKinlay, A. C.; Morris, R. E.; Horcajada, P.; Ferey, G.; Gref, R.; Couvreur, P.; Serre, C. *Angewandte Chemie-International Edition* 2010, *49*, 6260.
23. McKinlay, A. C.; Eubank, J. F.; Wuttke, S.; Xiao, B.; Wheadey, P. S.; Bazin, P.; Lavalley, J. C.; Daturi, M.; Vimont, A.; De Weireld, G.; Horcajada, P.; Serre, C.; Morris, R. E. *Chemistry of Materials* 2013, *25*, 1592.
24. Xiao, B.; Wheatley, P. S.; Zhao, X.; Fletcher, A. J.; Fox, s.; Rossi, A. G.; Megson, I. L.; Bordiga, S.; Regli, L.; Thomas, K. M.; Morris, R. *Journal of the American Chemical Society* 2007, *129*, 1203.
25. Lowe, A.; Chittajallu, P.; Gong, Q.; Li, J.; Balkus, K. J., Jr. *Microporous and Mesoporous Materials* 2013, *181*, 17.
26. Butler, A. R.; Rhodes, P. *Analytical Biochemistry* 1997, *249*, 1.
27. Giustarini, D.; Milzani, A.; Colombo, R.; Dalle-Donne, I.; Rossi, R. *Clinica Chimica Acta* 2003, *330*, 85.
28. Askew, S. C.; Barnett, D. J.; McAninly, J.; Williams, D. L. H. *Journal of the Chemical Society Perkin Transaction 2* 1995, *8*, 741.
29. Dicks, A. P.; Swift, H. R.; Williams, D. L. H.; Butler, A. R.; Al-Sa'doni, H. H.; Cox, B. G. *Journal of the Chemical Society Perkin Transactions 2* 1996, 481.
30. Farha, O. K.; Shultz, A. M.; Sarjeant, A. A.; Nguyen, S. T.; Hupp, J. T. *Journal of the American Chemical Society* 2011, *133*, 5652.
31. Chui, S.; Lo, S. M.; Charmant, J. P. H.; Orpen, A. G.; Williams, I. D. *Science* 1999, *283*, 1149.
32. Grajciar, L. s.; Bludský, O.; Nachtigall, P. *The Journal of Physical Chemistry Letters* 2010, *1*, 3354.

33. Alaerts, L.; Seguin, E.; Poelman, H.; Thibault-Starzyk, F.; Jacobs, P. A.; De Vos, D. E. *Chemistry European Journal* 2006, *12*, 7353.
34. Schlichte, K.; Kratzke, T.; Kaskel, S. *Micropourous and Mesoporous Materials* 2004, *73*, 81.
35. Widegren, J. A.; Finke, R. G. *Journal of Molecular Catalysis A: Chemical* 2003, *198*, 317.
36. Yu, Y.; Ren, Y.; Shen, W.; Deng, H.; Gao, Z. *TrAC Trends in Analytical Chemistry* 2013, *50*, 33.
37. Timerghazin, Q. K.; Peslherbe, G. H.; English, A. M. *Organic Letters* 2007, *9*, 3049.

Chapter 4

Development of Metal Organic Framework Catalysts for Biological Applications[3]

Synopsis

The versatile chemical and physical properties of metal organic frameworks (MOFs) have made them unique platforms for the design of biomimetic catalysts, but with only limited success to date due to instability of the MOFs employed in physiological environments. By adjusting the metal ligand acid base pairing a Cu-MOF with aqueous stability can be prepared using 1,3,5-Benzene-tris-triazole as the linking ligand to create CuBTTri. CuBTTri exhibited structural integrity in aqueous environments, including phosphate buffered saline (76 h, pH 7.4, 37 °C), cell media used for *in vitro* testing (76 h, pH 7.4, 37 °C), and fresh citrated whole blood (30 min, pH 7.4, 37 °C). Subsequently, CuBTTri was evaluated for catalytic generation of the bioactive agent nitric oxide (NO) from endogenous sources, *S*-nitrosothiols (RSNOs). The application of CuBTTri for use in polymeric medical devices was explored through the formation of a composite CuBTTri-poly by blending CuBTTri into biomedical grade polyurethane matrices. Once prepared, the CuBTTri-poly material retained the catalytic function towards the generation of NO with tunable release kinetics proportional to the total content of CuBTTri embedded into the polymeric material with a surface flux corresponding to the therapeutic range of 1-100 nM s^{-1} cm^{-2}, which was maintained even following exposure to blood.

[3] *The work presented herein is published in the journal Advanced Functional Materials with Jarid M. Metz and Melissa M. Reynolds as joint authors and is used with permission. The body of work presented here was assembled by this author.* *Adv. Funct. Mater. 2014, DOI:10.1002/adfm.201402529*

Introduction

The development of any material for a biological application requires that the material fulfills the intended function without resulting in any adverse effects. While there are many proposed applications for the use of MOFs in biomedicine, to date the development of bioMOFs remains limited by the susceptibility towards degradation in a biological environment.[1,2] While degradation may not be a limiting factor for materials targeted as drug delivery vehicles that need to be cleared after releasing their payloads, the use of MOFs as bioinspired catalysts requires that they be resistant towards degradation in the biological environment. The two primary components of the assembly of a MOF that dictate the stability of the material are the lattice type and the metal ligand interactions. While in many cases the resulting lattice is an artifact of synthetic conditions and the coordination cluster, the resulting metal-ligand interactions can be easily tuned based on the type of metal and ligand used in the preparation of the material. As a result the crucial challenge in the development of a bioMOF NO catalysts is the functionalization with a suitable biocompatible ligand while preserving catalytic function of the MOF.

The formation of a MOF is first and foremost dependent upon the type of coordination complex that forms between the metal ion and the ligand. This complex then proceeds to function as a secondary building unit (SBU) which is repeated throughout the MOF as a the nodes of the crystalline structure.[3-5] As a result the stability of the SBU assembly dictates the overall stability of the framework. As a coordination complex the stability is dictated by the same rules that apply to small molecule complexes including hard soft Lewis acid base theory. The use of carboxyl based ligands are amongst the favorites for the formation of MOFs, however the stability of the complexes formed are known to be subject to decomposition in air, as well as aqueous environments.[6,7] As a result the key factor towards the development of robust water stable MOFs relies in the appropriate selection of an alternative ligands.

A promising class of ligands for use in the construction of water stable MOFs are 5 member aromatic nitrogen heterocyles, officially classified as azoles.[8,9] While the formation of small molecule coordination

complexes with azole based ligands is well known to have a tendency to form insoluble salts, it wasn't until recently that exploration of MOFs with azole based ligands became of interest. Tetrazoles are commonly used as analogues to carboxylic acid ligands due to their very similar pKa values of 4.5. The preparation of Cu-MOFs with tetrazole based ligands results in porous 3D frameworks, yet the stability towards aqueous environments remains unimproved compared to carboxyl based MOFs.[10] Imidazole is an alternative azole based ligand known to construct Zn based frameworks with exceptional chemical and thermal stability.[11] However, the construction of Cu-imidazole MOFs results in frameworks which readily degrade in an aqueous environment. The reduced stability of Cu^{2+} ions with both imidazole and tetrazole based ligands is attributed to poor acid/base pairing. Cu^{2+} is considered a borderline ion in the hard/soft Lewis acid/base activity series whereas imidazole is strongly basic and tetrazole is an acidic species. Therefore a suitable ligand for the generation of a robust Cu-MOF would have a pKa value between tetrazole at 4.5 and imidazole at 14.5, resulting in the selection of triazole (pKa =9.2) ligands as suitable candidates for preparation of MOFs with aqueous stability.

Examination of literature reports for a reported framework which fits the criteria of a Cu-triazole MOF with coordinatively unsaturated metal centers revealed a report from the Long group of a water-stable Cu-MOF coordinated by 1,3,5-benzenetristriazole ligands referred to here on as CuBTTri (Figure 1).[12] While there are numerous reports of CuBTTri as an excellent material for the adsorption of CO_2[13,14] our aim in the present studies was to broaden the scope of CuBTTri applicability for use as a biocatalyst. Herein, the potential of CuBTTri as a MOF NO catalyst with the RSNO substrate, *S*-nitrosocysteamine (CysamNO) according to equation (2) is evaluated in conjunction with structural stability measurements via pXRD following reaction with CysamNO and in mediums routinely used for *in vitro* and *in vivo* experiments, including phosphate buffered saline (PBS), cell media, and whole blood. Subsequently, the development of a composite material with CuBTTri blended into biomedical polyurethane resulted in the capacity for localized catalytic generation of NO . Furthermore, kinetic control over the NO dosage is feasible and

here we demonstrate the capacity for tuning the NO surface flux of the material to lie within the physiologically relevant range.

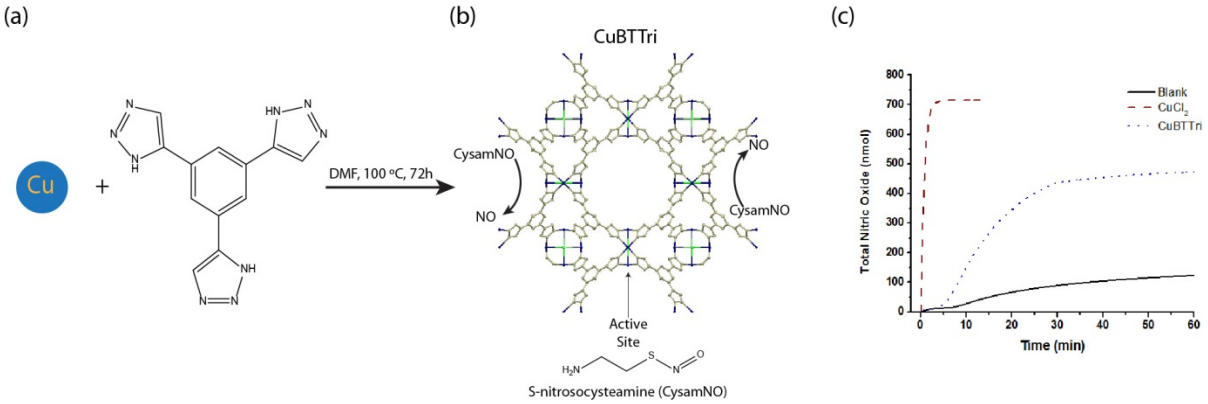

Figure 1. MOF biocatalyst, CuBTTri, for the catalytic generation of nitric oxide from bioavailable substrates. (A) Synthesis of CuBTTri, (B) Reactivity of CuBTTri with S-nitrosocysteamine (CysamNO), (C) Comparison of Total NO release rates between CuBTTri, uncatalyzed CysamNO decomposition, and solvated Cu^{2+} ions.

$$2\ \text{RSNO} \xrightarrow{\text{CuBTTri}} 2\ \text{NO} + \text{RSSR} \qquad (1)$$

Experimental Methods

Materials. All reagents and solvents were purchased from commercial vendors and used without further purification unless otherwise noted. 1,3,5-tribromobenzene (98%), trimethylsilyl azide (94%), (trimethylsilyl)acetylene (98%), and diethylamine (99%) were purchased from Alfa Aesar. Cysteamine hydrochloride (Fluka, 99%), ethylenediaminetetraacetic acid (EDTA) disodium salt (EMD, 99%), copper iodide (Sigma, 99.5%), bis(triphenylphosphine) palladium(II) chloride (TCI America, 98%), copper chloride dihydrate (EMD, 99%), potassium carbonate (Fisher, 99%), and *t*-butyl nitrite (Sigma, 90%). Ultra high purity N_2 and O_2 gases were supplied by Airgas (Denver, Colorado) and solvents PBS tablets (Calbiochem) and Endothelial cell Media MCMD151 (Invitrogen) for the NOA measurements. Water was purified using a Millipore purification system set at 18 MΩ for all experiments.

CuBTTri Synthesis: CuBTTri-H_2O.$H_3[(Cu_4Cl)_3(BTTri)_8(H2O)_{12}]$•$72H_2O$.[1] 1,3,5-tris(1H-1,2,3-triazol-5-yl)benzene (225mg) synthesized according to previously reported methods,[24] was dissolved in 30 mL DMF in a 120 mL vial. Triazole solution was adjusted to pH 4 with a dilute HCl solution. $CuCl_2$•$2H_2O$ (383 mg) was dissolved in 10 mL DMF and added to triazole solution. Vial was placed in oven at 100 °C for 72 hours followed by the reaction solution being kept at room temperature for 1 week. Resulting purple powder was centrifuged and washed with DMF 3 times. The percent yield of as synthesized CuBTTri-DMF was 75%. The powder was then placed in a Teflon lined Parr bomb along with 5 mL deionized water and heated in oven for 24 hours at 100 °C. Purple powder was again centrifuged, washed with water and allowed to air-dry in hood for several days.

Preparation of CuBTTri Films. Composite materials were prepared by dissolving 200 mg of Tygon polymer in 2 mL of THF. To the solvated polymer CuBTTri was added at 1 wt% (mg) and 4 wt% (mg). The CuBTTri polymer was cast into circular molds (radius of 2 mm) and allowed to cure under ambient conditions for 48 hours. For NO release experiments the films were punched into 4 mm disks. Leaching analysis for each film was determined by the copper content found in the reaction solution following each experiment.

Preparation of RSNOs. A fresh stock solution of each RSNO was prepared *in situ* prior to each reaction. In brief, 0.05 M cysteamine hydrochloride was nitrosated with excess *t*-butyl nitrite. After reacting for 10 minutes under agitation in an ice bath, the concentration of the red CysamNO solution was determined by UV-vis spectroscopy using characteristic absorption bands for RSNOs at 335 nm (ε = 793 M^{-1} cm^{-1}) and 545 nm (ε = 15 M^{-1} cm^{-1}).

Nitric Oxide Release Measurements. Nitric oxide generation was recorded in real time using a chemiluminescence based GE nitric oxide analyzer. To the NOA sampling vessel, 2 mL of PBS was added, where the PBS was treated with Chelex resin to remove trace amounts of Cu^{2+} ions and the pH was adjusted to 7.4. The catalyst CuBTTri (5 x10^{-7} mol Cu^{2+}, 0.00018 g) or CuBTTRi films were added

directly to the PBS solution and purged continuously for the duration of the experiment with ultrapure nitrogen gas. An aliquot of CysamNO was introduced directly into the solution in a gas tight Hamilton syringe through the side injection port of the NOA vessel. NO release was recorded in 1 second intervals as parts per billion with a gas sampling rate of 200mL/min. Raw data was processed using Microsoft Excel 2010.

The solution was maintained in a nitrogen atmosphere with bubbling of 16mL/min N_2 directly into the solution and flow gas introduced at 184mL/min into the remaining headspace, the system was continuously sampled under vacuum at 200mL/min.

SEM imaging and EDX analysis of CuBTTri-Poly Films. Using a JEOL JSM-6500F (FSEM) with an accelerating voltage of 20.0 kV and a working distance of 10.1 mm. Images were taken at magnification values of 500x and 5,000x and processed for copper distribution using EDX spectroscopy. The EDX spectrum was collected at an accelerating voltage of 20.0 kV at 130X magnification. All data was processed using Thermo NSS Release candidate 7 software.

Copper Leaching Studies. Inductively Coupled Plasma characterization was conducted on a Perkin Elmer Sciex DRC II . Table S1 displays pertinent information to ICP studies. A representative procedure is as follows: PBS (3mL) was added to a 20mL vial containing CuBTTri-H2O (5 mg). To this mixture 300µL S-nitrosocysteamine was added. The vial was placed in a preheated sand bath at 37°C for 12 hours. The mixture was then centrifuged and the supernatant was filtered through a syringe equipped with a 0.2µm filter. Filtered solutions were then sent for Cu analysis.

Statistical Analysis. Statistical t-tests were performed on each data set to determine statistical differences at the 95% confidence interval.

Results and Discussion

Heterogeneous vs Homogenous Catalyzed Reaction: Assessment of MOF Structural Stability. The resistance of CuBTTri towards degradation under aqueous conditions is critical towards the sustained use

of the material as a catalyst. Towards this end, we assessed the structural integrity of the catalyst based on the retained crystallinity of the material by powder X-ray diffraction and by elemental analysis of the post-reaction filtrate for residual Cu^{2+} ions. Evaluation of the soaking solution for Cu^{2+} content following the reaction indicated that 0.04 ± 0.01 % of the available Cu^{2+} ions from the initial CuBTTri added to the reaction is accounted for in the filtered reaction solution. At this concentration of Cu^{2+} ions, the rate of NO release from CysamNO is the same as that of the uncatalyzed reaction within experimental error, indicating that the observed increase in the rate of NO release is associated with Cu^{2+} ions bound in the CuBTTri framework. Assessment of MOFs using pXRD is an established method for indicating the structural integrity of the material based on the capacity of the material to retain its original crystallinity. In comparison to the parent diffraction pattern, when CuBTTri particles were immersed in PBS at 37 °C for 72 h, the CuBTTri particles post reaction with CysamNO (0.5 mM in PBS) retained their original diffraction pattern, as shown in Figure 2c. Since, the assembly of MOFs require the use of specific reaction conditions to a achieve a particular topology, the dissolution of the framework and subsequent recrystallization is not likely to result. Hence, the implied conclusion is that the framework is retaining heterogeneous character over the course of the reaction. In short, tunable release kinetics of a therapeutic agent from an endogenous source plus unprecedented stability of a MOF in PBS solution makes CuBTTri an excellent candidate for exploration in biotherapeutic applications.

Stability of CuBTTri under in vitro and in vivo conditions. The integration of MOFs in a biological setting further requires the evaluation of CuBTTri stability in cell media solutions used for *in vitro* testing and, most importantly, in body fluids. Hence, the crystallinity of CuBTTri was assessed after immersion in endothelial cell media maintained at pH 7.4 by a 5% CO_2 atmosphere for 72 h and in a separate experiment, following brief exposure (30 min) to fresh citrated whole blood the crystallinity was assessed. The representative diffraction patterns (Figure 2c) indicate that the structural integrity of the material was preserved. This is an important result because minimal biodegradation of CuBTTri has the potential to extend the lifetime of material use while minimizing toxicity associated risks. While rigorous

in vitro and *in vivo* testing remains to be done to determine any toxicity associated with CuBTTri, Cu remains an essential trace element in physiology rendering the body capable of uptake and clearance of MOF degradation products.[15]

Catalytic Activity of CuBTTri. The catalytic activity of CuBTTri towards the generation of NO when reacted with CysamNO in PBS was monitored *in situ* using chemiluminescence detection. The reactivity of CuBTTri was evaluated by comparing the rate of NO generation in the absence of a catalyst and with solvated Cu^{2+} ions as controls (Figure 1C). The average rate of NO generation in PBS at 25 °C when catalyzed by CuBTTri is 22.8 ± 2.1 nM s^{-1} and is an order of magnitude greater than the uncatalyzed reaction at 2.9 ± 0.6 nM s^{-1} (Table 1). Comparatively, in the presence of solvated Cu^{2+} ions (equation 1) the rate of the reaction increases an additional order of magnitude to 333.0 ± 5.1 nM s^{-1} when compared to CuBTTri. These results are consistent with the previous reports of the reactivity of solvated Cu^{2+} catalysts with RSNOs.[16] Specifically, Cu-MOF catalysts with RSNOs have shown the same reactivity trendior[17].

We further investigated the influence of the catalyst content with regard to substrate concentration on the rate of NO release (Figure 2). First, the influence of substrate concentration on the rate of NO generation was explored when the reaction content of the catalyst remained consistent as shown in Figure 2a. In these experiments, the rate of the reaction increased linearly as the concentration of the substrate was increased; however, the reaction with respect to CysamNO proceeded via zero-order reaction kinetics. Interestingly, in each case the amount of NO recovered was equal to 50% of the substrate conversion, leading to total turnover numbers ranging between 1.06 ± 0.04 to 3.90 ± 0.16, shown in Table 1. Notably, even when the reaction content of CuBTTri was in excess of the substrate, the conversion to NO remained consistent at 50%. When an additional aliquot of RSNO substrate was added, NO generation continued until equilibrium was reached again. As shown in Figure 2b, as the catalyst content in the reaction was increased, there was a linear correlation with the rate of NO release with second-order kinetics being followed. Taken together, these results indicate that CuBTTri successfully executes the role of a catalyst towards NO generation with RSNOs that is not impeded by mass-transfer effects or diffusion limitations.

Critical challenges in the development of NO releasing therapeutic materials are often due the difficultly in tuning NO delivery kinetics for therapeutic effectiveness. Additionally, it is critical to overcome the finite amounts of NO that can be incorporated into the material, which currently limit the active lifetime of the material.[18] However, the catalytic activity of CuBTTri exhibited herein towards NO generation is the highest reported delivery of NO to date at 10 mmol NO per g MOF, even exceeding highest previous NO-MOFs by the Morris group at 7mmol/g.[19] In addition, the NO generation capacity demonstrated herein is actually a lower, not an upper limit as is the case with traditional NO donor based materials, which rely on an incorporated reservoir of NO donors. This is true due to renewable sources of RSNO provided in the blood stream. When using the present catalyst, kinetic control over the amount of NO generated is possible via control of the catalyst content facilitating tunable dosages of NO for therapeutic applications and despite the likely fluctuation of RSNOs in the blood stream.

Table 1. Summary of rate of NO generation[a]

Catalyst[b]	**CysamNO (mM)**	**CysamNO:Cu^{2+}**	**NO Release Rate (nM s^{-1})**	**Total Turnovers**
None	0.50	n/a	2.88 ± 0.58	n/a
CuBTTri	0.25	2:1	17.3 ± 2.54	1.06 ± 0.04
CuBTTri	0.50	4:1	22.8 ± 2.08	1.90 ± 0.16
CuBTTri	1.0	8:1	24.2 ± 2.32	3.90 ± 0.16
$CuCl_2$	0.50	4:1	333 ± 5.10	1.43 ± 0.03

[a]All experiments performed in PBS (2mL, pH 7.4, 25 °C) at n=3 and reported at 95% confidence interval
[b]Catalyst content CuBTTri (0.2mg, $5x10^{-7}$ mol Cu^{2+}) and $CuCl_2$ ($5x10^{-7}$ mol Cu^{2+})

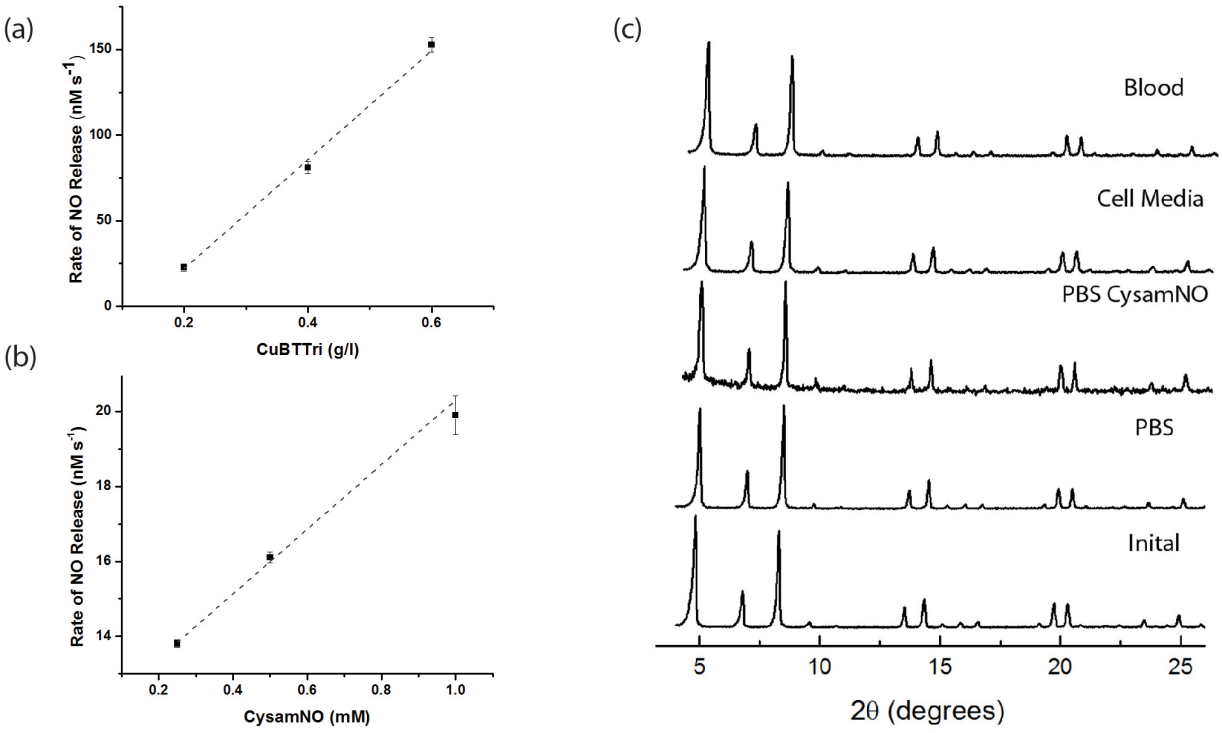

Figure 2. (a) Rate of NO generation from CysamNO (0.5mM) in PBS (2mL) catalyzed by CuBTTri at 25 °C. (b) Rate of NO generation from CysamNO catalyzed by CuBTTri (0.2mg) in PBS (2mL) at 25 °C. Values (n=3) and standard deviations reported to the 95% confidence interval. (c) Powder X-ray diffraction patterns of parent CuBTTri particles compared with CuBTTri particles immersed in PBS (37 °C, pH 7.4); 5mM CysamNO in PBS (37 °C, pH 7.4); Endothelial cell media (37 °C, pH 7.4 maintained with 5% CO_2 buffer); Fresh citrated whole blood (37 °C, pH 7.4).

Composite CuBTTri Biomedical Grade Polyurethanes. The administration of MOFs in biomedicine is achieved either through bulk administration in the blood stream or through the formation of composite materials. Composite materials are particularly advantageous in that they have the flexibility to be incorporated into a wide range of existing polymeric medical devices. Moreover, the immobilization in device matrices is expected to facilitate the site-localized delivery of the therapeutic. The high reactivity of NO necessitates site specific generation at the intended physiological site. Hence, we explored the activity of CuBTTri towards catalytic NO generation once embedded into a matrix of biomedical grade polyurethane. CuBTTri-poly films were prepared by incorporating CuBTTri at 1 or 4 wt% into a solution of THF solvated polyurethane polymer, followed by subsequent casting into 4 mm circular molds.

Examination of CuBTTri-polymer by SEM is shown in Figure 3, indicating that there are MOF particles on the surface the material, but that the majority of MOF particles remain embedded within the polymeric matrix. Dispersion of the CuBTTri particles throughout the polymeric matrix was assessed by analyzing the material for Cu content using SEM analysis accompanying energy dispersive X-ray analysis. As shown in Figure 3b, there is a relatively even dispersion of Cu atoms throughout the material, indicating that the CuBTTri particles are embedded within the polymer matrix.

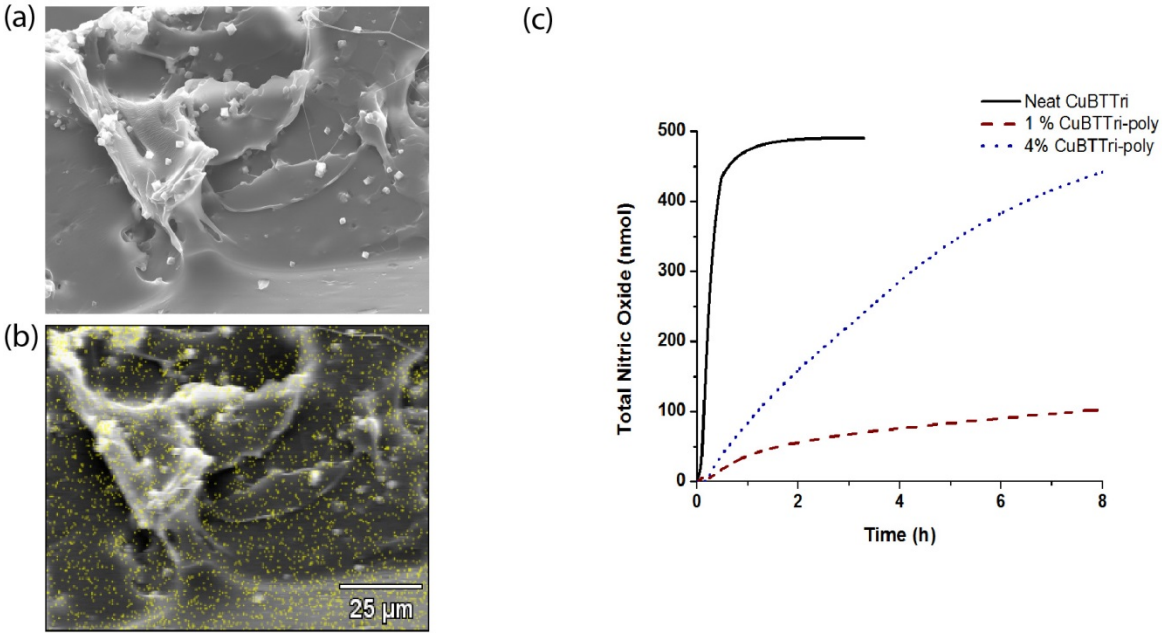

Figure 3. (a) SEM of CuBTTri- poly films at 1000x magnification, (b) SEM-EDX mapping of Cu content in CuBTTr-poly films at 1000x magnification, and (c) Total NO release from CysamNO, CuBTTri, 4% CuBTTri-poly film, 1% CuBTTri-poly film. Values (n=3) and standard deviations reported to the 95% confidence interval.

Catalytic Activity of CuBTTri-poly materials. The catalytic generation of CuBTTri once embedded into the polymeric matrix was evaluated by reacting 1 and 4 wt% CuBTTri-polymeric materials with CysamNO in PBS. To deduce the effects of encapsulation on the reactivity of CuBTTri, we compared the rate of NO generation between the free CuBTTri particles and the 4% CuBTTri films using an equivalent amount of CuBTTri (0.5 µmol Cu^{2+}) in each experiment. The results show that the rate of NO release is reduced 8-fold once the material is incorporated into the polymeric matrix in the otherwise identical

reaction to that observed with the non-embedded particles. The slowed reactivity of the polymer-encapsulated CuBTTri is the expected result of diffusion limitations of the substrate towards reaching the CuBTTri active sites. Reducing the total amount of CuBTTri incorporated into the polymeric matrix further reduces the rate of NO generation from CysamNO, which is consistent with our findings that kinetic control over the amount of NO generated is based on the availability of the catalyst, shown in Figure 3c. Following the reaction of the composite material with CysamNO, the reaction solution was evaluated by ICP-MS for Cu content in order to establish the extent of CuBTTri leaching from the polymer membrane. For both the 1% and 4% films, $\leq 0.47 \pm 0.03\%$ of the available Cu^{2+} ions were found in solution following removal of the CuBTTri-poly material.

Site Localized Delivery of Therapeutic NO Dosages. The *in vivo* effects of NO are concentration dependent resulting in protective and proliferative effects at low concentrations (0.1-10 nM), and cytotoxic effects at high concentrations (100 nM), requiring careful tuning of NO release properties to exhibit intended effects.[20] Since the rate of NO generation using CuBTTri is dependent upon the amount of available catalyst in the material, CuBTTri thereby provides a unique handle for mediating the surface flux of NO in CuBTTri-poly materials. The average surface fluxes from the 4% and 1% CuBTTri films are 1.87 ± 0.08 nM s^{-1} cm^{-1} and 0.77 ± 0.06 nM s^{-1} cm^{-1}, respectively, falling within the protective and proliferative therapeutic range.[21,22] Furthermore, we explored the effects of immersing CuBTTri-poly material in fresh citrated whole blood (37 °C, 30 min) on the reactivity of the material towards NO generation from CysamNO. Following immersion in blood, the CuBTTri-poly film was thoroughly rinsed with water and subsequently reacted with CysamNO in PBS to evaluate the materials capacity for generating NO. The resulting NO surface flux of the blood exposed CuBTTri-poly film (0.75 ± 0.08 nM s^{-1} cm^{-1}) remained consistent with the flux observed for the non-exposed film (0.77 ± 0.06 nM s^{-1} cm^{-1}). These results provide the first demonstration that a MOF biocatalyst can retain its therapeutic action following exposure to biological fluids.

Conclusion

The use of a triazole based ligand CuBTTri remains structurally intact in aqueous mediums including biological fluids. Contrary to previous inceptions of drug delivery vehicles, the use of an embedded catalyst liberates the materials dependence on the limited reservoirs of bioactive by relying on substrates (herein, RSNOs) supplied continuously in the physiological environment. The result is a resulting in a self-sustaining, therapeutic delivery system. In addition, tunable NO release kinetics were demonstrated based on the content of catalyst embedded into polymeric therapeutic materials. Most importantly, for the sustained use of the material, CuBTTri remains structurally intact in aqueous mediums including biological fluids, including whole blood, while retaining catalytic activity of the material. While rigorous *in vitro* and *in vivo* testing remains to be done to examine the full extent of the potential of CuBTTri in a therapeutic setting, this is the first report of a MOF which can catalytically generate a bioactive molecule from an endogenous source on the surface of a polymeric film with the capacity for tunable release kinetics in biological fluids.

References

1. Horcajada, P.; Gref, R.; Baati, T.; Allan, P. K.; Maurin, G.; Couvreur, P.; Férey, G.; Morris, R. E.; Serre, C. *Chemical Reviews* **2011**, *112*, 1232.
2. McKinlay, A. C.; Morris, R. E.; Horcajada, P.; Ferey, G.; Gref, R.; Couvreur, P.; Serre, C. *Angewandte Chemie-International Edition* **2010**, *49*, 6260.
3. Li, H.; Eddaoudi, M.; O'keeffe, M.; Yaghi, O. M. *Nature* **1999**, *402*, 276.
4. Yaghi, O. M.; Li, H.; Davis, C.; Richardson, D.; Groy, T. L. *Accounts of Chemical Research* **1998**, *31*, 474.
5. Yaghi, O. M.; O'Keeffe, M.; Ockwig, N. W.; Chae, H. K.; Eddaoudi, M.; Kim, J. *Nature* **2003**, *423*, 705.
6. Eddaoudi, M.; Kim, J.; Rosi, N.; Vodak, D.; Wachter, J.; O'Keeffe, M.; Yaghi, O. M. *Science* **2002**, *295*, 469.
7. Furukawa, H.; Yaghi, O. M. *Journal of the American Chemical Society* **2009**, *131*, 8875.
8. Aromi, G.; Barrios, L. A.; Roubeau, O.; Gamez, P. *Coordination Chemistry Reviews* **2011**, *255*, 485.
9. Zhang, J.-P.; Zhang, Y.-B.; Lin, J.-B.; Chen, X.-M. *Chemical Reviews* **2012**, *112*, 1001.
10. Dincă, M.; Yu, A. F.; Long, J. R. *Journal of the American Chemical Society* **2006**, *128*, 8904.
11. Park, K. S.; Ni, Z.; Cote, A. P.; Choi, J. Y.; Huang, R. D.; Uribe-Romo, F. J.; Chae, H. K.; O'Keeffe, M.; Yaghi, O. M. *Proceedings of the National Academy of Sciences of the United States of America* **2006**, *103*, 10186.
12. Demessence, A.; Dâ Alessandro, D. M.; Foo, M. L.; Long, J. R. *Journal of the American Chemical Society* **2009**, *131*, 8784.
13. McDonald, T. M.; D'Alessandro, D. M.; Krishna, R.; Long, J. R. *Chemical Science* **2011**, *2*, 2022.
14. Demessence, A.; D'Alessandro, D. M.; Foo, M. L.; Long, J. R. *Journal of the American Chemical Society* **2009**, *131*, 8784.

15. Tapiero, H.; Townsend, D. M.; Tew, K. D. *Biomedicine & Pharmacotherapy* **2003**, *57*, 386.
16. Askew, S. C.; Barnett, D. J.; McAninly, J.; Williams, D. L. H. *Journal of the Chemical Society Perkin Transaction 2* **1995**, *8*, 741.
17. Harding, J. L.; Reynolds, M. M. *Journal of the American Chemical Society* **2012**, *134*, 3330.
18. Carpenter, A. W.; Schoenfisch, M. H. *Chemical Society Reviews* **2012**, *41*, 3742.
19. McKinlay, A. C.; Xiao, B.; Wragg, D. S.; Wheatley, P. S.; Megson, I. L.; Morris, R. E. *Journal of the American Chemical Society* **2008**, *130*, 10440.
20. Coneski, P. N.; Schoenfisch, M. H. *Chemical Society Reviews* **2012**, *41*, 3753.
21. Thomas, D. D.; Ridnour, L. A.; Isenberg, J. S.; Flores-Santana, W.; Switzer, C. H.; Donzelli, S.; Hussain, P.; Vecoli, C.; Paolocci, N.; Ambs, S.; Colton, C. A.; Harris, C. C.; Roberts, D. D.; Wink, D. A. *Free Radical Biology and Medicine* **2008**, *45*, 18.
22. Yao, D. D.; Vlessidis, A. G.; Evmiridis, N. P. *Microchimica Acta* **2004**, *147*, 1.

Chapter 5

Processing of MOFs into Functional Biomaterials[4]

Synopsis

The preparation of MOF composite materials as blends incorporated into organic polymeric matrices is commonly referred to as the preparation of MOF mixed matrix membranes (MMMs).[1-4] The construction of MMMs are routinely used for liquid and gas phase separations of small molecules as well as use as immobilizing MOFs for catalytic applications. However, the development of MOFs as MMMs is routinely on a rather small scale when materials are cast from molds on laboratory bench tops. For commercialization purposes it is essential to investigate the capacity for MOFs to withstand commercial material manufacturing methods often involving extrusion. The critical requirement for MOF incorporation as a blended material is maintained structural stability after processing. This work aims to investigate the influence of commercial manufacturing processes on the structural and chemical stability of MOFs for the development of blended MOF-polymer composite materials.

Introduction

The integration of MOFs in biomedicine necessitates the use of a secondary support so as to provide site specific activity of the frameworks. Towards this end MOF composite materials can be formulated by

[4] *The work presented herein is published in the Journal of Materials Chemistry B with Melissa M. Reynolds as a joint author and is used with permission. The body of work presented here was assembled by this author. © 2014 Royal Society of Chemistry. J. Mater. Chem. B. 2014, 2, 2530.*

incorporating MOFs as dispersions in polymeric materials, commonly referred to as mixed matrix membranes.[1,5] The controlled integration of MOFs to form composite materials with either inorganic or organic substrates is advantageous for the development of functional materials which can complement the merits and mitigate shortcomings of existing material types thereby exceeding the functional capacity of the individual components. Polymeric materials are commonly used in the construction of biomedical devices and as such present an ideal substrate for investigating the feasibility of constructing MOF composite materials geared towards therapeutic applications. For the successful preparation of composite MOF biomaterials manufacturing must occur without significant modification to existing processes used in device construction. In this respect a critical test for the use of MOFs in device fabrication is their process ability into functional devices.

However the key requirement for the preparation of MOF composite materials is after fabrication of the material it is essential that the MOF remains structurally and chemically unaffected without compromising functionality. MMM's prepared on small laboratory scales utilize solvents based casting to shape materials into useable forms without impairing the MOF. However commercial manufacturing processes utilize heat and pressure to mold materials into desired shapes and sizes. Given the reported robustness of MOF capable of withstanding temperatures up to 500 °C and insoluble in organic solvents it is hypothesized that MOFs will be capable of withstanding manufacturing conditions. As such, the incorporation of structurally robust and catalytically active MOF particles in the matrix of biomedical devices has the potential to mediate negative interfacial material responses including reducing instances of surface biofouling and even mitigating proliferative effects towards the regeneration of healthy tissues.[6]

This work aims to investigate the influence of commercial manufacturing processes on the structural and chemical stability of MOFs for the development of blended MOF-polymer composite materials. Towards this end the structural integrity of CuBTC following extrusion with biomedical grade polyurethane into functional medical catheters was evaluated based on the crystalline diffraction pattern of the extruded

material with the parent CuBTC particles by powder X-ray diffraction (pXRD). Subsequently the relative dispersion of the particles within the blended composite was assessed SEM imaging coupled with elemental selective EDX analysis. The reactivity of CuBTC-poly material was evaluated for the capacity to catalytically generate NO from RSNO substrates.

Experimental Methods

Materials. All reagents were used as received without further purification. Cu-BTC was obtained from Sigma-Aldrich as Basolite® C300. Thiols used in this work include L-cysteine (Alfa Aesar), cysteamine (Fluka), and D,L-homocysteine (Sigma-Aldrich). The nitrosating agent *t*-butyl nitrite (90%) was obtained from Sigma-Aldrich. Cupric chloride ($CuCl_2 \cdot 2H_2O$) and reagent alcohol used in this work were obtained from EMD chemicals. Tecoflex SG80A polyurethane was obtained from Lubrizol. Compressed gas cylinders of O_2 and ultrapure N_2 (99.99%) were supplied by Airgas. Millipore purified water (18 MΩ) was used in the preparation of all *S*-nitrosothiol and $CuCl_2 \cdot 2H_2O$ stock solutions.

Preparation of S-nitrosothiols. RSNOs were prepared *in situ* by adding $5x10^{-5}$ moles of the appropriate thiol to 1mL of Millipore water followed by addition of excess ($1x10^{-4}$ mol) nitrosating agent, *t*-butyl nitrite. For each of the thiols investigated, the reaction solution was covered and protected from light with an aluminum foil wrapper and placed in an ice bath at 0 °C. After 15 min, the reaction solution was purged with N_2 under vacuum for 5 min to remove unreacted *t*-butyl nitrite. Complete removal of *t*-butyl nitrite was verified by UV-Vis spectroscopy following the disappearance of the characteristic 6 point absorbance features between 330-410 nm. The concentrations of the RSNO solutions were monitored by UV-Vis spectroscopy following the absorbance band at 545 nm , Thiol: λ(nm), (ε(M^{-1} cm^{-1})); *S*-nitrosocysteine (CysNO): 545, (14.5); *S*-nitrosocysteamine (CysamNO): 545, (14.5)); *S*-nitrosohomocysteine (HcysNO): 545, (16.5). The extent of nitrosation was determined by the quantification of thiol using the Ellman's assay.[7] The concentration of the RSNO in solution determined

by UV-vis was compared to the total amount of thiol in solution. Results from thiol quantification determined the total percent nitrosation for each of the substrates to be 91 ± 2%.

Quantification of NO. Direct NO measurements were made using chemiluminescent detection with a GE 280i Nitric Oxide Analyzer (NOA). The solvent ethanol was added in 2 mL quantities to a specialized reaction vessel and was deoxygenated with a flow of N_2 gas set to 200 mL/min with a simultaneous sampling rate of 200 mL/min under vacuum into the NOA reaction chamber. In reactions requiring a catalyst, the catalyst was added prior to the addition of RSNO. The MOF catalyst, Cu-BTC as either the free powder or the polymeric tubing was added directly to the NOA reaction vessel. Using an analytical balance, accurate to the one ten thousandth of a gram, 0.1 mg samples of Cu-BTC were massed to give a total copper content of 0.5 μmol Cu^{2+} in the sample. With a composition of 1.5% by weight of the Cu-BTC in the polymeric matrix 0.0067g of tubing were used for each experiment, in order to maintain the same amount of Cu-BTC for the reaction. In reactions utilizing solvated Cu^{2+} ion as the catalyst, a 10 μL aliquot of $CuCl_2 \cdot 2H_2O$ was injected from a 0.05 M stock solution directly into the ethanol reaction solution. The reaction vessel was protected from light with aluminum foil wrapping and exposed to ambient temperature at 22 °C. An aliquot containing 1 μmol RSNO ($2x10^{-5}$ L stock solution) was introduced to the reaction flask via a side injection port. The resulting NO product was collected at one second intervals and processed using Microsoft Excel 2010. All experiments were performed in triplicate and the average and standard deviation reported for the total NO recovered (mol) and the half-lives (s).

Preparation of Cu-BTC polymer composite materials. The preparation of the Cu-BTC-tubing materials was achieved by current industrial extrusion processing methods. The MOF was compounded into the polymer using a co-rotating twin screw extruder. The material was then pelletized and vacuum dried for 4 hours at 65°C under high vacuum. The compounded polymer was then extruded into a single lumen tube using a 1.5” single screw extruder running at a temperature of approximately 175°C. The tubing was water cooled, cut to length, and vacuum dried for 4 hours at 65°C under high vacuum before storage.

CuBTC-Poly Material SEM-EDX analysis. Using a JEOL JSM-6500F SEM with an accelerating voltage of 20,000 kV and a beam current of 7nA. A cross section of the Cu-BTC tubing was sputtered with 10 nm coating of gold. Images were taken at a 500x magnification and processed for copper content using adjunct EDX spectroscopy. Component mapping was evaluated between 4.5 keV and evaluated as generated auto phases. All data was recorded and processed using Thermo NSS Release candidate 7 software.

XRD measurements. Powder x-ray diffraction (pXRD) measurements were collected using a ScintagX2 pXRD equipped with a Cu Kα (λ=1.5406 Å) radiation source. Scans were taken at a speed of 3°/min and a step size of 0.02°. Data was plotted as intensity vs 2 theta in Sci Davis scientific data analysis software.

Results and Discussion

MOF Extrusion into Polymeric Materials. Composite MOF polymeric materials can be prepared by blending the MOF particles directly into a solution of solvated polymer. In scheme 1, Cu-BTC is incorporated at 1.5% by weight into a solution of solvated biomedical grade polymer SG-80A. The MOF-polymer composite materials are prepared through a two-step extrusion process. In the first step, the Cu-BTC particles are blended at 1.5wt% with the solvated polymer. Using a twin screw extruded composite material is formed into pellets and dried under vacuum. The resulting pellets are then extruded once more and formed into single lumen tubing with a diameter of 1.5 mm. The resulting tubing used for analysis in the remainder of this manuscript has a rich blue coloration as a result of the incorporation of Cu-BTC into the polymer matrix.

Scheme 1.

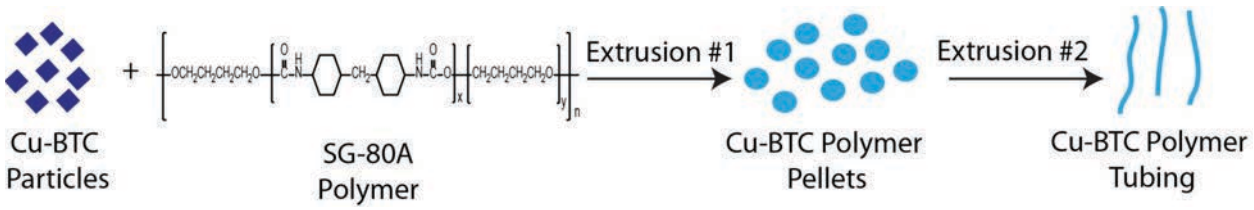

MOF Structural Robustness after Material Processing. The structural integrity of the composite tubing was assessed based on comparing the powder X-ray diffraction patterns with unmodified Cu-BTC crystals. Direct comparison of the powder pattern for the initial Cu-BTC and the polymer incorporated Cu-BTC is shown in Figure 1. The observed reflections at 6, 7, 9, 12, 14, and 18 degrees for each of the samples are characteristic of Cu-BTC. The large hump shown in the Cu-BTC polymer case (Figure 1) is a result of the polymer matrix and is not indicative of structural deviations in the MOF structure. The similarities in the two diffraction patterns between the incorporated Cu-BTC and the free particles indicate that the MOF remains structurally robust following processing into the polymeric material.

This is a significant finding given that over the last two decades countless reports of MOF structures have emerged, yet we have failed to capitalize on their potential for application. Propositions from gas storage,[8,9] drug delivery agents,[10-13] chromatographic separations,[14,15] and catalysis[11,16-18] applications have been the forerunners, but have failed to achieve true applicability. Incorporation of MOFs into biomedical polymers facilitates a new area of application for these types of materials. The proposed use of MOFs in this work facilitates the simultaneous application of MOFs as catalysts and drug delivery agents into one functional material. A new avenue of exploration for MOFs is in the field of biomedicine through their incorporation into existing medical devices. The extrusion of polymeric materials into desired shapes and sizes is a common manufacturing technique for biomedical devices.

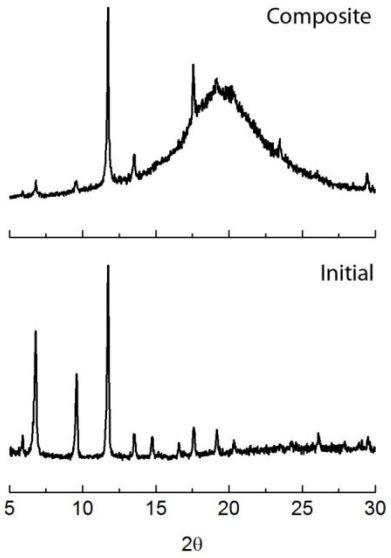

Figure 1. Powder X-ray diffraction pattern of polymer incorporated Cu-BTC – polymer composite (top) and the unmodified Cu-BTC powder (bottom).

Imaging of Cu-BTC Incorporated into a Polymeric Material. Even dispersion of CuBTC particles throughout the polymeric matrix is crucial for the consistent function of the device. Visual inspection with the naked eye reveals a uniform blue coloration throughout the entirety of the material, which is indicative of CuBTC particles. Upon closer inspection of the CuBTC-poly materials using SEM imaging (500x) of the material surface shown in Figure 2a, the majority of the MOF crystals remain embedded within the polymeric matrix. The relative dispersion of the embedded Cu-BTC particles underneath the polymer surface layer was determined by SEM-EDX analysis using copper as a probe molecule. In Figure 2b, the EDX phase representing the copper content and location is overlaid on the SEM image of the Cu-BTC-polymer tubing. From this experiment, the copper content of the material appears to be evenly dispersed. Although, depth profiling through the interior of the material is not accessible based on the 1 micron probing depth limitations of EDX. A large density of copper is detected on the surface particles attributed to the MOF crystals and is randomly dispersed over the entire area of the analyzed material. The copper content of the material was found to account for 4.2% of the total elemental composition of the Cu-BTC polymer material. The molecular formula of Cu-BTC is actually $Cu_3(BTC)_2$, indicating that

for every one mole of MOF, there are 3 mol of copper present and, based on the initial incorporation of Cu-BTC at 1.5%, the theoretical amount of copper contained within the material based on the initial incorporation of Cu-BTC is equal to approximately 4.5%. As such, the observed copper content observed for the material correlates with an even dispersion particles throughout the material.

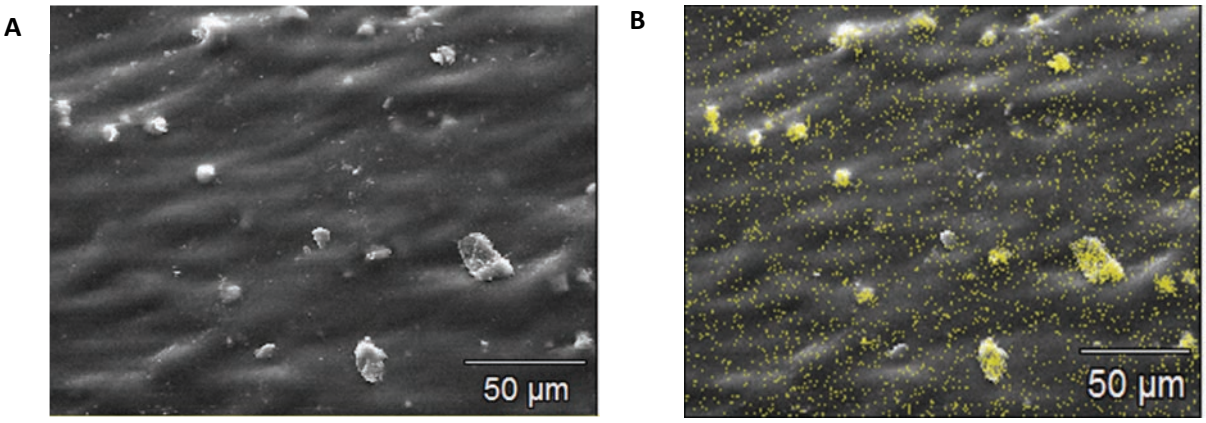

Figure 2. a) Representative SEM image of extruded Cu-BTC tubing (500x magnification). b) Representative SEM-EDX image of extruded Cu-BTC tubing including the overlaid elemental map where copper is indicated in gold.

Reactivity of Cu-BTC towards bioavailable RSNOs. Biologically occurring variants of RSNOs exist as a part of protein side chains and as small molecules.[19] Small molecule RSNOs such as *S*-nitrosocysteine (CysNO), *S*-nitrosocysteamine (CysamNO), and *S*-nitrosohomocysteine (HcysNO), shown in Figure 3, are responsible for the safe storage and transport of NO across cell membranes and through the blood stream. The degradation of RSNOs resulting in the generation of NO is well known to be catalyzed by Cu^{2+} ions and more recently by Cu-MOFs. Investigating structurally distinct RSNO species we can evaluate the role of substrate structure on the amount of NO generated using the extruded Cu-BTC polymer.

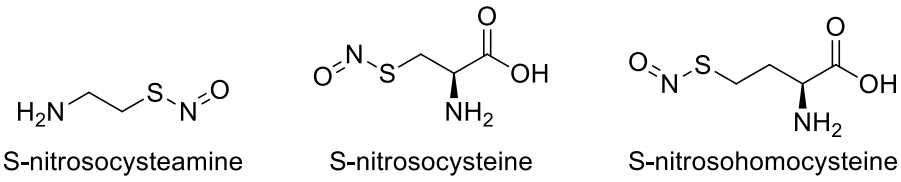

Figure 3. Molecular structures of bioavailable S-nitrosothiols

The decomposition of RSNOs in the presence of the extruded Cu-BTC polymer tubing was evaluated by monitoring the formation of the product NO (equation 1). Chemiluminescence is an ideal technique for measuring NO generation based on the selectivity for NO over other interfering NO_x species and the real-time sampling capabilities.[20] However, due to the fast reactivity of NO with O_2 in order to ascertain that an accurate measurement of the generated NO was accounted for, the reaction set-up required a closed system that was continuously deoxygenated using N_2 as a purge gas. The substitution of the reaction medium with ethanol in place of an aqueous solution was necessary due to the characteristic degradation of Cu-BTC in aqueous environments. As such this work demonstrates a proof of concept that MOF catalyst once incorporated into a polymeric membrane retains its capacity for facilitating the decomposition of bioavailable RSNOs resulting in the generation of NO. Therefore, by substituting the reaction medium we are able to ascertain that the reactivity observed is a result of the intact Cu-BTC particles and not free Cu^{2+} ions that have leached into solution. The investigation of MOF catalyst that is stable under truly physiological conditions is ongoing.

$$2\ \text{RSNO} \xrightarrow{\text{Cu-BTC -Polymer}} 2\ \text{NO} + \text{RSSR} \quad \text{(eq. 1)}$$

The reaction of the Cu-BTC polymer material with CysNO, CysamNO, or HcysNO resulted in the generation of NO, shown in Figure 4a. After a two hour reaction period with the Cu-BTC polymeric material the release of NO from CysNO and CysamNO stopped resulting in the generation of 75% of the theoretical NO. In contrast, after two hours the total amount of NO released from HcysNO was less than 10% of the theoretical amount of NO, however NO release is observed to continue over a 15 hour period. The generation of NO from CysNO and CysamNO started with an induction period that lasted 45 and 90 minutes, respectively. After the induction periods, a rapid release of NO was observed with the reactions proceeding to completion within a 1 hour time period. In order to determine if this observed induction period is a result of the polymeric material or the MOF we compared NO release with free Cu-BTC particles.

In Figure 4b, the generation of NO from CysNO, CysamNO, and HcysNO with the free Cu-BTC particles is shown. The reaction of CysamNO with Cu-BTC particles is the fastest reaching completion in 90 minutes and lacked an induction period. In contrast the induction period persisted over the initial 90 minute period for the Cu-BTC polymer material. The generation of NO from CysNO with the free particles was considerably slower with only 20% of the NO generated in the first 2 hours and lacked an induction period. The behavior of HcysNO with the free Cu-BTC particles corresponded to the encapsulated material with less than 10% of the total NO generated after 2 hours, yet still continued to produce NO for the next 15 hours.

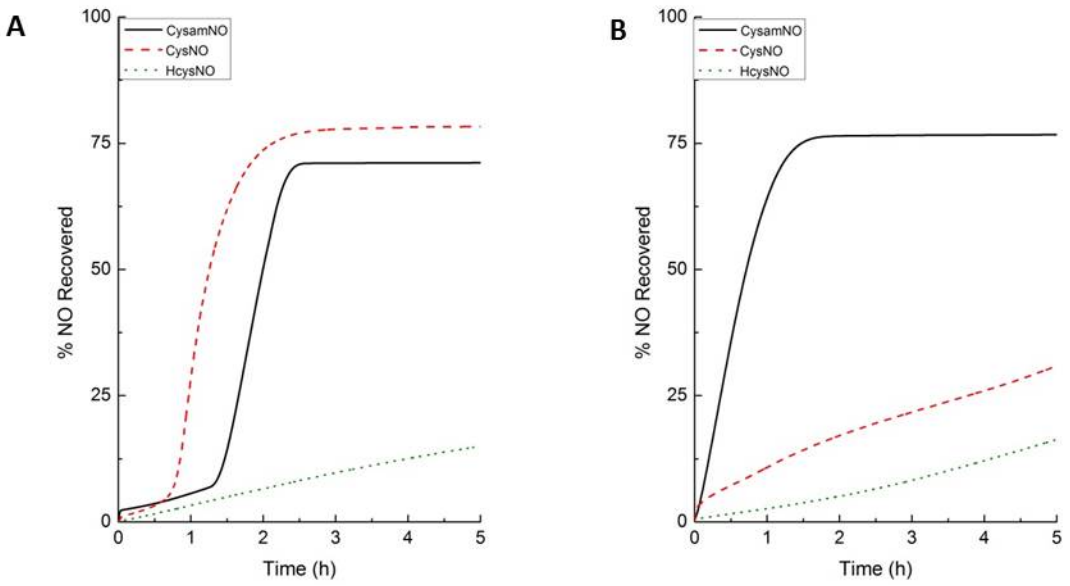

Figure 4. Representative NO release based on the percentage of theoretical NO recovered from CysNO, CysamNO, and HcysNO using a) extruded Cu-BTC polymer and b) Free Cu-BTC particles.

The variation in reactivity between the Cu-BTC tubing and the free particles is attributed to the presence of a polymeric barrier and the dispersion of the particles within the reaction medium. Embedding the Cu-BTC particles within the polymer matrix creates a barrier between the RSNO substrate and the active site Cu^{2+} sites contained within Cu-BTC, thus suggesting a diffusion mediated process that dictates the rates of reactivity. The similar reactivity of HcysNO with either the free particles or the polymer bound

particles suggests that the larger size of HcysNO restricts accessibility of the RSNO substrate to the active sites of the metal centers. As a result this diffusion driven process likely accounts for the induction period observed for CysNO and CysamNO. The faster reactivity of CysNO with the Cu-BTC polymer material compared to the free particles can be correlated to the requirement that once through the polymeric barrier it facilitates a close interaction between the Cu-BTC particles and the substrate. Furthermore, the dispersion of the Cu-BTC particles in the polymer increases the accessibility of the active sites, compared to the free particles where considerable aggregation of the particles is observed.

The resulting NO generated when the Cu-BTC catalyst is used is dependent on the substrate. Similar behavior has been noted previously for the reaction of RSNOs with solvated Cu^{2+} ions and is attributed to variations in the R substituent.[21] In the case of solvated Cu^{2+} ions, the differences in reactivity between the various substrates has been attributed to the capacity for each of the substrates to form stable bidentate cyclic intermediates with the metal ion.[22] Variations in the reactivity of RSNOs with Cu-BTC have been attributed to the presence of varying R groups and the resulting intermediates that are formed as a result of the coordination with the metal center resulting in CysamNO being more reactive towards NO generation than CysNO. Historically, HcysNO has been amongst the least reactive substrates as a result of the longer chain length and its propensity for forming an unfavorable 7 membered ring as the intermediate.[22] In this work, the coordination environment of the active site within the MOF architecture only allows for the coordination of one additional ligand and as a result likely impedes the formation of a cyclic transition state. At this point in time, little is known about the mechanistic activity of MOF catalysts and is beyond the scope of this paper. However, in regards to this reaction we have identified two potential reaction pathways that warrant further investigation. In the first we propose the possibility of a redox driven mechanism which is similar to that observed for the free ion. However, the feasibility of a MOF catalyst undergoing redox changes at the metal center without incurring structural damage is a major point of concern. Alternatively, we propose a Lewis acid driven mechanism of which Cu-BTC has been previously established to facilitate Lewis acid catalyzed reactions[23] and RSNOs have also been

shown to generate NO as a result of reactions with Lewis acids.[24] Exploration of the mechanistic avenues of reaction of RSNOs with Cu-MOFs will be the subject of future work.

Conclusion

The development of integrative materials is key for chronic medical device applications. This requires materials to have sustained biological activity for prolonged periods which has not been achieved through current approaches. Towards sustained release materials, this work demonstrates for the first time the development of a biomedical device, using a common manufacturing technique, with the capacity to generate NO from bioavailable sources. The MOF catalyst, Cu-BTC, upon interaction with the RSNO substrates, CysNO, CysamNO, and HcysNO, effectively produces NO. The rates of NO release from each of the substrates with the MOF catalyst varied based on the substitution of the R groups. Furthermore, the inherent structural robustness of the MOF catalyst facilitated its incorporation into a polymeric medical device tubing using a common commercial manufacturing technique and an even dispersion of the embedded particles. This work highlights the feasibility of incorporating embedded catalysts into bulk materials to produce NO utilizing external sources. Furthermore, the ability to tune the NO release function using a single catalyst in polymer tubing based on the NO donor it is exposed to is a promising approach towards integrating with chronic in-dwelling devices.

References

1. Adams, R.; Carson, C.; Ward, J.; Tannenbaum, R.; Koros, W. *Microporous and Mesoporous Materials* **2010**, *131*, 13.
2. Betard, A.; Fischer, R. A. *Chemical Reviews* **2012**, *112*, 1055.
3. Car, A.; Stropnik, C.; Peinemann, K.-V. *Desalination* **2006**, *200*, 424.
4. Hu, J.; Cai, H.; Ren, H.; Wei, Y.; Xu, Z.; Liu, H.; Hu, Y. *Industrial & Engineering Chemistry Research* **2010**, *49*, 12605.
5. Basu, S.; Cano-Odena, A.; Vankelecom, I. F. J. *Journal of Membrane Science* **2010**, *362*, 478.
6. Harding, J. L.; Reynolds, M. M. *Trends in Biotechnology* **2014**, *32*, 140.
7. Ellman, G. L. *Archives of Biochemistry and Biophysics* **1959**, *82*, 70.
8. Collins, D. J.; Zhou, H. C. *Journal of Materials Chemistry* **2007**, *17*, 3154.
9. Morris, R. E.; Wheatley, P. S. *Angew. Chem. Int. Ed.* **2008**, *47*, 4966.
10. Della Rocca, J.; Liu, D.; Lin, W. *Accounts of Chemical Research* **2011**, *44*, 957.
11. Keskin, S.; Kizilel, S. *Industrial & Engineering Chemistry Research* **2011**, *50*, 1799.
12. Rieter, W. J.; Pott, K. M.; Taylor, K. M. L.; Lin, W. *Journal of the American Chemical Society* **2008**, *130*, 11584.
13. Sun, C. Y.; Qin, C.; Wang, X. L.; Su, Z. M. *Expert Opinion on Drug Delivery* **2013**, *10*, 89.
14. Chen, B.; Liang, C.; Yang, J.; Contreras, D. S.; Clancy, Y. L.; Lobkovsky, E. B.; Yaghi, O. M.; Dai, S. *Angewandte Chemie International Edition* **2006**, *45*, 1390.
15. Yu, Y.; Ren, Y.; Shen, W.; Deng, H.; Gao, Z. *TrAC Trends in Analytical Chemistry* **2013**, *50*, 33.
16. Farha, O. K.; Shultz, A. M.; Sarjeant, A. A.; Nguyen, S. T.; Hupp, J. T. *Journal of the American Chemical Society* **2011**, *133*, 5652.

17. Lee, J.; Farha, O. K.; Roberts, J.; Scheidt, K. A.; Nguyen, S. T.; Hupp, J. T. *Chemical Society Reviews* **2009**, *38*, 1450.

18. Yoon, M.; Srirambalaji, R.; Kim, K. *Chemical Reviews* **2011**, *112*, 1196.

19. Hogg, N. *Free Radical Biology and Medicine* **2000**, *28*, 1478.

20. Bates, J. N. *Neuroprotocols: A Companion to Methods in Neurosciences* **1992**, *1*, 141.

21. Roy, B.; du Moulinet d'Hardemare, A.; Fontecave, M. *The Journal of Organic Chemistry* **1994**, *59*, 7019.

22. Askew, S. C.; Barnett, D. J.; McAninly, J.; Williams, D. L. H. *Journal of the Chemical Society Perkin Transaction 2* **1995**, *8*, 741.

23. Alaerts, L.; Seguin, E.; Poelman, H.; Thibault-Starzyk, F.; Jacobs, P. A.; De Vos, D. E. *Chemistry European Journal* **2006**, *12*, 7353.

24. Timerghazin, Q. K.; Peslherbe, G. H.; English, A. M. *Organic Letters* **2007**, *9*, 3049.

Chapter 6

Growth of Metal Organic Thin Films on the Surface of Flexible Polymeric Substrates

Synopsis

In order to expand the scope of applicability of MOFs, there is increasing interest in the process ability of MOFs into composite materials.[1,2] The preparation of MOF composite materials can be achieved either through the incorporation of MOF particles as blends into the matrix of polymeric materials or by in situ growth onto the surface of rigid substrates, to form what are known as SURMOFs.[3,4,] Advantageously, SURMOFs offer the capacity for functionalizing materials with uniform coatings of MOF thin films, with control over the thickness of the deposited layer, orientation of the crystal face, and even patterned surface deposition.[5,6] The growth of SURMOFs however is primarily limited to the growth on rigid inorganic substrates with only few reports of growth on organic substrates despite significant advantages towards the development of functional materials.

In this work, the surface functionalization of the flexible polymeric substrate Cellulose was adhered with CuBTC particles grown via epitaxial layer by layer growth under ambient conditions. The resulting CuBTC –Cellulose swatches were characterized for the formation of CuBTC particles by pXRD and ATR-IR spectroscopy. SEM imaging was used to evaluate the surface coverage and the uniformity of the crystals. Furthermore, the CuBTC-cellulose swatch is explored as a heterogeneous catalyst for the generation of the bioactive agent nitric oxide. This work highlights the feasibility of developing numerous MOF composite materials at polymer interfaces towards application for a wide range of polymeric materials and applications.

Introduction

The goal for the preparation of MOF biomaterials is to mediate interfacial responses between the foreign object and the host environment. As such the most crucial location for the placement of MOF materials is directly onto the device surface rather than as a blend where the majority of the included MOF is below the material surface. To this effect the uniform deposition of MOFs onto functionalized surfaces has been shown using in situ synthetic growth methods.[7,] Biomaterials are fabricated to take on various shapes and sizes in order to accommodate numerous functionalities. As such a synthetic method which can accommodate a wide range of substrates that is indifferent to size, topology, and even varied topographies would be advantageous for the preparation of MOF coated biomaterials.[8]

For the synthesis of surface grown MOFs (SURMOFs) it is essential that the growth substrate remains intact over the course of MOF synthesis. As such many reports for the growth of SURMOFs are for robust inorganic substrates, gold, silica, or alumina.[6,9,10,11] However, with the emerging interest of MOFs in sensing, chromatographic, filtration, and even protective textiles it is essential to expand the capacity for the growth of SURMOFs on flexible organic substrates.[12] The critical requirement for the attachment of the MOF to a polymer surface is tuning of the surface functionality such that it corresponds with the coordinating ligand of the MOF. Towards this end, there are few reports of the successful in situ growth of MOFs on polymeric substrate using microwave assisted, slow diffusion reactions, and layer by layer (LbL) epitaxial growth methods.[13,14,15,16,] There is particular interest in the use of the LbL method due to its effectiveness under mild reaction conditions at room temperature in aqueous solvents compared to solvothermal methods.[17,5] The layer by layer method relies on alternating between metal ion and ligand precursor solutions, with the number of cycles directly corresponds the film thickness. Therefore, using the LbL approach we propose the growth of SURMOFs on flexible organic substrates that is impartial to shape, topography, or topology.

Presented herein is the rapid growth of the archetypal MOF, CuBTC directly onto the surface of the flexible polymeric substrate, Cellulose, using room temperature epitaxial LbL deposition. CuBTC is assembled into a permanently porous crystalline network of Cu^{2+} metal ions coordinated to the carboxyl functionalities of 1,3,5-benzenetricarboxylic acid, as such it is essential that the surface of the polymer be derivatized to include carboxyl pendant groups through carboxymethylation of polymeric hydroxyl groups. Subsequently, CuBTC particles were synthesized directly on the polymeric surface by incorporating the swatches of the carboxymethylated cellulose into a saturated solution of Cu(II)Acetate in water for 5 minutes followed by immersion of the swatch in the ligand solution of 0.2M 1,3,5-Benzenetricarboxylate for an additional 5 minutes. This process was repeated for a total of 8 cycles. The characterization of the resulting CuBTC-Cellulose swatches was evaluated visually for MOF surface coverage and uniformity by SEM imaging; structurally by pXRD and ATR-IR spectroscopy; and for fixation to the substrate through leaching studies. Furthermore, we explored the utility of the CuBTC-cellulose swatch as a heterogeneous catalyst for the generation of the bioactive agent nitric oxide.

Experimental Methods

Materials. The natural cotton fabric (TIC/400) was obtained from SDL Atlas and used as received. Reagents used in this work include, copper (II) acetate ($Cu(OAc)_2 \bullet H_2O$) (Sigma Aldrich), 1,3,5-benzentricarboxylic acid (H_3BTC) (Acros Organics) and sodium chloroacetate ($C_2H_2ClNaO_2$) (Alfa Aesar). Dimethylformamide (DMF), reagent alcohol and sodium hydroxide were all obtained from Fischer Scientific. All reagents were used as received without any further purification.

Carboxymethylation of Cellulose fabric. In order to obtain an anchoring point for the deposition of Cu-BTC onto the cellulose matrix, the cellulose fabric was carboxymethylated using sodium hydroxide as the catalyst, shown in Scheme 1. A 1M solution of sodium chloroacetate (1.16 g) and 5% NaOH (2.5 mL) was prepared by dissolving in a total volume of 10 ml, followed by the cellulose being allowed to react for an hour under stirring.

Surface Deposition of Cu-BTC. Copper Acetate (1.078 g) was mixed in 15 mL of millipore water (18 MΩ) and allowed to completely dissolve to create a 0.36 mM solution. H_3BTC (631 g) was dissolved in 15 mL of a 1:1:1 ratio DMF:ethanol:water to obtain a 0.2 M solution. Cotton samples were sequentially dipped in the copper acetate ($Cu(OAc)_2*2H_2O$) solution, followed by the H_3BTC solution, 5 min each, for a total of 8 alternating cycles. After each dipping the cotton fabric was rinsed thoroughly with millipore water to remove any excess reagents. After 8 cycles, the samples were washed for 5 hours each, in ethanol followed by DMF to remove any Cu-BTC which was not covalently bonded to the cellulose.

Material Imaging: Using a JEOL JSM-6500F (FSEM) with an accelerating voltage of 3.0 kV and a working distance of 4.0 mm. Images were taken at magnification values of 500x, 2,000x and 9,000x and processed for copper distribution using EDX spectroscopy. The EDX spectrum was collected at an accelerating voltage of 5 kV at 130X magnification. All data was processed using Thermo NSS Release candidate 7 software.

XRD measurements. Powder X-ray diffraction (pXRD) measurements were carried out using a Scintag X2 pXRD with CuKα radiation.

Results and Discussion

Carboxymethylation of Cellulose to include anchor sites. As shown in Scheme 1, the hydroxyl groups incorporated onto the polymeric backbone of cellulose were derivatized with chloroacetate to form pendant carboxylic acid groups on the polymeric surface. Carboxymethylation of the cellulose was evaluated my comparing the infrared spectrum of parent cellulose and the reacted material, shown in Figure 2. The appearance of the adsorption peak at 1590 cm^{-1} for the reacted particles is indicative of a C=O stretch corresponding to the incorporation of carboxyl functionalities.[16] The successful modification of the cellulose with carboxyl groups provides the necessary surface composition for the attachment and subsequent growth of MOFs on the material surface.

Scheme 1. Carboxymethylation of cellulose

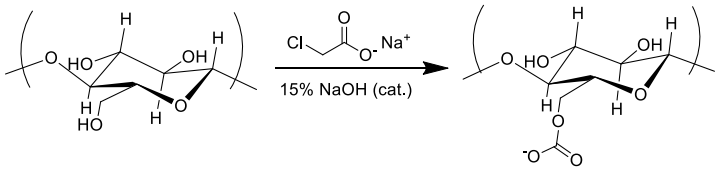

Surface Growth of CuBTC. Next *in situ* growth of Cu-BTC onto the carboxylated polymers through LBL synthesis, under ambient conditions, where the polymer undergoes alternative immersion in solutions of $Cu(OAc)_2*H_2O$ and the ligand H_3BTC for 5 minutes periods constituting a cycle, is shown in Scheme 2. The process was repeated for a total of 8 cycles, with each cycle beginning with immersion in the copper solution, since the coordination environment of the metal ion creates an anchor point for the attachment of the particles to the surface. Furthermore, the coordination cluster serves as a platform for the growth of CuBTC particles, where each subsequent immersion cycle facilitates the stepwise growth of CuBTC onto the material surface and the resulting thickness of the surface grown crystal layer is well known to be directly correlated with number of repeated cycles. With each cycle the polymeric material gradually up took a turquoise coloration, which even after thorough washing and leaching studies was determined to be adhered to the surface and subsequent desolvation of the material resulted in the transformation to a royal blue coloration. These results are consistent with the well-defined behavior of solvated versus desolvated CuBTC particles. To further confirm the synthesis of surface adhered CuBTC particles, we assessed structural properties through attenuated total reflectance infrared spectroscopy (ATR-IR) and powder X-ray diffraction (pXRD) and visually inspected the deposited particle through SEM imaging.

Scheme 2. Layer by layer growth of CuBTC onto carboxymethylated cellulose substrates

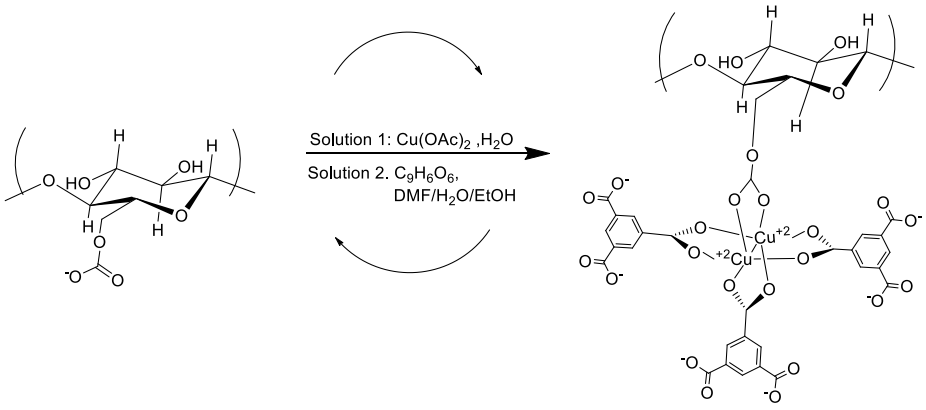

Characterization of CuBTC-Cellulose swatch. The formation of CuBTC onto the polymeric surface was evaluated based on a comparison of the crystalline signature of the material with traditionally prepared CuBTC particles using pXRD. As shown in Figure 1, the diffraction pattern of CuBTC-Cellulose corresponds with the diffraction pattern for the free particles. However, in the case of CuBTC-cellulose material there are additionally diffraction peaks present at 15 degrees and 23 degrees, which are artifacts of diffraction associated with the polymeric surface, shown in Figure 1. Overall, the presence of the matching diffraction peaks signifies the successful deposition of a crystalline material, not just an amorphous salt. Subsequently, we investigated the structural identity of the crystals by ATR-IR spectroscopy. The resulting IR spectra of CuBTC cellulose material, shown in Figure 1, corresponds with CuBTC particles. Notably, the spectral properties associated with the polymeric substrate are not evident, providing further evidence for the exceptional surface coverage of CuBTC on the polymeric substrate.

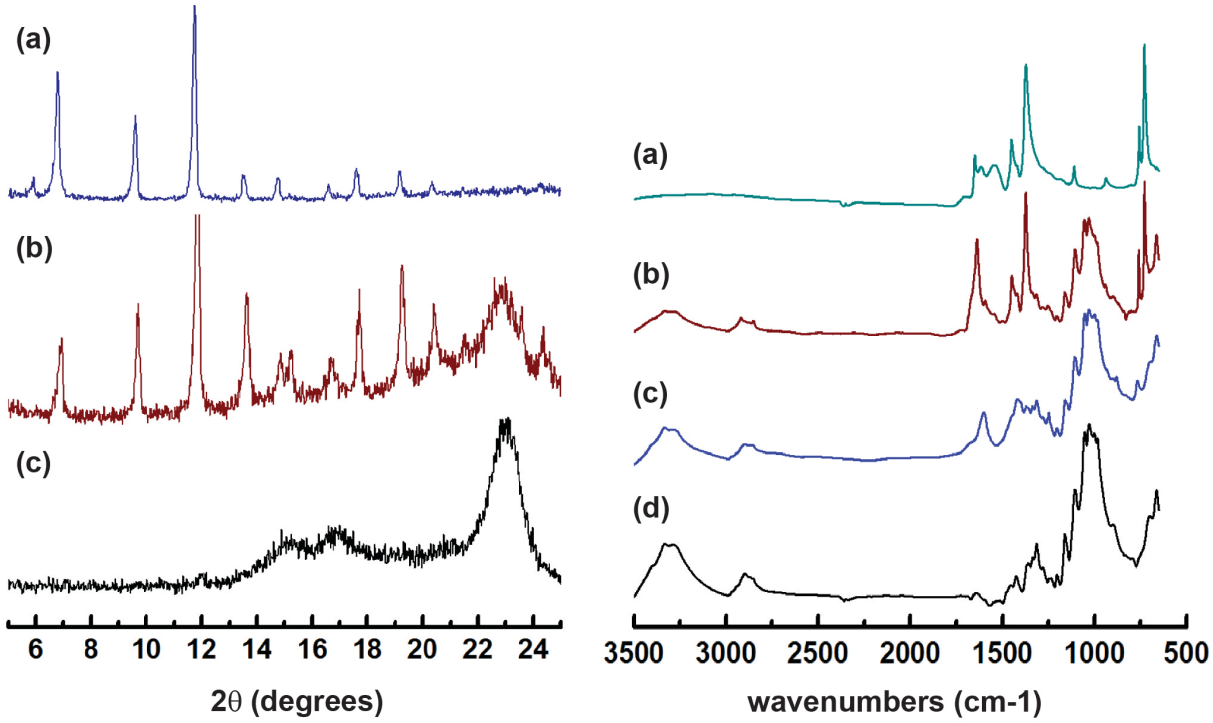

Figure 1. (left) pXRD diffraction patterns of a) CuBTC powder b) composite material c) cellulose diffraction patterns. (right) and ATR-IR spectra of a) CuBTC powder b) composite material c) carboxymethylated cellulose d) cellulose.

SEM Imaging and Leaching Studies. We visually inspected the formation of MOF particles on the surface of the polymeric substrate by SEM at 500x and 5000x magnification, shown in Figure 2. At 500x magnification we observe the fibrous strands of cellulose are deposited with the CuBTC crystals with excellent surface coverage over the entire surface. Upon closer inspection of the CuBTC partcles we observe that well defined octahedral crystals with an average particle size of 10.55 ± 4.01 μM are formed across the curved surface of the fiber. The adhesion of the particles to the surface was subsequently evaluated by leaching studies where CuBTC Cellulose swatches were immersed in ethanol over a one week period. In Figure 3 the resulting weight percentage of the material is presented for swatches which were immersed continuously in the soak solution. Following removal of the swatch from the soak solution the material was dried and weighed and the soak solution was evaluated for copper content by elemental analysis. After a 1 week period the swatches retained in ≥95% of the initial weight and elemental analysis of the solution indicated the solution copper content was <1% of the total Cu content

of polymer bound CuBTC particles. Taken together these results indicate that the deposited CuBTC particles are anchored to the surface of the polymeric cellulose substrates.

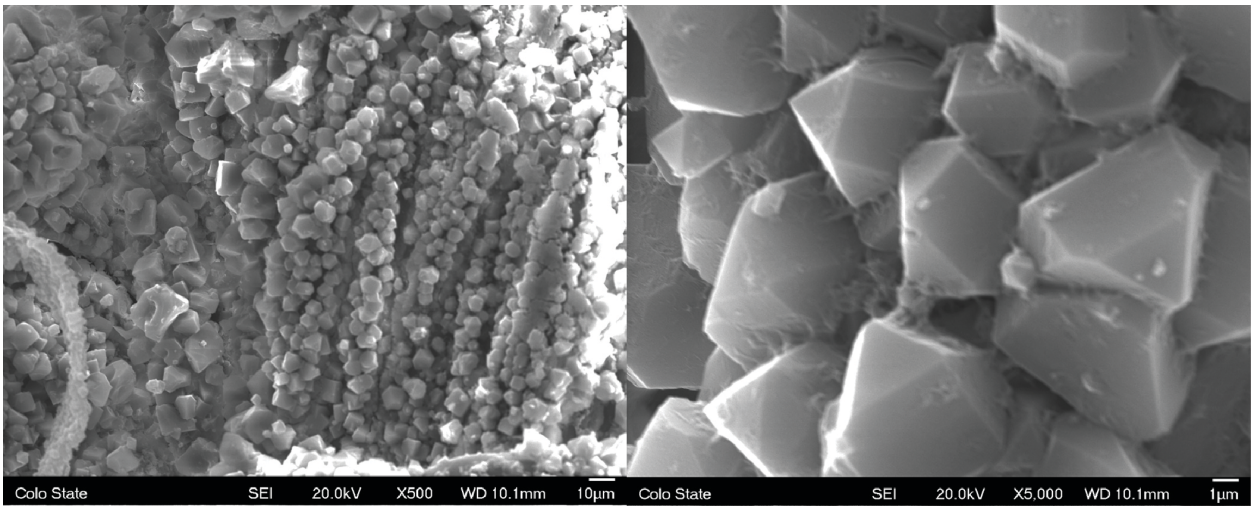

Figure 2. SEM images of CuBTC-Cellulose swatches at 500x (left) and 5,000x (right) magnification after leaching analysis studies.

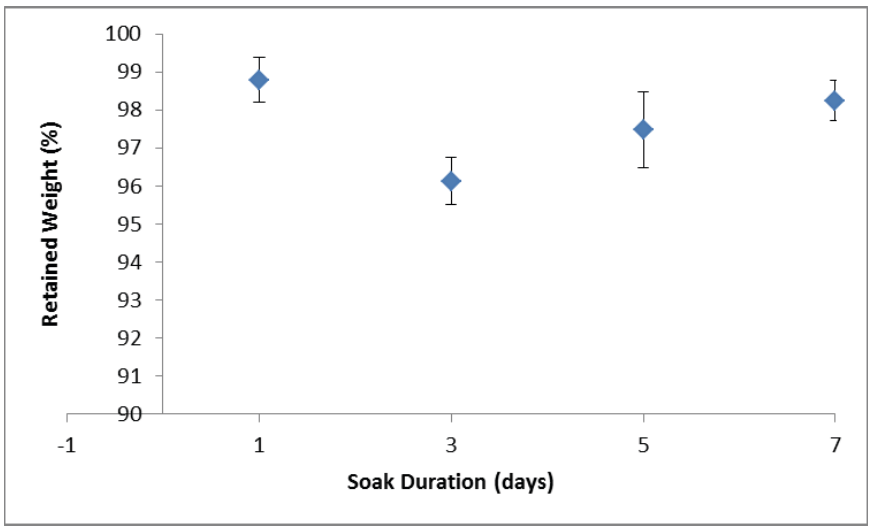

Figure 3. Leaching studies for CuBTC . Elemental analysis studies indicated no detectable Cu in solution over the 1 week period.

We have demonstrated the development of a synthetic method for the functionalization of preformed polymeric surfaces that is irrelevant towards the size, shape, or topology with a uniform coating of

CuBTC crystals under ambient conditions. Notably the fibrous polymeric network associated with Cellulose is composed of a weave type configuration which does not compromise the surface coverage of the materials nor does it impact the uniformity in crystalline deposition on the material surface. Based on this exceptional demonstration for the formation of a MOF composite material the next logical step is to apply the material in an application based setting. The use of fibrous materials are often found in the development of protective textiles including bandages and through the incorporation of MOFs, the materials can be tuned to mediate interfacial responses between damaged tissues and the bandage for minimizing the risk of infection and promoting wound healing responses.[18] As an essential bioagent for mediating proliferative cellular effects and immune responses, nitric oxide, is a target therapeutic to investigate for wound healing applications.[19] Towards this end we have explored the functionality of the CuBTC-Cellulose swatch for the catalytic generation of nitric oxide from bioavailable substrates, S-nitrosothiols.

Heterogeneous Catalysis Mediated by CuBTC-Cellulose Swatches. The reactivity of CuBTC-Cellulose swatches as heterogeneous catalysts for the generation of NO from select bioavailable NO donors shown in Figure 4, S-nitrosocysteine (CysNO), S-nitrosocysteamine (CysamnNO), and S-nitrosohomocysteine (HCysNO) were evaluated by monitoring the formation of the product NO via chemiluminescence detection. The resulting rate of NO generation from each RSNO increased in order of HCysNO>CysNO>>CysamNO as shown in Table 1. These results concur with the previous findings utilizing the unsupported CuBTC particles (ref Ch 3). As shown in Table 1, the reactivity of the CuBTC swatches towards NO generation is analogous to that of the free particles.

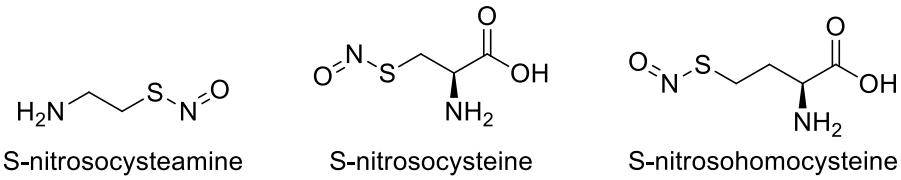

Figure 4. Molecular structures of Bioavailable RSNOs

Table 1. Summary of Rate of NO Generation from Various RSNOs

Donor	Blank (nM s^{-1})	Swatch (nM s^{-1})	Neat (nM s^{-1})	Cu^{2+} (nM s^{-1})
CysNO	2.05 ± 0.88	7.46 ± 0.83	9.64 ± 0.26	161 ± 18
CysamNO	2.11 ± 0.29	20.3 ± 0.63	21.3 ± 0.82	231 ± 13
HcysNO	3.22 ± 0.19	1.94 ± 0.15	3.10 ± 0.09	163 ± 3

Subsequently, the CuBTC swatch was confirmed as the catalyst responsible for the generation of NO and not the leached copper ions or unadhered CuBTC particles. Towards this end, in a classical evaluation for a heterogeneous catalyst the swatch was removed from solution during the reaction and the resulting NO release following removal was examined. Since NO release measurements are recorded in real time we are able to determine the instantaneous effects of the removal of the catalyst from solution. As shown in Figure R, removal of the swatch immediately halted the generation of NO and returned the levels of NO generation to a baseline reading observed in the absence of the catalyst. Subsequently, reintroduction of the CuBTC swatch resulted in the return of catalyzed NO generation. Based on these experiments we are confident that the catalyzed generation of NO is a result of the covalently bound CuBTC particles present on the CuBTC swatch is responsible for the observed catalytic activity and not Cu^{2+} ions leached into solution.

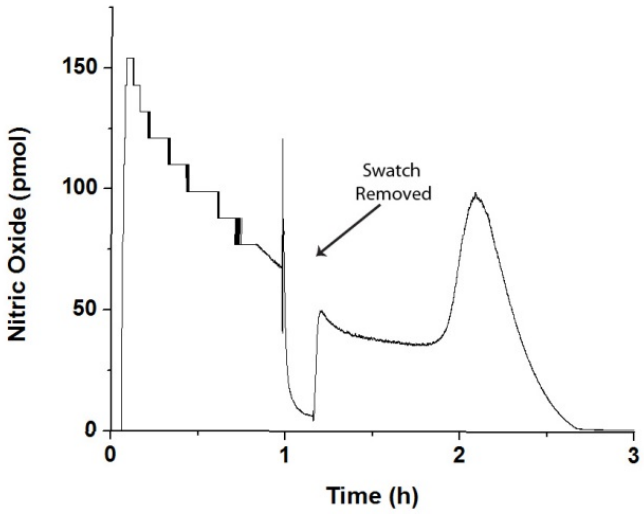

Figure 5. Real time NO release curve of CysamNO as the substrate in the presence of CuBTC-Cellulose swatch. Where removal of the swatch results in a return to baseline of the NO generation.

Conclusion

In summary we present the first instance of in situ growth a MOF onto a preformed polymeric substrate. Utilizing a layer by layer approach CuBTC crystals were deposited onto carboxymethylated cellulose under ambient conditions. Notably, excellent surface coverage with well-defined CuBTC crystals was evident on the uneven surface associated with the fibrous composition of the cellulose. This work highlights the feasibility of developing numerous MOF composite materials at polymer interfaces towards application for a wide range of polymeric materials and applications.

References

1. Bradshaw, D.; Garai, A.; Huo, J., *Chemical Society Reviews* **2012,** *41* (6), 2344-2381.
2. Shekhah, O.; Liu, J.; Fischer, R. A.; Woll, C., *Chemical Society Reviews* **2011,** *40* (2), 1081-1106.
3. Hinterholzinger, F.; Scherb, C.; Ahnfeldt, T.; Stock, N.; Bein, T., *Physical Chemistry Chemical Physics* **2010,** *12* (17), 4515-4520.
4. Shekhah, O.; Wang, H.; Kowarik, S.; Schreiber, F.; Paulus, M.; Tolan, M.; Sternemann, C.; Evers, F.; Zacher, D.; Fischer, R. A.; Woll, C., *Journal of the American Chemical Society* **2007,** *129* (49), 15118-+.
5. Shekhah, O., *Materials* **2010,** *3* (2), 1302-1315.
6. Liu, B.; Tu, M.; Zacher, D.; Fischer, R. A., *Advanced Functional Materials* **2013,** *23* (30), 3790-3798.
7. Zhuang, J. L.; Ceglarek, D.; Pethuraj, S.; Terfort, A., *Advanced Functional Materials* **2011,** *21* (8), 1442-1447.
8. Stock, N.; Biswas, S., *Chemical Reviews* **2012,** *112* (2), 933-969.
9. Wu, Y. N.; Li, F. T.; Xu, Y. X.; Zhu, W.; Tao, C. A.; Cui, J. C.; Li, G. T., *Chemical Communications* **2011,** *47* (36), 10094-10096.
10. Gascon, J.; Aguado, S.; Kapteijn, F., *Microporous and Mesoporous Materials* **2008,** *113* (1-3), 132-138.
11. Tu, M.; Wannapaiboon, S.; Fischer, R. A., *Dalton Transactions* **2013,** *42* (45), 16029-16035.
12. Centrone, A.; Yang, Y.; Speakman, S.; Bromberg, L.; Rutledge, G. C.; Hatton, T. A., *Journal of the American Chemical Society* **2010,** *132* (44), 15687-15691.
13. O'Neill, L. D.; Zhang, H. F.; Bradshaw, D., *Journal of Materials Chemistry* **2010,** *20* (27), 5720-5726.
14. Abbasi, A. R.; Akhbari, K.; Morsali, A., *Ultrasonics Sonochemistry* **2012,** *19* (4), 846-852.

15. Meilikhov, M.; Yusenko, K.; Schollmeyer, E.; Mayer, C.; Buschmann, H. J.; Fischer, R. A., *Dalton Transactions* **2011,** *40* (18), 4838-4841.
16. Pinto, M. D.; Sierra-Avila, C. A.; Hinestroza, J. P., *Cellulose* **2012,** *19* (5), 1771-1779.
17. Shekhah, O.; Wang, H.; Strunskus, T.; Cyganik, P.; Zacher, D.; Fischer, R.; Woll, C., *Langmuir* **2007,** *23* (14), 7440-7442.
18. Tsotsalas, M.; Liu, J. X.; Tettmann, B.; Grosjean, S.; Shahnas, A.; Wang, Z. B.; Azucena, C.; Addicoat, M.; Heine, T.; Lahann, J.; Overhage, J.; Brase, S.; Gliemann, H.; Woll, C., *Journal of the American Chemical Society* **2014,** *136* (1), 8-11.
19. Bogdan, C., *Nature Immunology* **2001,** *2* (10), 907-916.

Chapter 7

Summary

The primary goal of the research contained within this dissertation is to develop a therapeutic material which generates the bioactive agent nitric oxide from an endogenous source. Nitric oxide (NO) is a bioactive agent generated by most nucleated cells in the human body known to mediate antimicrobial effects and promote the proliferation of healthy tissues.[1] Therefore, the development of an NO releasing material which can sustain the generation of physiologically relevant levels of NO by relying on endogenous supplies of NO over the device lifetime will result in the development of an antifouling material surface with potentially regenerative effects. Achieving this goal requires the separation into three parts: First the development of a measurement method to quantify NO; second identification of catalytic material which not only catalyzes the generation of NO from bioavailable substrates but also remains structurally intact in the physiological environment. Lastly, the NO catalyst must be incorporated into a polymeric secondary support for use in biomedical devices.

The development of any material requires a means to evaluate its effectiveness. Therefore, in order to evaluate any NO materials that may be prepared a method for the accurate quantification of generated NO must first be developed. In this work chemiluminescence based NO detection was established as reliable method for the accurate quantification of NO generated from small molecule donors in cell media solution.[2] Riboflavin was identified as a NO scavenging agent included in cell media solutions as a vitamin additive. Variations in the concentration of riboflavin and the rate of NO release from the NO donors was found to influence the amount of NO scavenged from solution. Based on these results many discrepancies in the literature regarding the therapeutic range of NO can be rectified by taking into account the NO scavenging capacity of the media solutions.

The development of an NO catalyst for the sustained generation of NO from bioavailable S-nitrosothiol (RSNO) substrates requires accessible Cu^{2+} catalytic sites and structural integrity in the physiological environment, shown in Figure 1.[3] The use of a solid state catalyst is advantageous based on the ease of incorporation into secondary supports and the inherent robustness of the material. In particular metal organic frameworks are regularly explored as both drug delivery vehicles and heterogenous catalysts making them attractive targets for use as NO catalysts. The variable chemical and physical properties of MOFs make them promising platforms for biomedical applications due to their potential design for biodegradability and chemical and structural tunability.

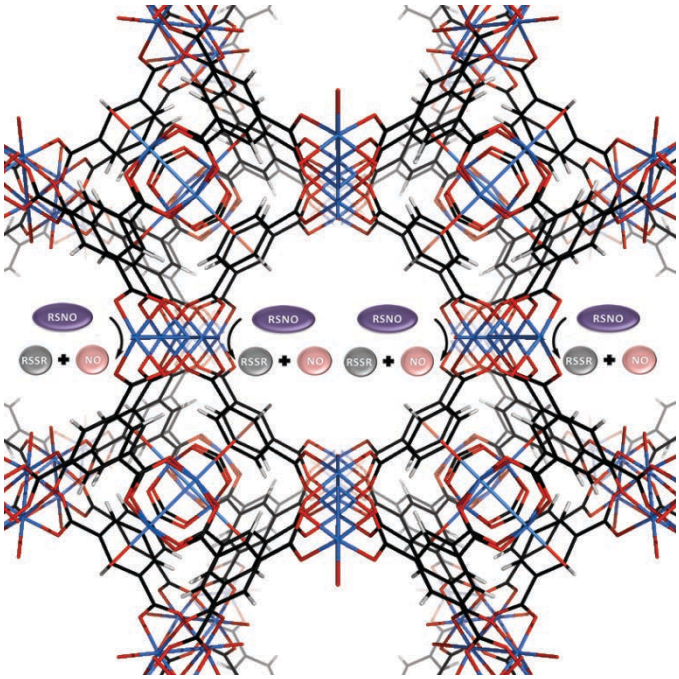

Figure 1. Illustration of RSNO decomposition to produce NO via a MOF catalyst with coordinatively unsaturated Cu^{2+} metal centers

Initial exploration of MOFs as NO catalysts in this work focused on the use of the classic and commercially available MOF, CuBTC. The use of CuBTC demonstrated proof of principle that Cu-MOFs can drive the catalytic generation of NO from RSNO's, where the rate of NO generation from structurally distinct RSNOs (Table 1) was dependent on substrate size and polarity of the functional groups. The summary of the rate of NO generation from each RSNO substrate reacted with CuBTC compared to

solvated Cu^{2+} ions and the blank is shown in Table 1. The limitation of CuBTC as a NO catalyst for biological applications was the limited moisture stability of the framework, which necessitated that all catalytic activity be evaluated in a non aqueous solvent (ethanol).

Table 2. Rate of NO Generation from various RSNOs

RSNO	Blank (nM s^{-1})	CuBTC (nM s^{-1})	$CuCl_2$ (nM s^{-1})
CysNO	2.55 ± 0.21	10.4 ± 0.2	161 ± 18
CysamNO	2.23 ± 0.30	21.3 ± 0.9	231 ± 12
HcysNO	3.22 ± 0.19	3.10 ± 0.94	157 ± 12
MPANO	2.80 ± 0.11	4.56 ± 0.68	214 ± 19
MeNO	1.60 ± 0.27	11.1 ± 1.6	264 ± 23
TGANO	2.30 ± 0.60	20.1 ± 1.1	515 ± 73
TLANO	1.23 ± 0.10	26.1 ± 1.7	441 ± 45

All rates are reported at 25 °C. Data points were run in triplicate and reported to the 95% confidence interval.

Encouraged by the success of CuBTC as a MOF NO catalyst, alternative MOFs with increasing stability in aqueous solutions were sought. Substitution of the carboxyl ligand (1,3,5-benzetricarboxylic acid) contained with CuBTC for a triazolate analogue (1,3,5-benzenetristriazole) results in the formation of a robust water stable MOF with coordinatively unsaturated Cu^{2+} metal centers, CuBTTri.[4] Investigation of CuBTTri structural stability in aqueous mediums routinely used for *in vitro* and *in vivo* experiments, including phosphate buffered saline (PBS), cell media, and whole blood by assessing the resultant crystallinity of the material by pXRD revealed the material remains intact, shown in Figure 2. Subsequently, the reaction of CuBTTri with an RSNO substrates resulted in the catalytic generation of NO with kinetic control imparted as a function of catalyst loading. While rigorous *in vitro* and *in vivo* testing remains to be done to examine the full extent of the potential of CuBTTri in a therapeutic setting, this is the first report of a MOF which can catalytically generate a bioactive molecule from an endogenous source on the surface of a polymeric film with the capacity for tunable release kinetics in biological fluids.

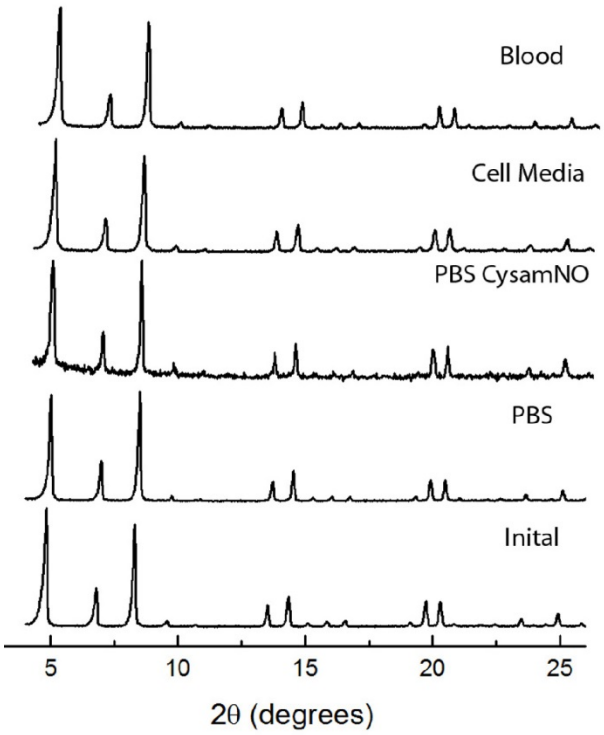

Figure 2. pXRD patterns of CuBTTri particles as the initial unreacted particles and following immersion in phosphate buffered saline, cell media, and fresh whole blood.

Finally the feasibility of developing composite MOF-polymer biomedical devices was investigated. The development of MOF composite materials can proceed by either embedding preformed MOF particles within the polymeric matrix prior to manufacturing of the device or MOFs can be grown in situ as thin films directly onto the surface of a preformed substrate. In this account both approaches to MOF composite material preparations were pursued. The preparation of blended composites was demonstrated via processing into single lumen tubing via a commercial extrusion process.[5] Evaluation of the processed material indicated that the structural integrity of the MOF was preserved as well as the reactivity as an NO catalyst.

Use of the blended approach is favorable when the material comes direct from a manufacturer, however in many cases the preparation of a composite MOF material with already prepared substrates is more accessible. The majority of surface grown MOFs are reported for rigid inorganic substrates rather than

flexible organic polymers used for the construction of many biomedical devices. As a result this work demonstrated room temperature epitaxial growth of CuBTC particles onto the surface of the natural organic polymer cellulose (cotton fabric). The deposited MOF crystals confirmed by pXRD as CuBTC crystals and were determined to be adhered to the material surface after vigorous washing and leaching studies. In Figure 4, SEM imaging of the material indicated that the crystals exhibited excellent surface coverage across the uneven cellulose fabric strands with well-defined 10μM MOF crystals. Evaluation of the CuBTC-cellulose swatches indicated that the material catalyzed the generation of NO at rates comparable to unsupported CuBTC particles. Subsequent removal of the CuBTC-cellulose material halted the reaction progress, confirming its presence as a heterogeneous catalyst.

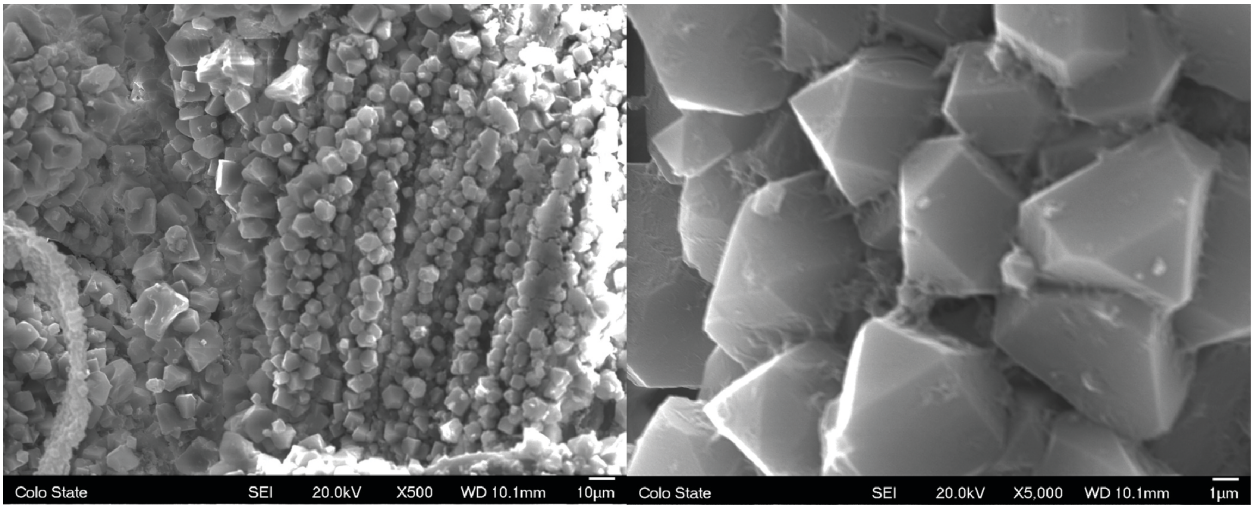

Figure 4. SEM images of CuBTC-Cellulose swatches at 500x (left) and 5,000x (right) magnification after leaching analysis studies.

The research presented in this dissertation was undertaken with the intention of making a significant contribution to the field. In order to fulfil the stated goal of developing a catalytic NO material for the long term applications in biomaterials it was necessary to start from the ground up requiring the development of a measurement method for assessing the materials, identification of a suitable catalytic material, and ultimately processing into usable devices. In light of the success of this work it is important to consider that it remains the first of its kind in a very young field. As such continued work in this field

will likely explore the development BioMOFs aimed at mimicking enzymatic process or perhaps even as scaffolds for use in tissue regeneration.

References

1. Giustarini, D.; Milzani, A.; Colombo, R.; Dalle-Donne, I.; Rossi, R. *Clinica Chimica Acta* **2003**, *330*, 85.
2. Harding, J. L.; Reynolds, M. M. *Analytical Chemistry* **2014**, *86*, 2025.
3. Harding, J. L.; Reynolds, M. M. *Journal of the American Chemical Society* **2012**, *134*, 3330.
4. Demessence, A.; Dâ Alessandro, D. M.; Foo, M. L.; Long, J. R. *Journal of the American Chemical Society* **2009**, *131*, 8784.
5. Harding, J. L.; Reynolds, M. M. *Journal of Materials Chemistry B* **2014**, *2*, 2530.

Appendix 1

Table S1. Summary of Cell Media Components		
	EC* (mM)	NB** (mM)
Amino Acids		
Glycine	0.0307	0.4
L-Alanine	0.0303	0.0225
L-Arginine hydrochloride	0.3	0.398
L-Asparagine-H2O	0.1	0.00553
L-Aspartic acid	0.1	0
L-Cysteine 2HCl. H2O	0.199	0.26
L-Glutamic Acid	0.0299	0
L-Histidine hydrochloride-H2O	0.2	0.2
L-Isoleucine	0.504	0.802
L-Leucine	1	0.802
L-Lysine hydrochloride	0.995	0.798
L-Methionine	0.101	0.201
L-Phenylalanine	0.2	0.4
L-Proline	0.1	0.0675
L-Serine	0.305	0.4
L-Threonine	0.101	0.798
L-Tryptophan	0.0201	0.0784
L-Tyrosine	0.1	0.398
L-Valine	1	0.803
Vitamins		
Biotin	2.99E-05	0
Choline chloride	0.1	0.0286
D-Calcium pantothenate	0.0252	0.00839
Folic Acid	0	0.00907
Folinic Acid Calcium salt	0.00117	0
Niacinamide	0.05	0.0328
Pyridoxine hydrochloride	0.0102	0.0196
Riboflavin	1.01E-05	0.00106
Thiamine hydrochloride	0.0101	0.0119
Vitamin B12	0.00001	0.000005

i-Inositol	0.04	0.04
Inorganic Salts		
Ammonium Metavanadate NaVO3	4.9E-06	0
Ammonium Molybdate ((NH4)6Mo7O24-4H2O)	0.000003	0
Calcium Chloride (CaCl2-2H2O)	1.6	1.8
Cupric sulfate (CuSO4-5H2O)	4.8E-06	0
Ferric sulfate (FeSO4-7H2O)	0.00102	0
Ferric Nitrate (Fe(NO3)3"9H2O)	0	0.000248
Magnesium Chloride (anhydrous)	0	0.814
Magnesium Sulfate (MgSO4-7H2O)	10.02	0
Manganese Sulfate (MnSO4-H20)	1.2E-06	0
Nickelous Chloride NiCl2 6H2O	3E-07	0
Potassium Chloride (KCl)	3.97	5.33
Selenious Acid H2SeO3	2.95E-05	0
Sodium Bicarbonate (NaHCO3)	14	26.19
Sodium Chloride (NaCl)	110.86	68.97
Sodium Meta Silicate Na2SiO3 9H2O	0.00986	0
Sodium Phosphate dibasic (Na2HPO4-7H2O)	0.5	0.906
Zinc Sulfate (ZnSO4-H2O)	0.000001	0.000674
Other Components		
Adenine	0.001	0
D-Glucose (Dextrose)	5.56	0
Lipoic Acid	1.02E-05	0
Phenol Red	0.0329	0.0736
Putrescine 2HCl	1.2E-06	0
Sodium Pyruvate	1	0
Thymidine	9.92E-05	0
HEPES	0	10.92

*EC - MCDB 131, no Glutamine
*NB - NEUROBASAL™ Medium (1X) liquid